

Experimental Investigation of the Mechanical
Behavior of 3D Printed Co-Continuous Composite Polymers
under Static and Cyclic Loadings

by

Madhava Reddy Varakantham

A Thesis Presented in Partial Fulfillment
of the Requirements for the Degree
Master of Science

Approved July 2019 by the
Graduate Supervisory Committee:

Yongming Liu, Chair
Hanqing Jiang
Jay Patel

ARIZONA STATE UNIVERSITY

August 2019

ABSTRACT

Essential knowledge of Co-continuous composite material properties are explored in this thesis. Mechanical characterization of these materials gives a detailed outlook to use them in design, manufacture and tailor make the products.

Soft and hard polymer materials have extensive properties individually, but when combined to make a single structure, they give an exceptional combination of properties. In this study, Polymer materials used are in the form of Co-Continuous structures (i.e., both soft and hard polymers are continuous throughout the microstructure) fabricated into several microstructures namely, Simple Cubic (SC), Body-Centered Cubic (BCC) and Face Centered Cubic (FCC) shapes. An experimental process is designed and fine-tuned from existing methods to understand and record the mechanical response of these co-continuous polymers. Experimental testing is used to gather detailed information about several constituencies namely stress behavior and damage progression. A 3D imaging technique, Microtomography is used to visualize damage initiation and progression in the sample. Variations in energy absorption, fracture initiation and damage propagation in samples are observed and correlated analysis is performed to provide a logical explanation. Comparative studies are performed as well for different structures.

Based on the Knowledge gained from the above study on co-continuous polymer composites, several conclusions are drawn, and future work directions are suggested.

ACKNOWLEDGMENTS

My thesis study and this report would not have been possible without the valuable assistance and guidance of several individuals who contributed to my study and research in one way or another.

First and foremost, I would like to express my sincere gratitude to my advisor Dr. Yongming Liu, for accepting me into his student group and giving me the opportunity and continuous support for my thesis study. I appreciate all his guidance during the time of my research.

Also, I would like to thank the members of my thesis committee, Dr. Hanqing Jiang and Dr. Jay Patel for spending their valuable time supporting me in the stages of hardships, in reading and reviewing my work.

I extend my gratitude to Arizona State University for giving me this opportunity.

Finally, I would like to thank my parents and friends who are being there as my emotional support which gave me the courage to complete this study successfully.

TABLE OF CONTENTS

	Page
LIST OF TABLES.....	vi
LIST OF FIGURES.....	vii
LIST OF PLOTS.....	ix
LIST OF ABBREVIATIONS AND SYMBOLS.....	xi
CHAPTER	
1 INTRODUCTION.....	1
1.1 Composite Materials.....	1
1.2 Applications of Composite Materials.....	2
1.3 3d Printing (Additive Manufacturing).....	3
1.4 Applications of 3d Printing Technology.....	6
2 BACKGROUND AND TESTING FACILITIES.....	7
2.1 Background.....	7
2.2 Purpose of the Thesis.....	8
2.3 Sample Fabrication and Material Properties.....	10
2.3.1 Materials and their Properties.....	10
2.4 Laboratory Equipment.....	13
2.4.1 MTS Machine.....	14
2.4.2 Micro CT Machine.....	16
2.4.2.1 Micro CT Machine Scanning Procedure.....	17

CHAPTER	Page
3	DESIGN OF EXPERIMENTAL PROCESS.....20
3.1	Experimental Design.....20
3.2	Static Analysis Process.....21
3.3	Multi-Cycle Analysis Process.....24
4	STATIC ANALYSIS RESULTS.....26
4.1	Data Analysis and Results Discussion.....28
4.1.1	Load vs Deformation.....28
4.1.2	Stress vs Strain.....29
4.2	Microtomography Images and Discussion.....31
5	MULTICYCLE ANALYSIS RESULTS.....38
5.1	Data analysis and Results for 50 cycles.....38
5.1.1	Stress vs Number of cycles.....38
5.1.2	Stress vs Strain.....39
5.1.3	Imaging of Samples.....40
5.2	Data Analysis and Results for 500 Cycles for SC Sample.....44
5.2.1	Imaging of SC Sample.....48
5.3	Data Analysis and Results for 500 Cycles for BCC Sample.....54
5.3.1	Imaging of BCC Sample.....58
5.4	Data Analysis and Results for 500 Cycles for FCC Sample.....61
5.4.1	Imaging of FCC Sample.....66

CHAPTER	Page
5.5	Image Processing.....70
5.5.1	Methodology.....70
5.5.2	Results.....78
6	CONCLUSION AND FUTURE WORK.....85
6.1	Conclusion.....85
6.2	Future Work.....86
6.2.1	FEA Analysis.....87
6.2.2	Material Calibration.....88
6.2.3	Characterization of 3D Printed Metal Sample.....89
	REFERENCES.....91
	APPENDIX.....93
	A. MICROSOFT VISUAL STUDIO CODE DEVELOPED AND USED FOR THE IMAGE ANALYSIS.....93

LIST OF TABLES

Table	Page
1.1 Types of 3D Printing Technologies.....	6
2.1 VeroWhite Material Properties.....	11
2.2 Tango Plus Material Properties.....	12
3.1 Static Analysis Input Parameters into Testworks Software.....	22
3.2 Multi-Cycle Analysis Input Parameters into Testworks Software.....	25
5.1 Time Lapse between the Tests of SC Sample.....	45
5.2 Time Lapse between the Tests of BCC Sample.....	55
5.3 Time Lapse between the Tests of FCC Sample.....	61

LIST OF FIGURES

Figure	Page
2.1 Lattice Structures SC, BCC, and FCC.....	9
2.2 Samples used for Testing.....	10
2.3 Morphology of the Sample.....	11
2.4 MTS Machine used for Testing.....	14
2.5 Testworks Software Input Window.....	15
2.6 Micro CT Machine.....	16
3.1 Flow Chart Showing Complete Experimental Procedure.....	21
4.1 Sample Placement on MTS Machine for Testing.....	26
4.2 BCC Structure after Testing.....	27
4.3 FCC structure after Testing.....	27
4.4 SC structure after Testing.....	27
4.5 Microtomography Images of SC Sample.....	32
4.6 Microtomography Images of BCC Sample.....	35
4.7 Microtomography Images of FCC Sample.....	36
5.1 3D Scanning Images of SC Sample for 50 Cycles.....	40
5.2 3D Scanning Images of BCC Sample for 50 Cycles.....	42
5.3 3D Scanning Images of FCC Sample for 50 Cycles.....	43
5.4 3D Scanning Images of SC Sample for 500 Cycles.....	48
5.5 3D Scanning Images of SC Sample for 1500 Cycles.....	51
5.6 3D Scanning Images of SC Sample for 3500 Cycles.....	53

Figure	Page
5.7 3D Scanning Images of BCC Sample for 500 Cycles.....	58
5.8 3D Scanning Images of BCC Sample for 1000 Cycles.....	59
5.9 3D Scanning Images of BCC Sample for 1500 Cycles.....	60
5.10 3D Scanning Images of FCC Sample for 500 Cycles.....	66
5.11 3D Scanning Images of FCC Sample for 2000 Cycles.....	67
5.12 3D Scanning Images of FCC Sample for 3000 Cycles.....	69
5.13 Overview of the algorithm to approximate void area.....	71
5.14 Overview of image analysis to filter void area.....	71
5.15 Canny edge detector algorithm.....	73
5.16 Contours extraction from SC sample images.....	76
5.17 Contours extraction from BCC sample images.....	77
5.18 Contours extraction from FCC sample images.....	78
6.1 BCC 3D CAD Model for FEA Simulation.....	87
6.2 SC 3D CAD Model for FEA Simulation.....	87
6.3 3D Printed Stainless Steel 316L Alloy Sample.....	89
6.4 Micro CT Imaging Showing Voids in Different Layers of Dogbone shape.....	90

LIST OF PLOTS

Plot	Page
4.1 Load vs Deformation Plot for all Samples.....	28
4.2 Stress vs Strain Plot for all Samples.....	30
5.1 SN Plot for 50 Cycles.....	39
5.2 Stress-Strain Plot for 50 Cycles.....	39
5.3 SN Plot of SC Sample for 500 to 1500 Cycles.....	44
5.4 SN Plot of SC Sample for 2000 to 4500 Cycles.....	45
5.5 Stress-Strain Plot of SC Sample for 500 to 1500 Cycles.....	46
5.6 Stress-Strain Plot of SC Sample for 2000 to 4500 Cycles.....	46
5.7 Peak Stress Degradation of SC Sample for 500 to 4500 Cycles.....	47
5.8 Stiffness Reduction of SC Sample for 500 to 4500 Cycles.....	47
5.9 SN Plot of BCC Sample for 500 to 2000 Cycles.....	55
5.10 Stress-Strain Plot of BCC Sample for 500 to 2000 Cycles.....	56
5.11 Peak Stress Regression of BCC Sample for 500 to 2000 Cycles.....	56
5.12 Stiffness Reduction of BCC Sample for 500 to 2000 Cycles.....	57
5.13 SN Plot of FCC Sample for 500 to 2000 Cycles.....	62
5.14 SN Plot of FCC Sample for 2500 to 4000 Cycles.....	63
5.15 Stress-Strain Plot of FCC Sample for 500 to 2000 Cycles.....	63
5.16 Stress-Strain Plot of FCC Sample for 2500 to 4000 Cycles.....	64
5.17 Peak Stress Regression of FCC Sample for 500 to 4000 Cycles.....	64
5.18 Stiffness Regression of FCC Sample for 500 to 4000 Cycles.....	65

Plot	Page
5.19 Void area increase in SC Sample	79
5.20 Void area increase in BCC Sample	79
5.21 Void area increase in FCC Sample	79
5.22 Damage variation inside of SC sample for 500 cycles.....	80
5.23 Damage variation inside of SC sample for 1500 cycles.....	81
5.24 Damage variation inside of SC sample for 3500 cycles.....	81
5.25 Damage variation inside of BCC sample for 500 cycles.....	82
5.26 Damage variation inside of BCC sample for 1000 cycles.....	82
5.27 Damage variation inside of BCC sample for 1500 cycles.....	83
5.28 Damage variation inside of FCC sample for 500 cycles.....	83
5.29 Damage variation inside of FCC sample for 2000 cycles.....	84
5.30 Damage variation inside of FCC sample for 3500 cycles.....	84
6.1 Material Calibration of Samples.....	89

LIST OF ABBREVIATIONS AND SYMBOLS

SC	Simple Cubic
BCC	Body-Centered Cubic
FCC	Face Centered Cubic
ε	Strain
σ	Stress
δl	Deformation
l	Length of the Sample
T1, T2	Hysteresis Thresholds
Hij	Kernel matrix
σ^*	Standard deviation
Gx, Gy	Sobel Filters

CHAPTER – 1

INTRODUCTION

1.1 Composite Materials

Materials are often chosen to fulfill requirements like in the areas of manufacturing as raw materials and in the structures for reinforcement. Not every material has the desired properties. Two or more material must be chosen to fulfill the requirements of the task at hand. But as the requirements became more demanding, scientific advancements have made the possibility of combining two or more materials chemically to get the materials with desired properties. These new materials are known as composites with components either metallic or nonmetallic.

Composites are used in many areas and for many reasons, for example, one single composite part can replace many metallic parts. These metallic parts could take a lot of time and resources to acquire the shape of the desired part but in the case of composites, parts can be made into customized designs utilizing less time and resources. Flexural properties of Composite materials are better compared to metals. Composites are good dampers, able to reduce vibration and sound.

Composite materials are heterogeneous which are made by combining two completely different material. Each individual material has its own set of properties, but when combined synthetically or chemically we will get properties that not seen in any of the individual materials. These materials can be tailor-made to complex parts, unlike metals.

1.2 Applications of Composite Materials

It is important to list all the commercial and industrial applications of the composites.

Aerospace

Since composites are versatile materials, these are used in the aerospace industry.

- Aircraft brakes, Heat pipes, joints, and holding equipment
- Passenger doors, engine nacelle, slats, ailerons, spoilers, flaps, wing skin, fuselage skin, wingtips, horizontal and vertical stabilizers, undercarriage doors.
- In case of the helicopters, rotor blades, stabilizers, fuselage, doors, cowling.

Rockets and Launch vehicles

Rocket motor cases, High-Temperature nozzles, Igniters, Nose cone, interstage structure, Equipment section, Aerodynamic fairings, Control Surfaces, Payload fairing and dispensers, Pressurized containers (fuel tanks latest research)

Sports

Tennis rackets, Golf balls, Surfing & Skating boards, canoes, Speed boats, climbing ropes, scuba diving tanks, race cars, baseball bats, skis, hockey sticks, Yachting rope, paddles, helmets and a lot more.

Automotive

Lightweight, Greater durability, corrosion, wear a& impact resistance. Drive shafts, fan blades and shrouds, interior panels, brake shoes, belts, and engine parts. Mirror & headlamp housings, radiator end caps, air filter housing, accelerating pedals, intake

manifolds, bumpers, fuel tanks. Motorcycle and automotive bodies, Bicycles, tire frames
Railway carriages, truck body.

Infrastructure

Skeletal structures, Walls and panels, Doors, Windows, Ladders, Staircases, Water
and chemical tanks, Cooling towers, Windmills, and turbines, Antenna dishes

Industrial

Drive shafts, Conveyer belts, Hoses and cables, Ropes, Tear and puncture
resistance fabrics, Mandrels, Rotor vanes

Medical

Wheelchairs, Crutches, Hip joints, Dentistry, Surgical Equipment's, Prosthetics
and Artificial limbs, X-ray tables, Composite bolts used in bones, Exoskeletons,
Biomedical implants

Military

Helmets, Bulletproof vests, Impact resistant vehicles, Portable bridges, Engine and
equipment foundations, Rudders, Hovercrafts

1.3 3D Printing (Additive Manufacturing)

3D printing in other terms Additive manufacturing is a process which adds material
to make components in successive patterns instead of removing material. It is an innovative
manufacturing method that uses a 3D printer which runs on three axis system X, Y & Z.
This is a technique where the material is deposited layer by layer then it is solidified to
form a complete part. This process is completely computer controlled. This manufacturing
process reduced the process time and labor, made the production of parts lot faster and

easier. Recent developments in this process made the possibility of printing of plastics, metallic powder, and the polymers.

Traditional manufacturing methods evolved over time from hand-based manufacturing to fully automated process, such as machining, casting, forming, molding. For numerous reasons this process poses unacceptable constraints like fixtures, expensive tooling, need for assembly of complex parts. Even though they are fully automated they demand substantive manufacturing which results in almost 90 percent of the original block material as waste. In contrast to this, the 3D printing process can create parts by adding material.

The entire 3D printing process from design to final product can be explained into three steps, Design, Slicing & Printing.

First a 3D CAD (Computer Aided Design) model of the required component is created by using any CAD software available. Then that model further processed through Slicer software which slices the CAD model into thin layers of about 0.01mm thickness and generates G Code which is readable by 3D printer. Then the 3D printer used this G code and prints the designed component layer by layer.

Advantages

Customization of components, Feasibility of manufacturing more efficient designs light, strong and less assembly required, one machine with multiple productions of parts, Minimal material wastage, Complex geometries can be made, Parts ranging from Nano size to very large size can be manufactured, Rapid prototyping can be possible, Manufacturing speed is high, Decentralization , Reduced costs of production

Disadvantages

Less Manufacturing jobs, Limited materials, Size of the parts manufactured, Copyright parts can be printed, Printing of dangerous material like weapons.

There are numerous 3D printing techniques developed in the past few years after introducing this technology. Every technique has its own benefits, limitations, requirements, processing speeds and timing. Some of the 3D printing technologies along with some specifications are explained below.

Several types of available 3D printing techniques are summarized with materials used in it in the following table

Process	Technology	Materials used
Material Extrusion	Fused Deposition Molding (FDM)	Thermoplastics (PLA, ABS) Eutectic metals, edible materials
Granular or powder bed	Direct Metal Laser Sintering (DMLS)	Any metal alloy
	Electron beam melting (EBM)	Titanium alloys
	Selective heat sintering (SHS)	Thermoplastic powder
	Selective laser sintering (SLS)	Thermoplastics, metal powders, ceramic powders

	Powder-based and inkjet head 3d printing, plaster-based 3D printing (PP)	Plaster
Laminated	Laminated object manufacturing (LOM)	Paper, metal foil, plastic film
Light polymerized	Stereolithography (SLA)	Photopolymer
	Digital light processing (DLP)	Liquid resin

Table 1.1: Types of 3D printing Technologies

1.4 Applications of 3D printing Technology

In the last decade, 3D printing has developed enough to replace all the crucial techniques until now used in many fields. It has the potential to be applied in the promising areas, mainly to say in the fields of manufacturing, medicine, industrial and lot more. Here quick points of the potential applications of 3D printing in these areas are specified.

Manufacturing field: Product development, Rapid manufacturing & prototyping, Mass customization & production, Jigs, and fixtures

Medical Applications: Surgical & Medical devices, Bio Printing, Pills

Industrial Applications: Apparel (3D printed clothing), Jewelry and art, Automotive industry, Construction, Firearms, Robots and computers

CHAPTER – 2

BACKGROUND AND TESTING FACILITIES

2.1 Background

Polymer materials are mainly used because of their processability, design flexibility, availability and more importantly lightweight. However, when compared to other material like metals these materials exhibit less suitable mechanical properties. One way to improve the properties of polymers is to add a high modulus reinforcement phase to make a polymer composite. This will give rise to a peculiar polymer structure which exhibits not only structural rigidity but also have an exceptional combination of the properties of both material phases in it.

Dr. Lifeng Wang (Wang, Lau, Thomas, & Boyce, 2011)^[1] is one of the researchers who worked on one of these peculiar polymer structures which is co-continuous polymer structure which have superiority of the properties compared to normal composites and the 3d printed materials. This newly proposed design has high energy absorption, stiffness, and strength. Generally, when composite material is subjected, there might be a possibility of cracks or defects formation inside the structure. Then under the continuous loading, the transfer of loading between the material phases is not possible, that results in the progression of the damage. But in the co-continuous polymer structures, made from materials which have completely different properties support each other, in certain stages the load transfer is a possibility in between the phases, which results in the restriction of crack or damage propagation by allowing the sample to provide more stiffness.

Now the major point of concern is that the mechanical response of these type of morphologies and the state of the structure after the investigation.

2.2 Purpose of the Thesis

Cellular material optimization for different loading conditions has enabled the development of the lattice structures, which is based on the repetition of the architecture of the unit cell. High-end applications of the materials included in the fields of aeronautics, medicine with the tradeoff between strength and stiffness which enabled the production of lightweight structures. Lattice structures provide the possibility of studying them as material on classical mechanics basis. Study over the lattice structures provides a basic understanding of the behavior as well as provides the necessary information on manipulating the properties in the macroscale structure of the material.

This thesis aims to achieve the full understanding of the material behavior in the form of co-continuous polymer structures, in order to customize and tailor make the products needed based on the requirement at hand. Here the analysis of the base level patterns is necessary to fully grasp the knowledge of the mechanical response of each sample in the form of a different design.

This investigation is done on three different types of lattice structures, these are simplest and most commonly found structures in materials. Simple Cubic (SC), Body-Centered Cubic (BCC) and lastly Face Centered Cubic (FCC). Generally, these lattice structures are mainly discussed in the basic chemistry as the Bravais lattices or crystal structures which are usually a cubical crystal system where the unit cell is in the shape of a cube. Here different types of these crystal structures are SC, BCC, and FCC. SC has a cubic void at the center with one atom at each corner. BCC has one atom at the center of the cube and with one at each corner. FCC has the atoms placed on each face of the cube

along with each one at the corner. Study on this lattice structure provides basic information about the change in local properties deformation and the damage.

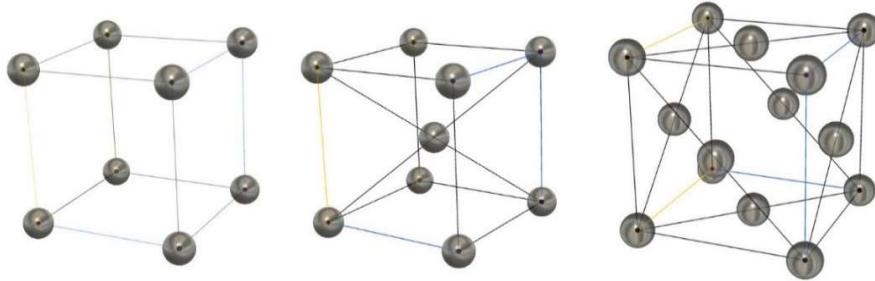


Fig 2.1: Lattice Structures SC, BCC, and FCC

The approach of this study is completely based on an experimental investigation in order to determine the mechanical behavior of the samples which are fabricated using 3D printing technique in a unique structure which is co-continuous structure using polymer materials in the form of lattice structures. Here the important thing to be noted that the mechanical testing is performed to gather the required information on the samples used.

Micro Tomographic method is a 3D imaging technique, which is used along with the mechanical testing of samples that reveals the behavior of the material like the progression of deformation in the structure of the sample internally. The non-uniform strain distribution within the struacts of a single cell, that is completely affected by the material phase inside of the sample. Here the stress distribution is not completely homogeneous because of the localized collapse mechanism or vice versa. Here in this sample where the transition between the two regions was smoother, this gives the concept of co-continuous composites.

Samples are fabricated using the Connex 500 printer. Detailed information on the properties of materials used for the sample printing is explained later in this chapter.

2.3 Sample Fabrication and Material properties

Samples that are used in this study are 3D printed using the Connex500, which is a multi-material 3D printer. Two different polymer materials are used to print these samples. VeroWhite an acrylic based glassy polymer and Tango plus a hyperelastic material simply elastomer. These two materials are used to print the samples in the shape of lattice structures, namely Simple cubic (SC), Body-centered Cubic (BCC) and Face-centered Cubic (FCC). These lattice structures are in the form of cubes. All these samples are in the form of a cube with dimensions of 15mm X 15mm X 15mm

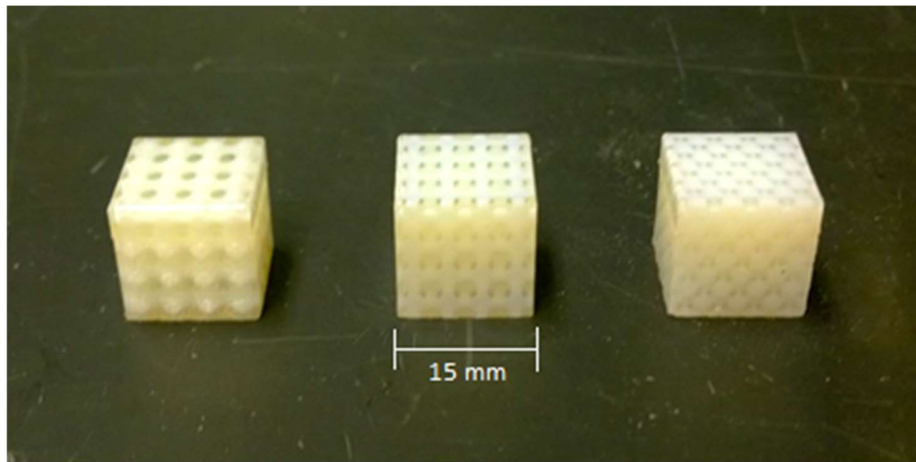


Fig2.2: Samples used for testing

2.3.1 Materials and their properties

VeroWhite is also known as a Polyjet material because this is widely used in the Polyjet 3d printing machines. This material is opaque with high resolution, gives a smooth surface finish of the parts.

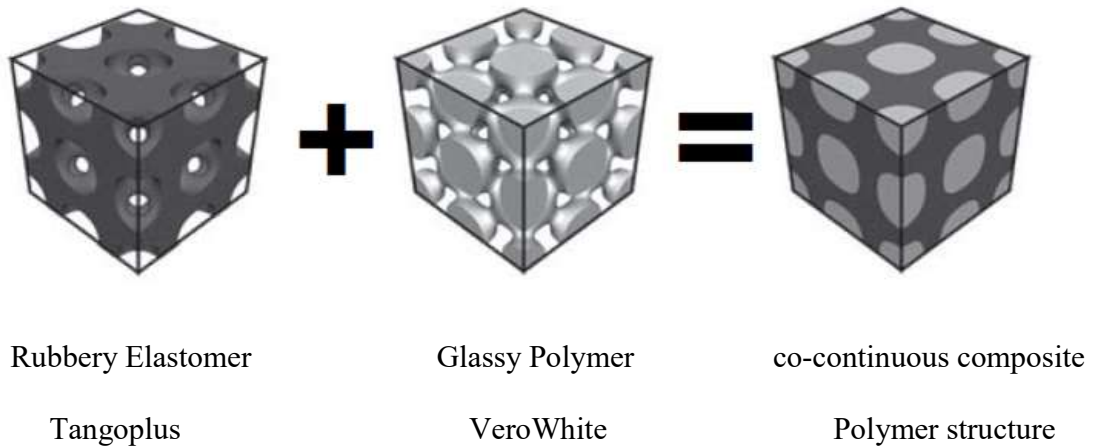


Fig 2.3: Morphology of the sample

Some of the mechanical properties of this material are sated below

Tensile Strength	50 MPa
Modulus of elasticity	2.5 GPa
Percentage of elongation at break	10 to 25
Flexural strength	93 MPa
Density	1174 kg/m ³
Impact strength (notched)	24 J/m

Table 2.1: VeroWhite Material properties

“All this data is taken from the manufacturer documentation for this material”.

Benefits of using this material are it is opaque and have high detail on final parts. This material is rigid and durable, also great for molds and patterns. Also widely used in the presentation models.

Tangoplus is one of the tango materials which are known for their hyperelastic nature. This material is well suited to be used in the Polyjet printing machine. Tangoplus is a clear and translucent material, this comes in a variety of colors like grey and black. This material is well suited in the applications of damping, making gaskets, overmolds, etc. Some of the mechanical properties of this material are as stated below.

Tensile Strength	1.45 GPa
Tensile tear resistance	20 lb/in
Percentage of elongation at break	218
Modulus of elasticity 20% strain	0.1 MPa
Density	1141 kg/m ³
Shear modulus	0.213 MPa

Table 2.2: Tango Plus Material properties

“All this data is taken from the manufacturer documentation for this material”

Benefits of using this material are to simulate rubber parts, bumpers, and buttons. Parts made using this material have high resolution, perfect for testing because this material has excellent flex memory and allows the shortening of product design life cycle.

When we talk about materials, we must discuss the properties of them like elasticity, plasticity and other properties exhibited by the material under loading conditions. Here various properties are discussed which are exhibited by the materials used for making the samples for this study.

First, VeroWhite which is a glassy polymer exhibits properties like elasticity, plasticity before failure. Mainly this material is considered to be viscoelastic material.

Elasticity means the tendency of a material to return to its original shape without undergoing any permanent deformation under marginal allowed loading. When the forces are removed the material will return to its original shape or state.

Plasticity, means, the permanent deformation of the material once it crossed its elastic limit. After removal of load also the material does not return to its original state.

Numerous polymers which appear to be solid shows behavior between those of liquids and solids under stress, they also show continuous liquid like deformation while under loading condition, this deformation tends to change the structure. These materials are often termed as Viscoplastic materials

Second, Tango plus is a rubbery polymer behaves as hyperelastic material. This material has very little plastic region compared to the glassy polymer.

Hyperelasticity of a material can also be said as the material having very high elastic nature compared to normal elastic materials. As tested, this material has high flex memory which enables it to return to its original shape in a certain time span, say almost immediately after removal of load without showing any traces of permanent deformation.

2.4 Laboratory Equipment

For the testing purpose of the samples, two different types of equipment available in the laboratory are used. One is for testing of samples and another one is for scanning of the tested samples.

2.4.1 MTS Machine

Electromechanical loading system by MTS is used for the testing of samples. This machine can apply about 10KN of loading. It can be used to study the fatigue analysis of samples along with pure tension and compression tests. It can apply to load on the sample and record the values of stress, strain, percentage of compression as well as the displacement or deformation of the sample. The only tradeoff to get these values is to give proper dimensions of the sample into the software.

This machine applies Electromechanical loading on the sample. It has loading lever which is attached to the crosshead that moves vertically up and down to apply tension and compressive loading. Two vertical stands like structures on the machine have screw heads which control the motion of the crosshead. The following picture shows the MTS system used for testing the samples for this study.



Fig 2.4: MTS Machine (Electromechanical Loading system) used for testing

Here in response to the given inputs into the software, the testing is performed on the samples. Here, Test works are the controlling software used to operate the machine as well as to test the samples. This software is provided along with the machine.

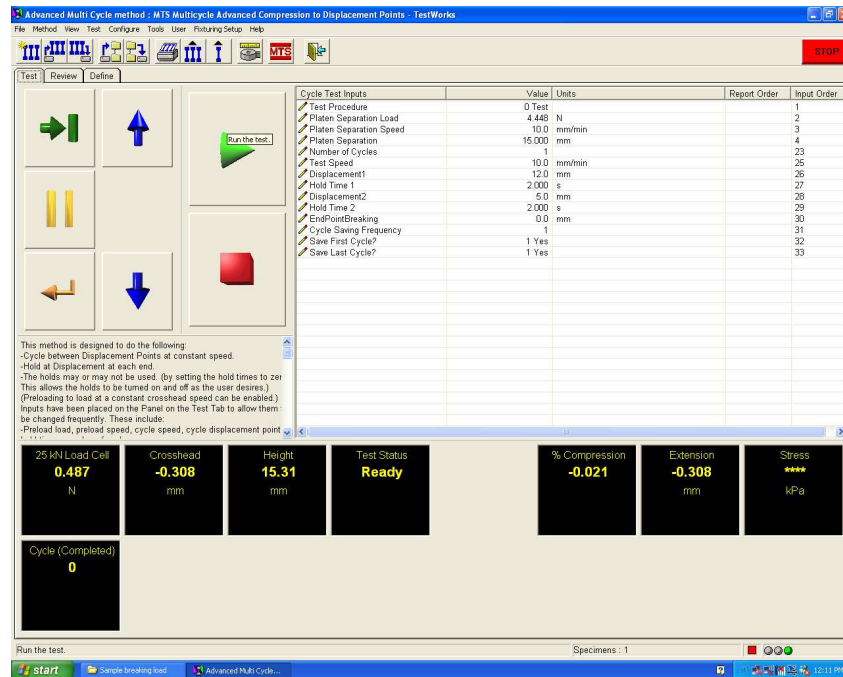


Fig 2.5: Testworks software input window

Here in this software, all the required parameters are given as inputs. Like sample dimensions, test speed which was chosen to be 5mm/min based on the trial testing on the samples, displacement limits, and one important input is the hold time after reaching the intended displacement, this is given to stabilize the stress values inside the sample after reaching the limited displacement point without giving any noise in the output data. In this panel, the dials at that bottom indicate Load in kN, Crosshead position, these values are set to zero or can say adjusted to zero before testing is started. Then all the other values are cross-checked before testing is initiated.

2.4.2 Micro CT machine

Hereafter the testing's are done using MTS machine, samples immediately transferred into the Micro CT machine which used x-ray as an energy source to scan the sample and give the detailed information about the sample in 3D model with all the internal features. Here this x-ray tomography machine produces 2D shadow images of the complete 3D internal structure of the sample which is scanned without sample preparation or chemical fixation.

The process of operating this machine to scan the sample explained later in this chapter.



Fig 2.6: Micro CT machine

This machine is manufactured and distributed by Bruker. The sample is held onto the sample holder. The problem is that the sample holder absorbs the x-rays, so the sample must be placed above the holder. For that a special type of clay is used to make the sample stick to the sample holder, the only problem is that the clay absorbs the x-rays in the process of scanning, so to avoid the loss of features of the sample in contact with the clay, a layer of thermocol is placed in between the clay and sample, then a thin plastic film is wrapped around it to hold sample firmly. After all these steps are done sample is placed inside the

machine. Skyscan is the controlling software used to operate, scan and generate the results in this machine.

2.4.2.1 Micro CT machine Scanning procedure

Micro CT imaging process gives the detailed imaging of the internal structure of the specimen without damaging it. This process is done in four steps, scanning, reconstruction, visualization and animation. The machine is capable of HD, 2K, 3K, and 4K scanning to give high-quality images and videos as explained earlier. But the time consumption to complete the process is very high.

Here, the collected samples were carefully placed onto the sample holder and then in the machine by following the proper procedure for the safety of the equipment because the hardware and the sensors in the machine are complex and too fragile. Once the initial process is done the moved onto the next step of setting up the scanning parameters in the software. Step by step process of complete scanning procedure is as follows.

First, an x-ray is warmed up which usually takes about 15 min. Then the screen capture option is turned on so that the camera inside the staging area captures the sample that can be seen on the screen. Now Sample is set onto the screen then checked for rotation to make sure that the sample is at the exact center. After that zoom in of the sample is checked. If the sample is overly zoomed in, the sensors might collide with the sample while scanning. Now the resolution is selected, and also appropriate filter is selected to energize the x-rays to get highly detailed images after scanning. But for the materials I am using for scanning filter is not needed. Once this step is done sample is moved down so that there is nothing showing up on the screen. Now for the next step, flatfield correction is turned off and intensity is checked by right clicking mouse on the screen. Average value chowing

must be in between 58 to 62. If not, this can be adjusted using scanning modes option in the options menu. After getting intended value flatfield modes are turned on then updated into the software. Once the update is done with the latest settings, flatfield correction is turned on. This time average intensity value must be in between 86 to 90. It will show a close value to 88. Then after this moving onto the final step in the scanning process is initiating the scan itself. After selecting the option, it will ask to save the file and select the directory to save it. Then we must select the average rotation speed, which determines the rotation of the sample to get the highest possible resolution images as output. Once all the settings are given, then scanning is initiated. On an average, the scanning process is dependent on rotation speed, as lower the rotation speed, the longer it takes to scan the sample. For the value i used, scanning took about 8 to 10 hours for each sample. The same value is used for all the samples. Once the scanning is done then proceeded to the next step which is Reconstruction.

The scanning process produces images with some irregularities like misalignment of the layers scanned, rings on the images because of the minor irregularities in the layers of the sample. By using the reconstruction step these errors are corrected. Once done with all these steps, reconstruction is initiated, which reconstructs the whole sample by applying all these corrections to all the layers. usually, this process takes about 4 to 6 hours depending on the scanning resolution. Once this step is done then moved onto the third step which is visualization. Images produced by the reconstruction step are stacked in this step and the 3D model of the sample can be formed. Or in the simple file used to make the 3D model of the sample. This step usually takes about 1 to 2 hours. Then lastly moved onto

the animation step where we can combine the files and see the 3D configuration of the sample scanned.

In the final step, which is Animation, files generated by visualization are loaded, the software stocks every file in a sequence and generated a perfect 3D model of the sample. We can adjust color and opacity to make the features more noticeable. This process usually takes about 25 to 40 min of time to complete. The complete scanning process takes about 48 to 56 hours, which completely depend on the resolution of the images which we choose to get as output for each sample.

By understanding the full functionality and procedure to operate these specific machines, the experimental design to perform the testing is carried on.

CHAPTER – 3

DESIGN OF EXPERIMENTAL PROCESS

To study the behavior of the samples, the mechanical analysis must be done. To observe the nature of the sample under loading conditions, two different types of testing processes were assumed. The detailed explanation of the processes is given further in this chapter. The laboratory equipment explained in the earlier chapter is used for the testing of the samples and to acquire detailed imaging to visualize the internal structure.

3.1 Experimental Design

In general, variation in the behavior of these samples might be observed under the conditions they put up to. Here three samples have different morphologies, so common understanding is that the change in the structure and the response they give for different testing's will be variant. To get full information on the behavior of the samples, the testing process is divided into two modules. One to get the general idea of how it is reacts to the test and then using the results acquired from the testing as inputs for final testing of the sample. Then the final stage is imaging. The process followed for this analysis is completely sequential.

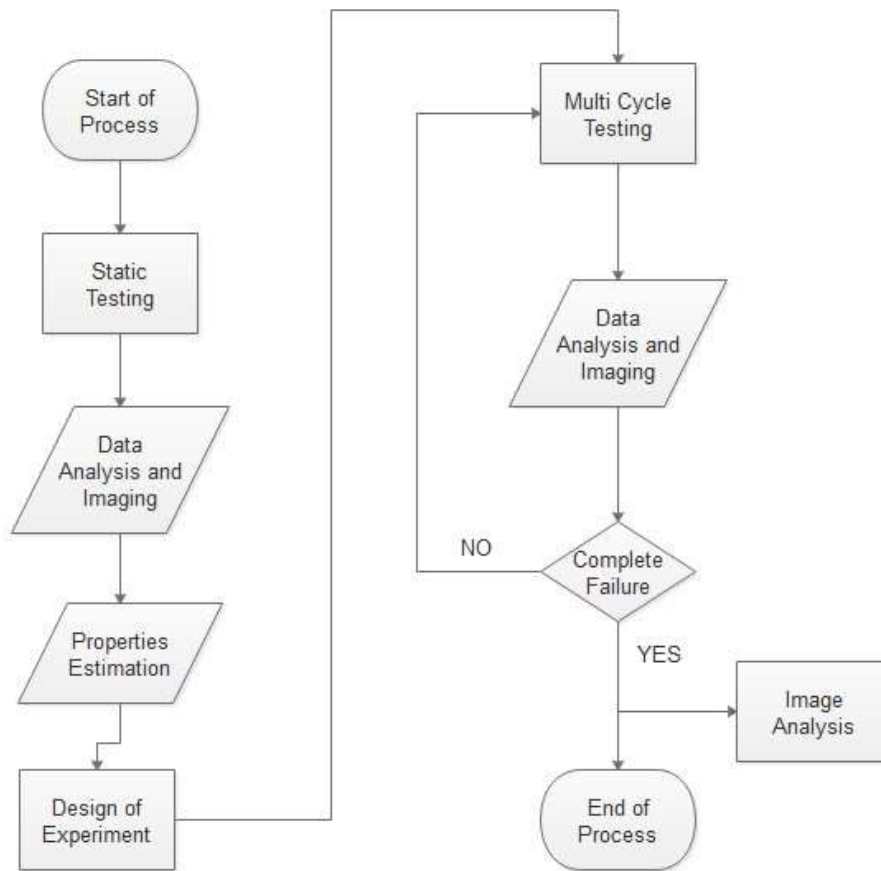


Fig 3.1: Flowchart showing Complete experimental procedure

3.2 Static Analysis Process

The testing process is carefully designed so that the data gathered from it is accurate. Here the first static analysis is performed on the sample by giving necessary inputs into networks software.

Samples were measured for the dimensions that must be given as one of the inputs in the software. Here to test the samples Testworls4 is used, which is controlling software of the MTS machine used. Here for the initial test, sample holder distance on the machine is adjusted to that of the sample size, then given the inputs as stated below.

Test Procedure	0
Platen separation load	4.448 N
Platen separation speed	10 mm/min
Platen separation & Sample Height	15mm
Number of cycles	1
Test speed	10mm/ min
Displacement 1	12mm
Hold time	2 sec
Displacement 2	5 mm
Hold time	2 sec
Endpoint breaking	0
Cycle saving frequency	1
Save the first cycle	yes
Save the last cycle	yes

Table 3.1: Static analysis input parameters into test works software

Here predefined process for the compression testing is already recorded in the software. Based on the sample dimensions and the output requirements the steps in this process are slightly modified to fit the need. The complete process is tailored down to the steps shown above. In the process, the test procedure is the constant number given in the

software to recognize the saved testing process. Platen separation load is also the initial load for the software to counter the weight of the loading lever and the support structure. Test speed is controlled by giving the input to test speed. Then the displacement 1 and 2 are the limits given for the loading anvil to move. Here for the static loading purpose only displacement 1 taken into consideration. Hold time is the amount of time the anvil rest after reaching the intended displacement. Here frequency is set to 1. Last commands are given to save the cycles and the data recorded during testing.

Since here the testing on the samples are done for measuring the sample braking load and deformation, data is collected slowly until the sample is completely crushed. Here in this testing, we can observe the change in structure based on the data acquired. Like the start of breaking point, stages of breaking of samples. The important observation is, completely different behavior shown by these three samples.

Here properties of the sample like stress and strain are calculated using formulae

$$\sigma = \frac{\text{Load}}{\text{Cross Seccional Area}} \dots\dots\dots(1)$$

$$\varepsilon = \frac{\delta l}{l} \dots\dots\dots(2)$$

Experimental load over cross-sectional area of the sample gives Stress value, then the change in length or deformation in the sample to the original length gives strain values.

Structural sustainability and integrity might depend on the deformations inside and on the stress induced because of loading. So static analysis alone is not sufficient, so a different method is opted to test these parameters.

3.3 Multicycle Analysis Process

The process to test the samples under multiple cycles to see how the sample reacts is carried out by using the results got from the static analysis. The main points considered are breaking displacement. Here the breaking displacement is considered, where the sample transitions into the plastic region from the elastic region. Here these values are different for these three samples. Now, the strain is calculated based on the deformation values gathered then the 90 percent of that strain value is considered as the input for the next stage. Simple, 90 percent of the deformation value at first yield point is considered, the reason is to keep the sample in elastic region while testing.

While performing the trial testing on the sample the hold time on the sample is tested, for zero seconds of the hold time, the stress value seemed to be a bit considerate, to avoid that and to visualize the stress stabilization at that maximum point, hold time of 1sec given for loading and unloading limits. Then comes the main point where this testing is performed by assuming two different criteria, a low multicycle analysis which is for 50 cycles and high multicycle analysis which is for 500 cycles. After performing the 50 cycles on each sample it is observed from the images that the damage inside the sample is not initiated which doesn't help to record the behavior of the sample, so 500 cycles are opted by allowing the sample to rest between the testing's to observe the sample relaxation. The process is completely identical to static analysis with minor changes in it as stated below.

Test Procedure	0
Platen separation load	4.448 N
Platen separation speed	10 mm/min

Platen separation & Sample Height	15mm
Number of cycles	50 or 500
Test speed	5 mm/ min
Displacement 1	90 Percent of deformation at first yield point
Hold time	1 sec
Displacement 2	0.2 mm
Hold time	1 sec
Endpoint breaking	0
Cycle saving frequency	1
Save the first cycle	yes
Save the last cycle	yes

Table 3.2: Multicycle analysis input parameters into test works software

Here for two criteria of this module, all other inputs are the same except a number of cycles. Test speed is chosen to be 5 mm/min after observing the minimal change of stress values for the test speeds of 5mm/min and more. After fully understanding the processes in the software, necessary inputs are given and testing on the samples is carried out by gathering the data. Necessary values are analyzed using proprietary software and plotted. For the final step, imaging is carried out on the samples immediately after the testing is done. Acquired the imaging data and presented all these results in the later chapters.

CHAPTER – 4

STATIC ANALYSIS RESULTS

A testing process designed in the previous chapters was followed and completed. This testing is purely compressive. The sample is small, so custom platens to hold the sample on the MTS machine is not designed. The sample is placed onto the machine as shown below.

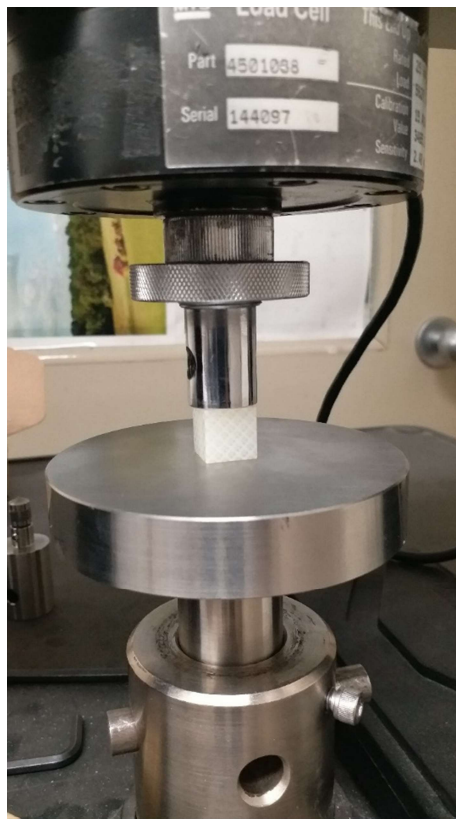


Fig 4.1: Sample placement on MTS machine for testing

Loading is applied to the sample and continued until the point where the sample started to fall apart, observed the variations in the data displayed on the computer screen. Terminated the process when sample is almost crushed. Then the imaging process is initiated to record the structure of the sample after testing.

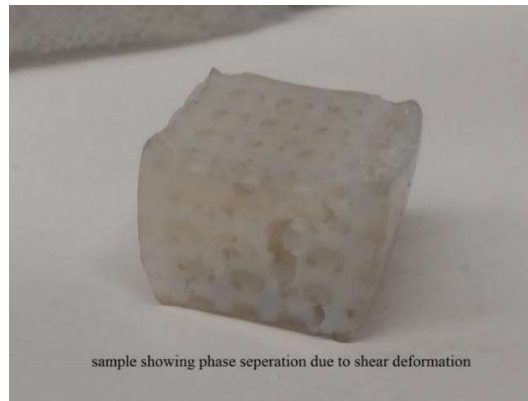


Fig 4.2: BCC structures after testing



Fig 4.3: FCC structures after testing



Fig 4.4: SC structures after testing

Detailed explanation about the behavior of the samples given later in the chapter.

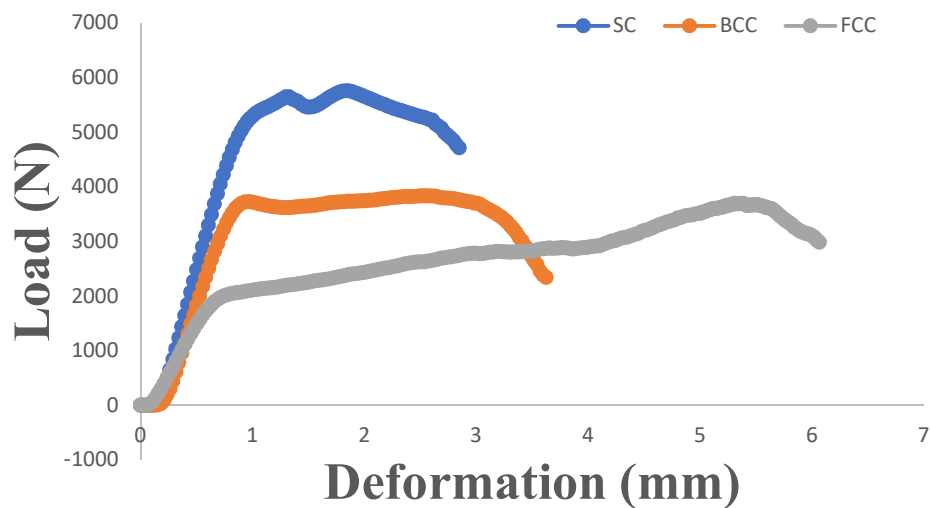
The results from the testing gave the information like the peak load of the samples at the break, peak height along with the percentage of compression at each displacement point recorded.

4.1 Data Analysis and Results discussion

The present analysis is involved in the inspection of the behavior of the samples under the static loading. Here the data is collected after the testing and sorted out for the required values and generated the plots showing the variation of required quantities.

4.1.1 Load vs Deformation

Applied load on the samples resulted in the deformation and finally failure of the sample. Different morphologies of these samples show variations in the behavior under loading.



Plot 4.1: Load vs Deformation plot for all samples

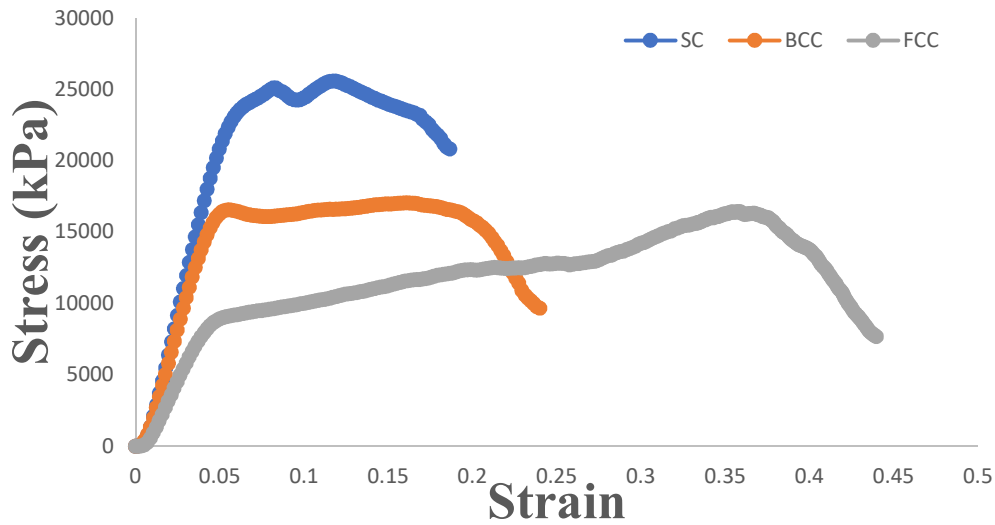
It is noticeable that the SC sample is showing high response to the loading compared to other samples. Here transition of SC sample from elastic deformation to

plastic deformation happened at 1.29 mm of deformation under loading of 5756.4 N of loading. But for BCC this transition started earlier at 0.955mm at a load of 3728.29 N, even after this transition sample continued to show response to applying load until the point where the load on the sample reached 3836.41 N while showing the deformation of 2.55 mm where it is considered the complete crushing load of the sample. For FCC sample transition point is at the deformation of 0.85 mm at the loading of 2059 N, same as BCC this sample also showed response until it reached the load of 3673 N with deformation of 5.5mm this point is considered as complete crushing load.

The area under load vs displacement curve represents the amount of energy absorbed while testing of the sample. The simple cubic sample shows the highest energy absorption capability out of all three samples. Glassy polymer inside the SC sample is axially oriented in the loading direction, this type of arrangement supports the compressive loading, so this might be the reason for SC sample to provide such higher energy absorption. Unlike SC, loading carried inside FCC and BCC structure may be due to bending or shear deformation due to which it shows lower energy absorption.

4.1.2 Stress vs Strain

From the testing data, stress and strain values were extracted, calculated and plotted to show the response of the samples under compressive loading.



Plot 4.2: Stress vs Strain plot for all samples

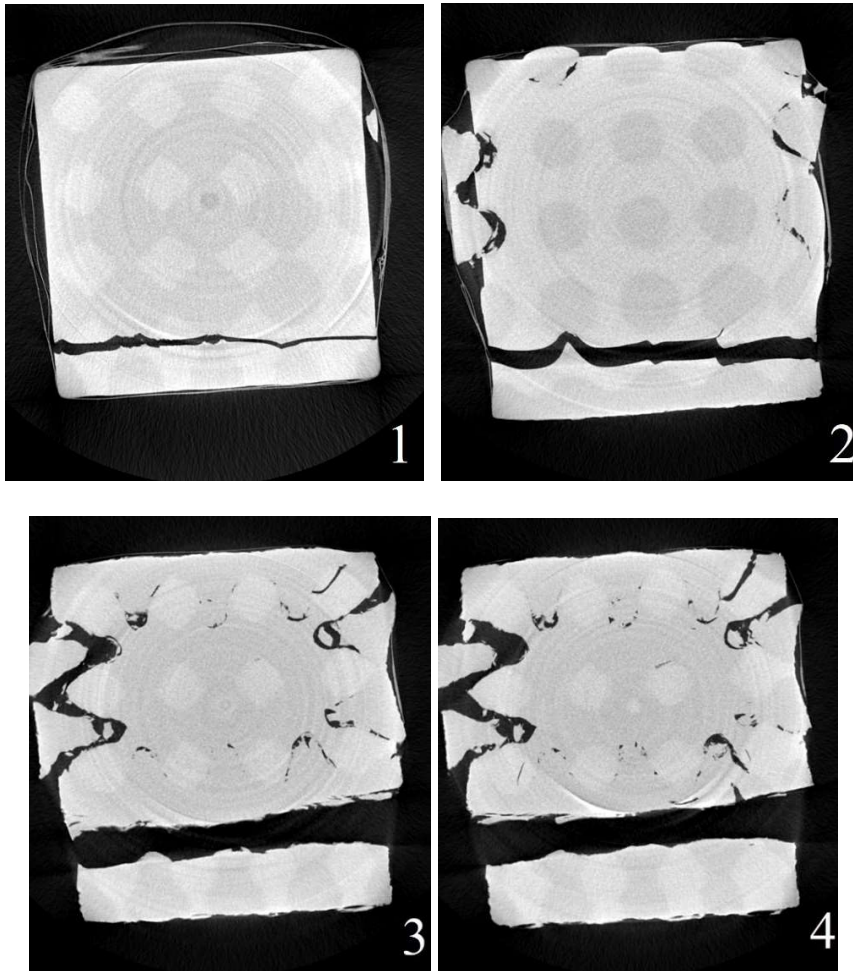
This figure shows the mechanical response of the glassy polymer/elastomer co-continuous structure under compressive loading in terms of stress and strain. From the curves, we can see the yielding points and the strain hardening. For simple cubic there is minimum strain hardening phase then failure after the second yielding point, for BCC after the first yielding point it has longer strain hardening phase, this might be due to the shear forces acting in the sample due to loading. Lastly, for FCC sample the strain hardening phase is largest comparatively of SC and BCC. This might be due to the closely packed material phase involved in sharing the incoming load throughout the structure. Even though it has the largest strain hardening state, this sample also damaged through shear deformation just as BCC but unlike to SC which is broke because of the buckling in the plastic phase.

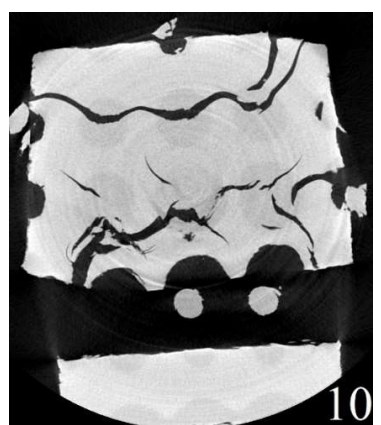
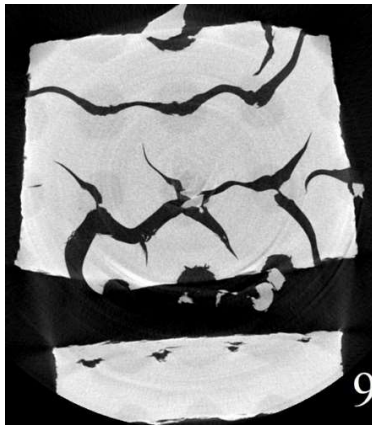
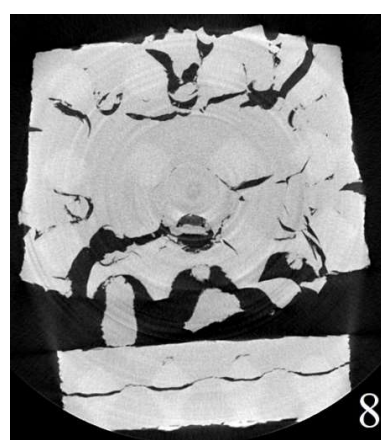
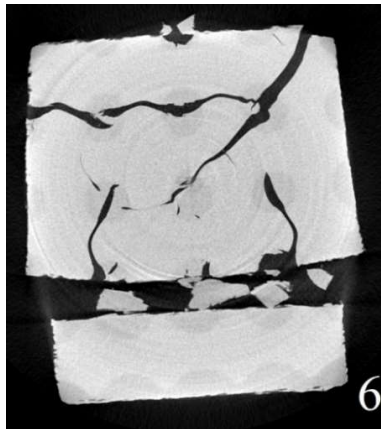
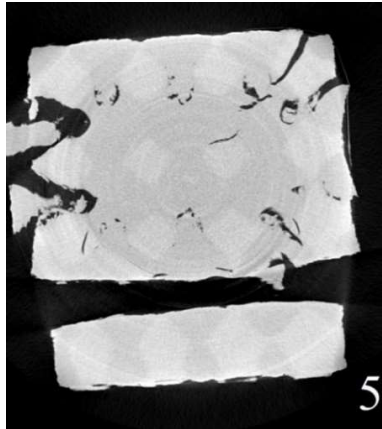
The area under this curve represents the energy absorbed before breaking which gives modulus of toughness. So, in the same as load-displacement curve, here simple cubic

showing highest toughness modulus compared to other samples probably because of the same reasons stated above.

4.2 Microtomography Images and Discussion

Images are gathered after static analysis to visualize the damage pattern inside due to compressive loading.





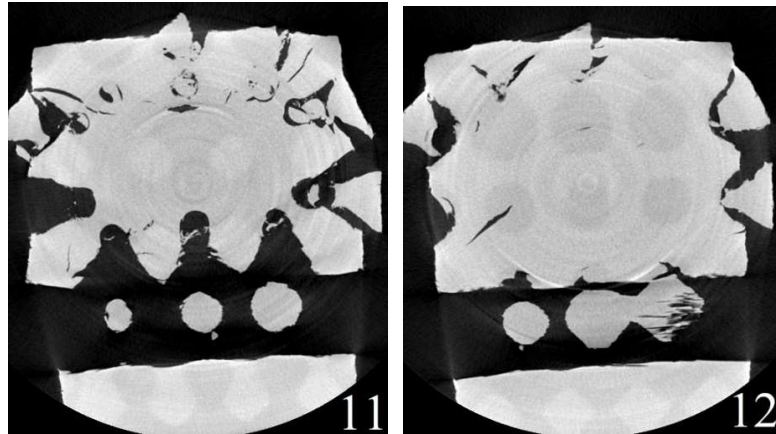
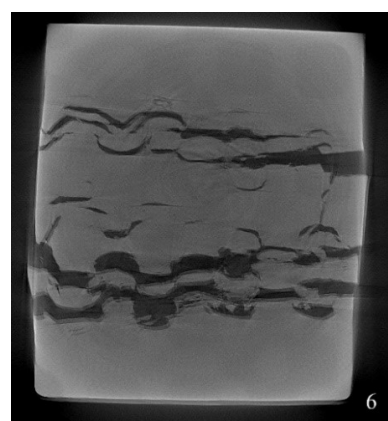
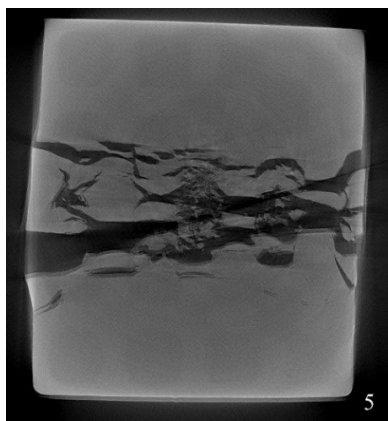
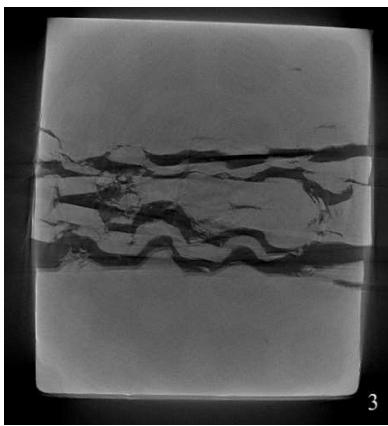
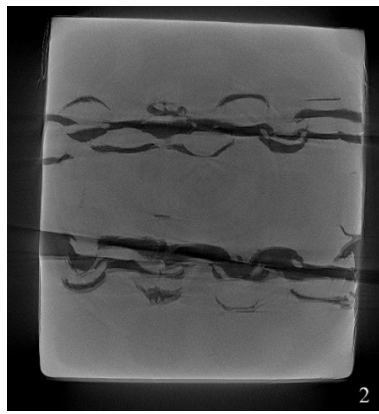
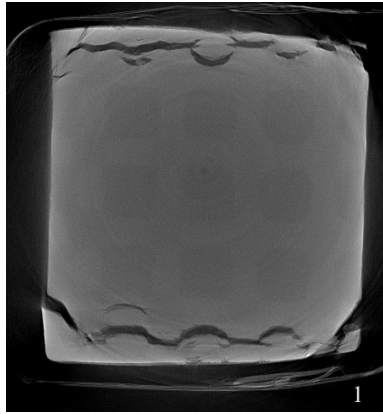


Fig 4.5: Microtomography images of SC sample

Here each image with the number on it shows the damage in different layers in the sample from the top surface to the bottom surface, light grey color represents Plastic phase in the material which is VeroWhite and the dark grey color represents elastomer phase which is Tangoplus. From these images, it is evident that damage inside the sample is catastrophic since the sample is tested till it is completely fallen apart. Here from image 1 is closer to the layer on which load is applied and the breaking in the sample started there, as the continued, images 2, 3, 4 shows the signs of heavy damage inside not only on single location but damage in multiple locations on the same layer. Now from images 5 to 8, the damage increased and the separation between phases happened completely with small strands of material in between, from last four images, the sample almost in two pieces as there is no linking strands in between. This mainly happened due to the buckling of the plastic phase as it is aligned in the same axis as loading. So purely compression resulted in the plastic phase to completely fail and separate the sample.



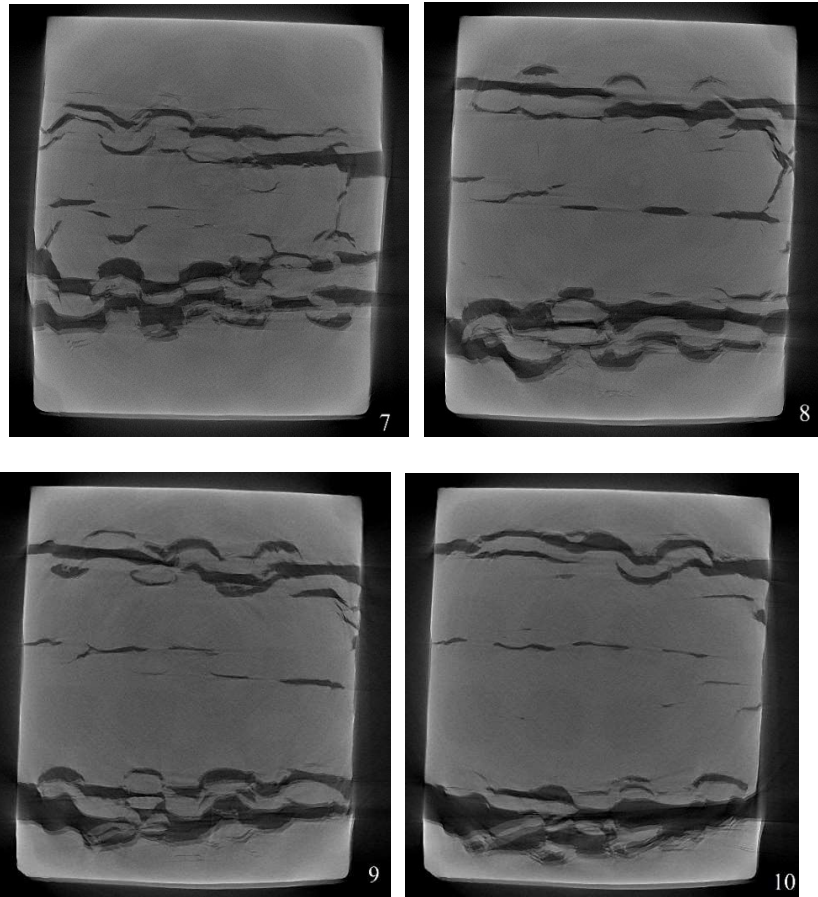
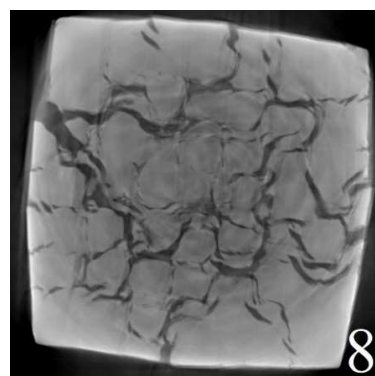
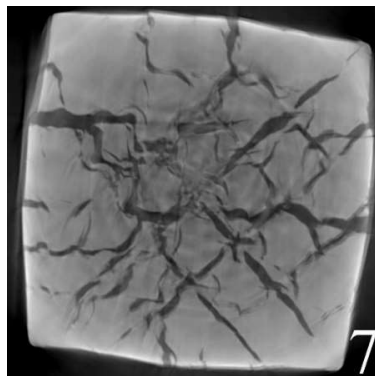
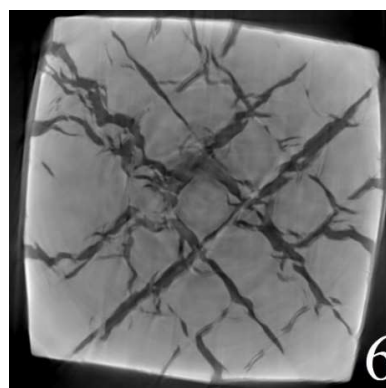
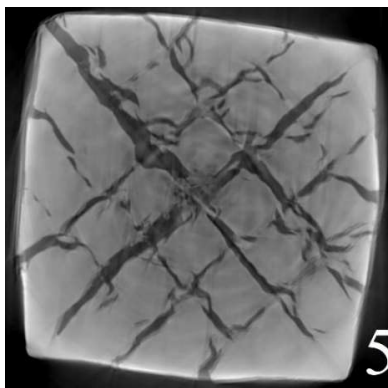
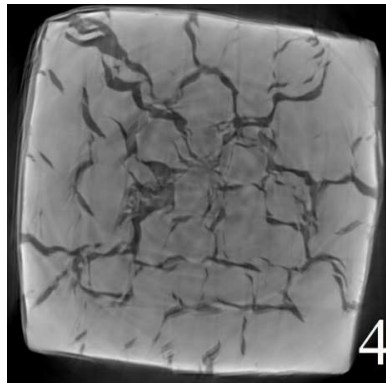
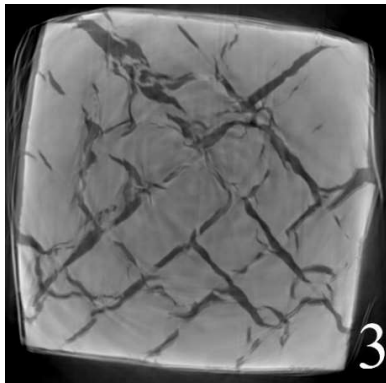
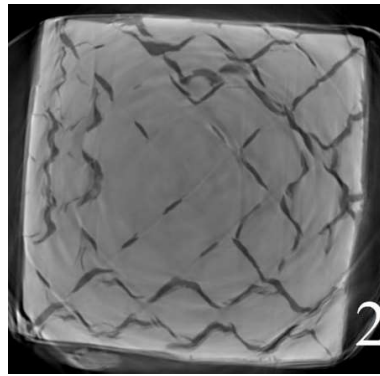
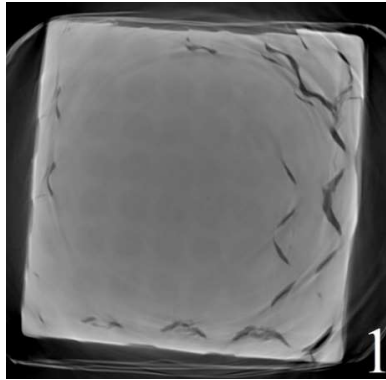


Fig 4.6: Microtomography images of BCC sample

From the top layer, the damage almost started near the edges of the sample. from the images 1 to 4, the damage seems to be moving closer towards the center and from images 5 to 10 the damage is spreading towards the corners that indicated the damage is not in the axis of loading. From these images, we can say that the damage inside the sample is almost angular to the loading axis which states that the deformation in the sample is purely shear.



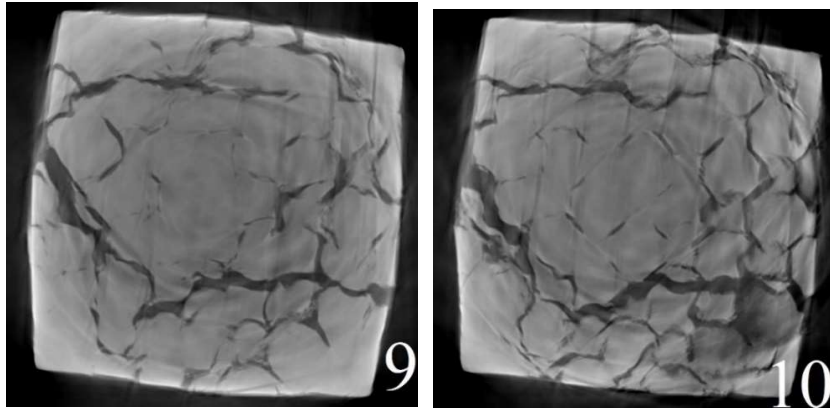


Fig 4.7: Microtomography images of FCC sample

From the images 1 to 4 it is observed that the damage initiated near the edges and slowly progressed towards the center, but the damage is consistent, unlike SC and BCC in which damage is in random locations. From the rest of the images, the damage inside the sample continues to spread almost in evenly and the break patterns appear that separated the phases inside the sample which are closely packed compared to BCC and SC. This morphology of FCC sample resulted in the sharing of incoming load in between the strands of plastic phase, that gave out drastic failure all over the sample, this might result in giving the superior stress values than BCC whose structure is not as densely packed as FCC. It is also clear that this sample also underwent purely shear deformation because of the loading applied to it.

Here the damage mechanism in the samples are understood and the necessary values are gathered. So, this investigation can be moved to the next step.

CHAPTER – 5

MULTICYCLE ANALYSIS RESULTS

As explained in earlier chapters, to understand the behavior of the samples from mechanical testing, static analysis is not enough so the multicyclic procedure is designed and samples are tested. Results gathered from the static analysis, mainly deformation is taken into consideration for multicycle analysis by altering the number of cycles.

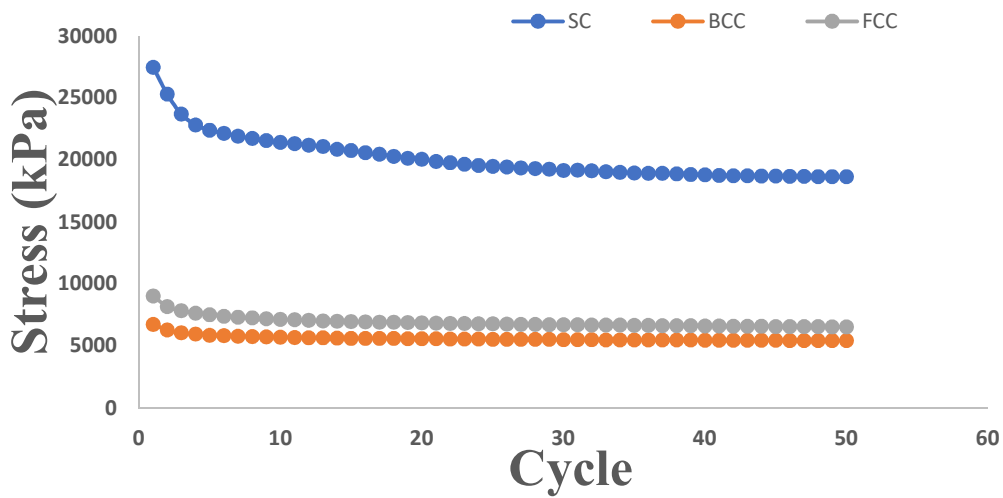
5.1 Data analysis and Results for 50 cycles

First, the testing is performed for 50 cycles to generate information about the behavior of samples. Data gathered from the testing, extracted and calculated the necessary values then plotted.

5.1.1 Stress vs Number of cycles

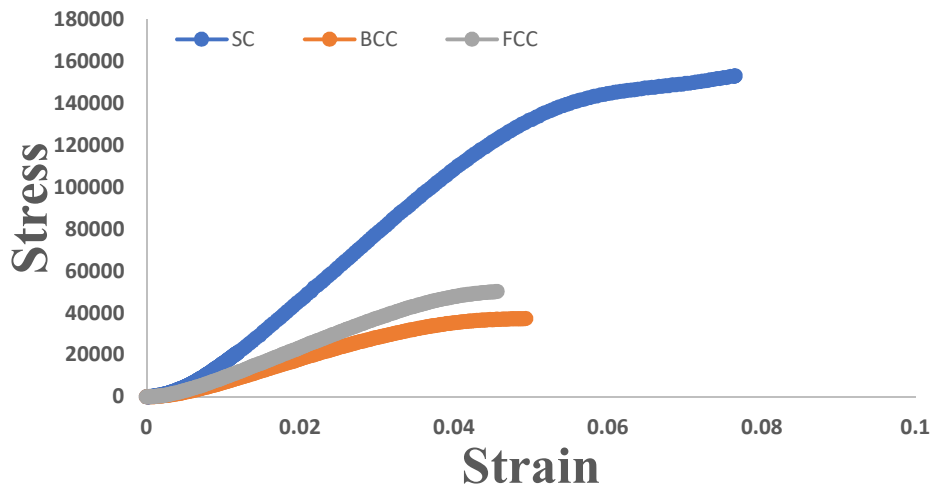
Here, the SN curve is plotted for the values gathered from testing, for all the samples. Multicycle testing is performed, so that the variations in the stress is observed while testing.

Form the plot below it is observed that the samples are showing the sudden decline in stress in the initial stages of cyclic loading this might be because of the plastic deformation in the sample, then the stress levels are linearly declining because of the elastic phase in the sample which restricts the plastic phase inside of the sample. FCC sample shows higher stress levels than BCC because of the load distribution inside the sample through the phases is not same and the reason is that these two samples undergo shear deformation under loading and the energy absorbed during loading is completely different depending on the microstructure of the sample.



Plot 5.1: SN plot for 50 Cycles

5.1.2 Stress vs Strain



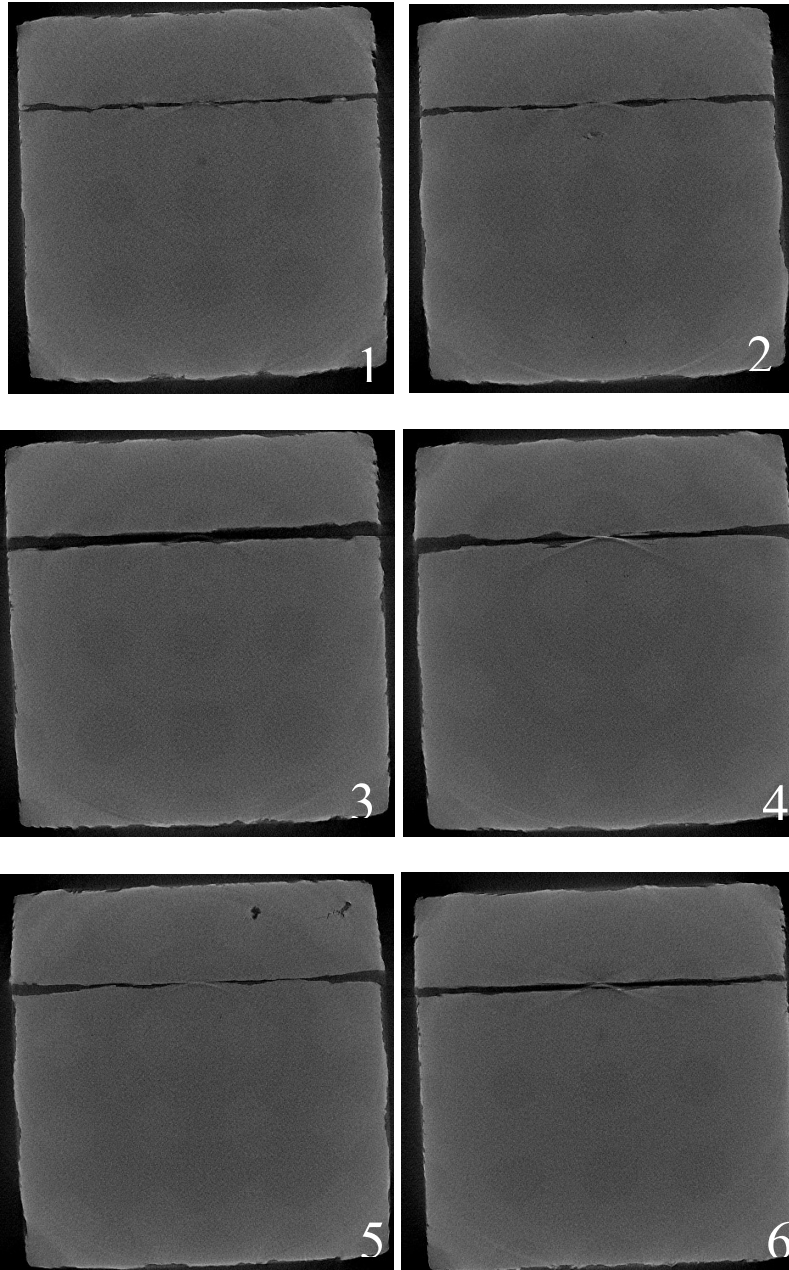
Plot 5.2: Stress-Strain plot for 50 cycles

From the Stress strain plot for the samples under 50 cycles, it is observed that the SC sample showing the maximum response to load when compared to other samples BCC and FCC. The area under the stress-strain curve shows the modulus of toughness, so from the plot, it is evident that SC sample providing the highest toughness. Even though the

energy absorption for the other samples is less compared to SC they also show fair toughness.

5.1.3 Imaging of samples

Samples are scanned for the traces of damage due to low cyclic loading



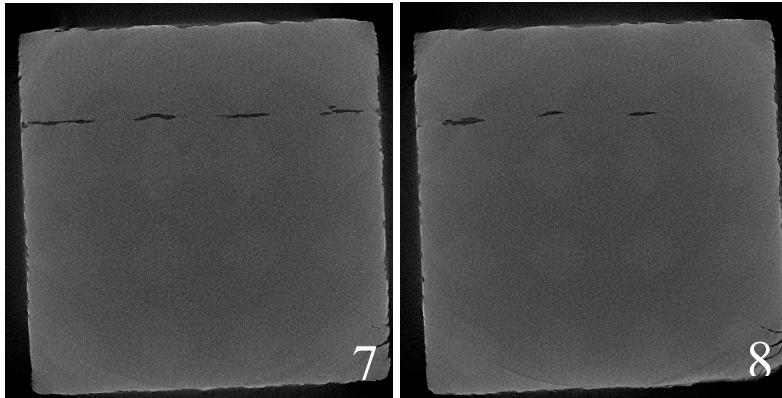
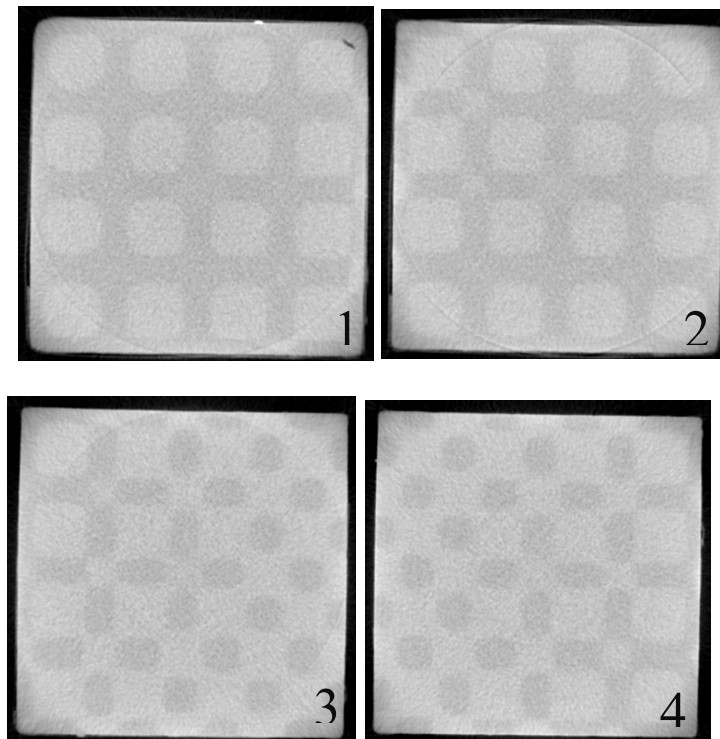


Fig 5.1: 3D scanning images of SC sample for 50 cycles

From the above images, images 1 to 8 shows signs of damage inflicted because of the low cyclic loading, that is different layers of the sample, from top surface to the bottom surface in random locations.



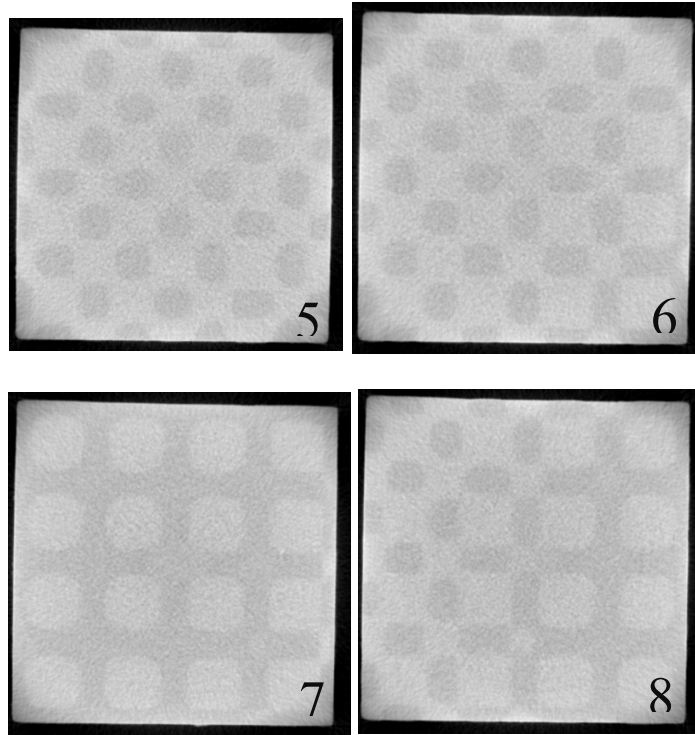
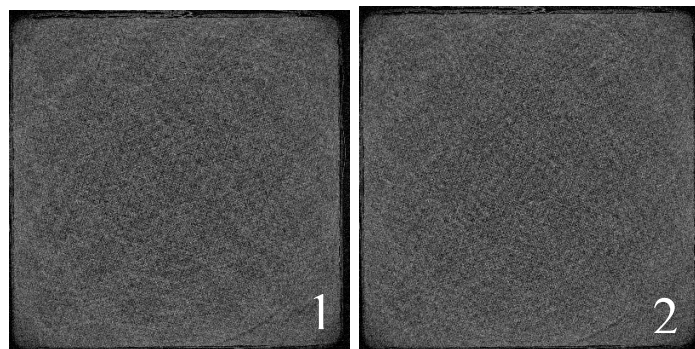


Fig 5.2: 3D scanning images of BCC sample for 50 cycles

For BCC sample, the imaging results show no sign of damage initiation. Images 1, to 8 taken from different locations on the sample, it is observed that the sample is fine without any damage.



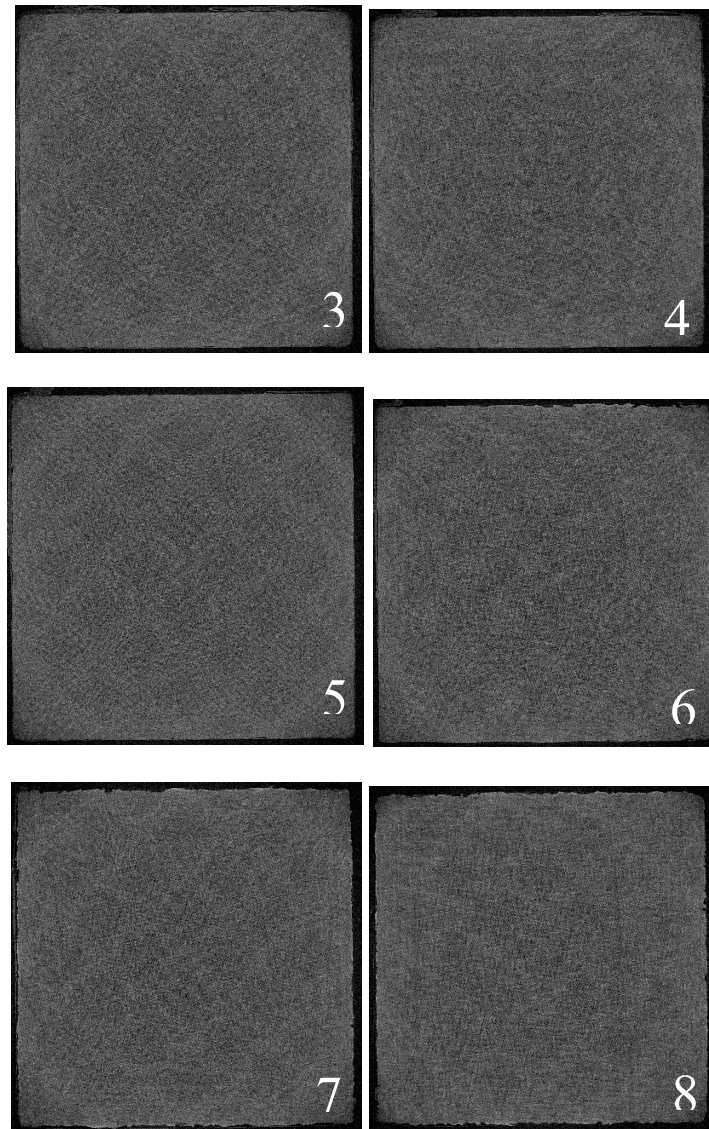


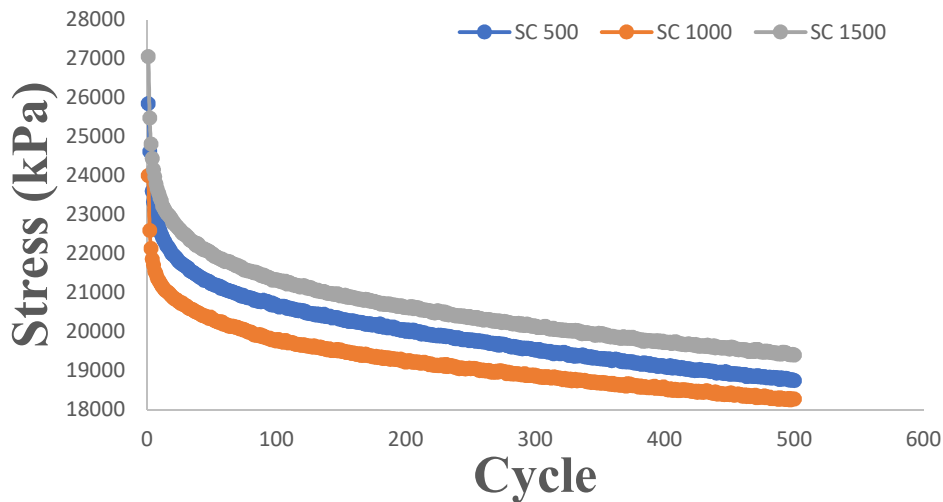
Fig 5.3: 3D scanning images of FCC sample for 50 cycles

For FCC sample It's the same case as BCC there are no signs of damage to be seen in the imaging.

Unlike SC in which there is damage but minimal, BCC and FCC samples did not show any damage for 50 cycles testing.

5.2 Data analysis and Results for 500 cycles for SC sample

Once all the necessary calculations and results are gathered for the 50 cycles testing, it was clear that the behavior of the samples is not clear enough to understand. So, the testing process is altered to perform high cyclic loading to perform a proper analysis. Testing for 500 cycles is performed and data is gathered for analysis.



Plot 5.3: SN plot of SC sample for 500 to 1500 cycles

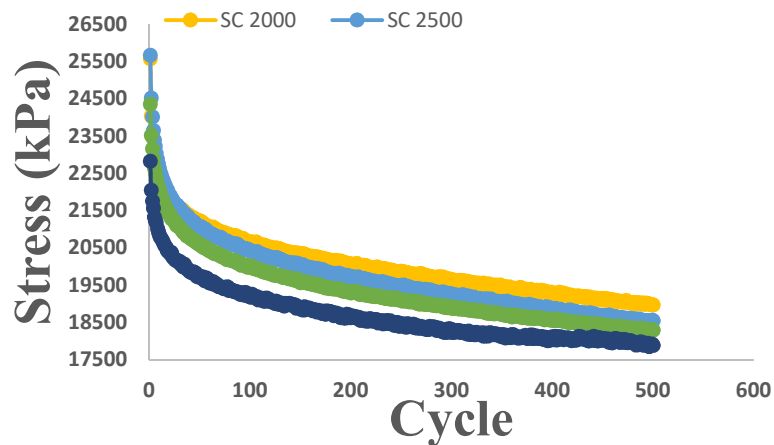
One of each sample is put up to multi cyclic loading testing with time lapses in between. Same as in the 50-cycle analysis, the degradation in the stress initially is due to the deformations in the plastic phase but as the testing is progressed, the elastic phase constraints the plastic phase. A table is provided for the time lapse of the samples between the testing's at room temperature.

Test (Cycles)	Relaxation time (days)
500	
1000	1
1500	7
2000	1
2500	1
3000	1
3500	1

4000	10
4500	10

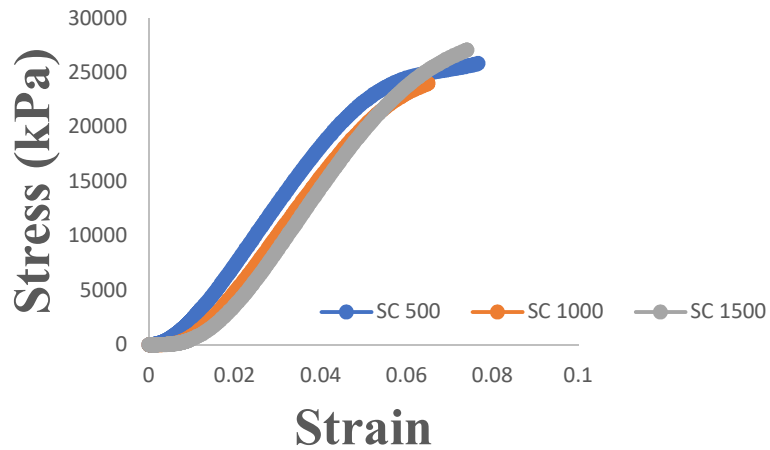
Table 5.1: Time lapse between the tests of SC sample

For the first three tests of the SC sample as the above plot showed the stress degradation is almost the same as 50 cycle analysis. And the time lapse between the testing's is one day. After the third test sample is allowed to rest for seven days and the results are quite peculiar. the sample gave a reasonable response, but because of the time constraint of the testing process, all the other testing on the SC samples are carried out with one day of time lapse.



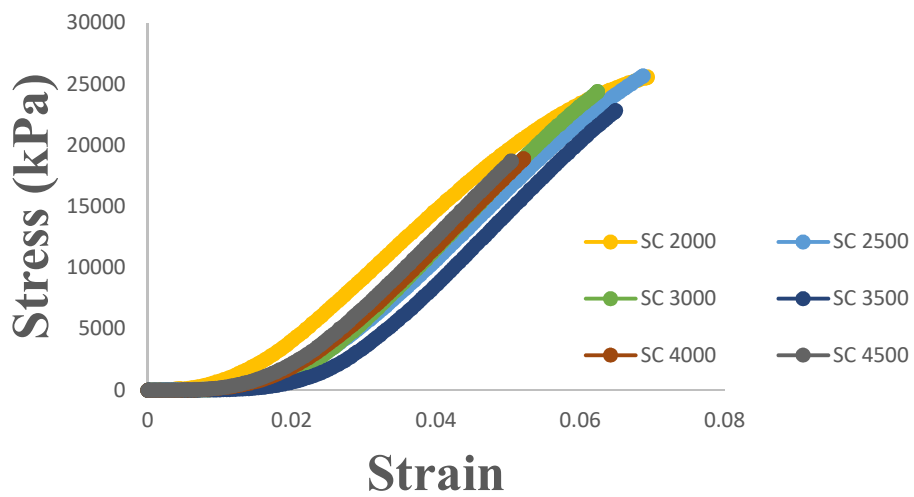
Plot 5.4: SN plot of SC sample for 2000 to 4500 cycles

Now for the stress-strain behavior of the SC sample for different tests, it is observed From the plot that as the sample is subjected to continuous loading under cyclic analysis, it is not affecting the stress value that much, even though the slope of the curve decreasing as the tests, the peak stress values seems to be maintained consistently in the first three tests with one day of relaxation time.

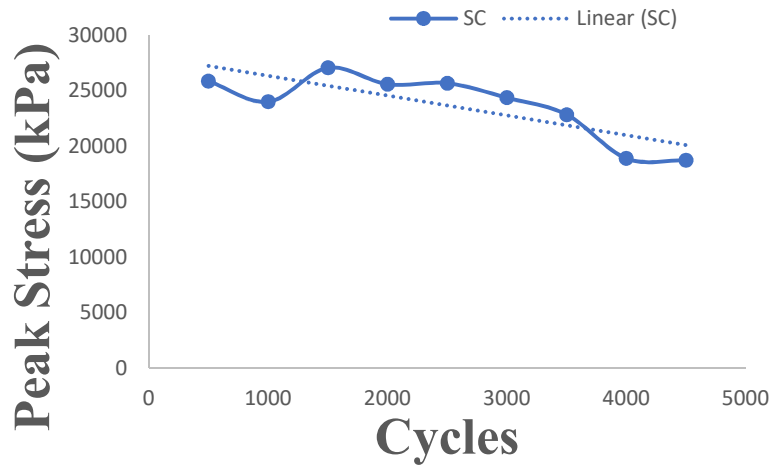


Plot 5.5: Stress-Strain plot of SC sample for 500 to 1500 cycles

From the below plot it is observed in the decrease of stress peak value for every other test. Overall peak stress values of the sample for different tests can be seen in the plot.

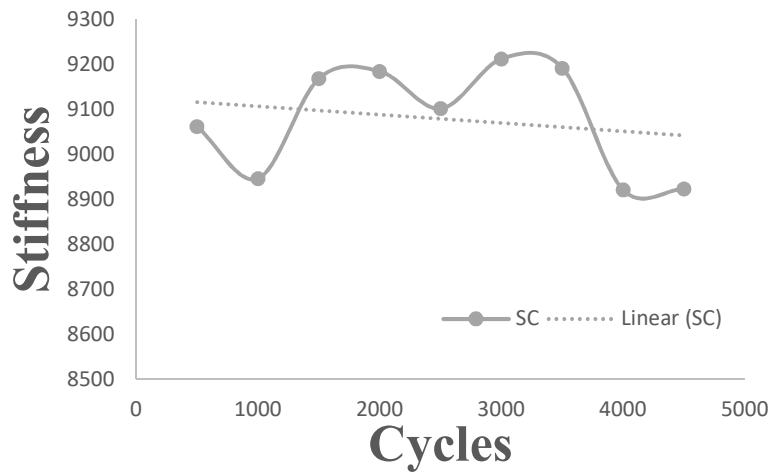


Plot 5.6: Stress-Strain plot of SC sample for 2000 to 4500 cycles



Plot 5.7: Peak stress degradation of SC sample for 500 to 4500 cycles

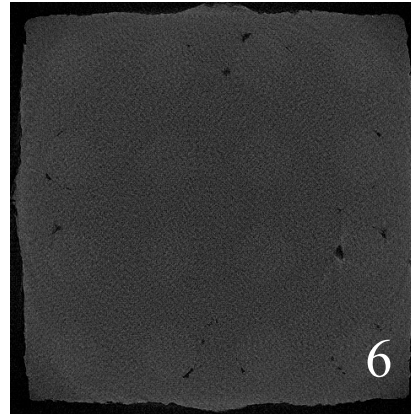
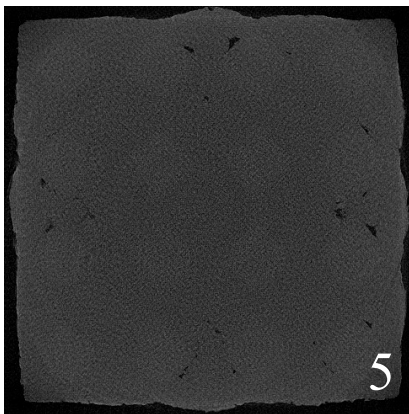
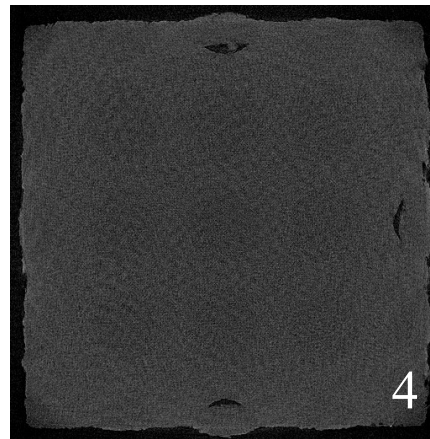
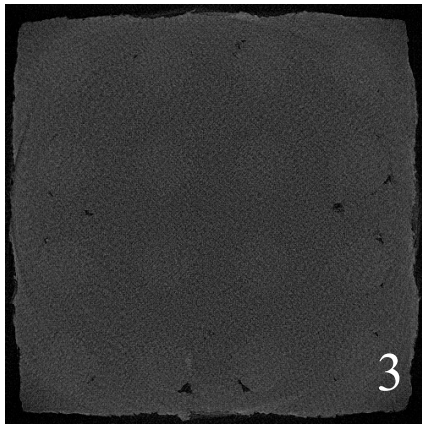
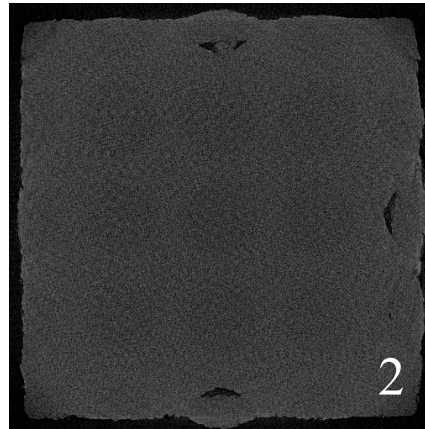
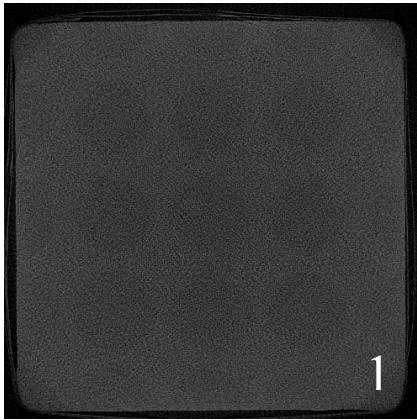
As a linear regression is performed to state the decreasing trend in the stress values. From the experimental data, stiffness is calculated and estimated the regression. This is calculated by taking the slope of load vs deformation curve. The regression is quite a lot.



Plot 5.8: Stiffness reduction of SC sample for 500 to 4500 cycles

Now, from the images of the sample that was gathered from 3D scanning, we can visualize how the damage is initiated and progresses in the sample.

5.2.1 Imaging of SC sample



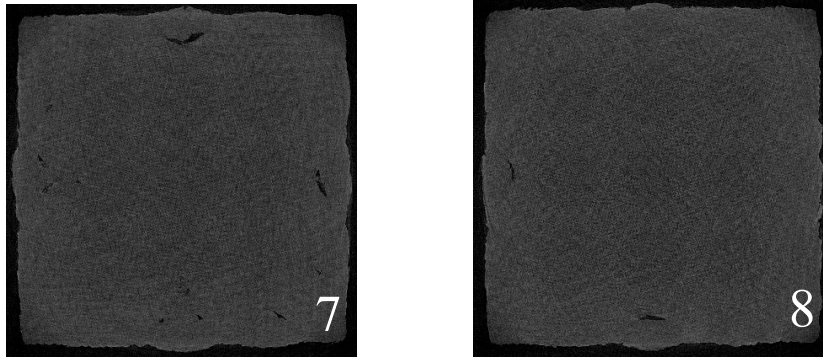
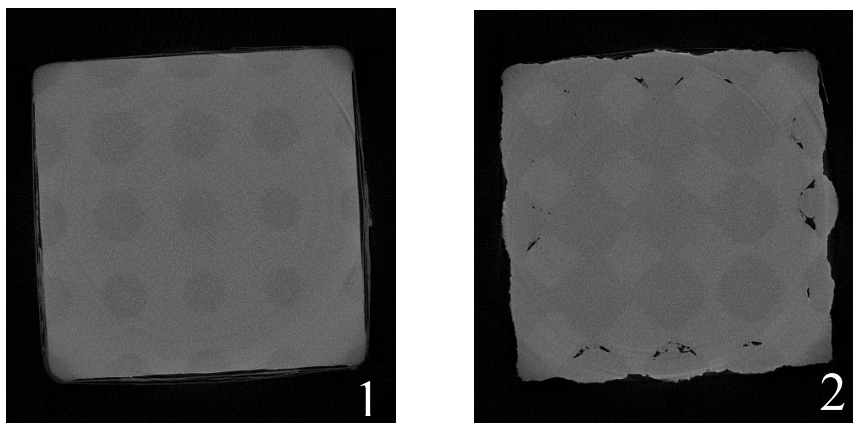
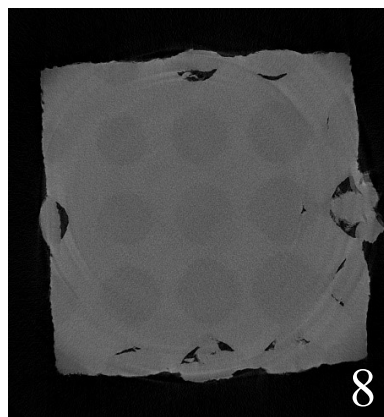
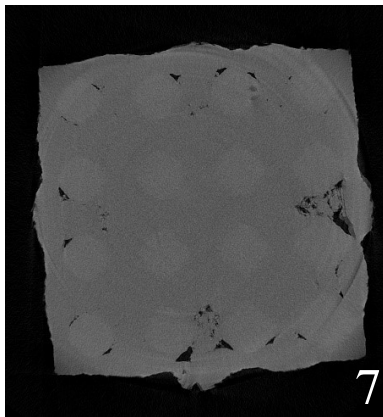
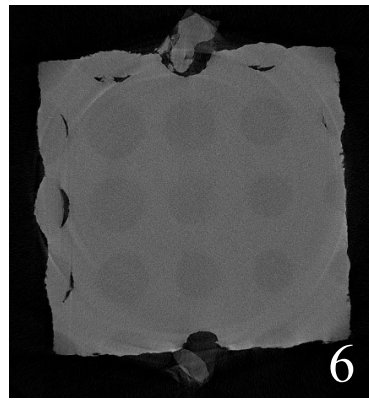
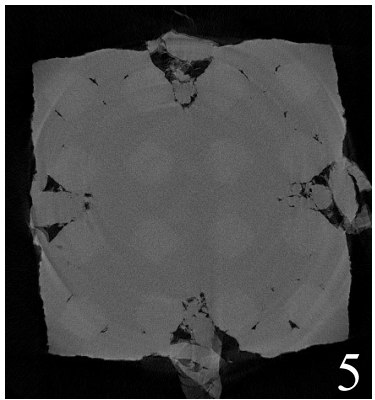
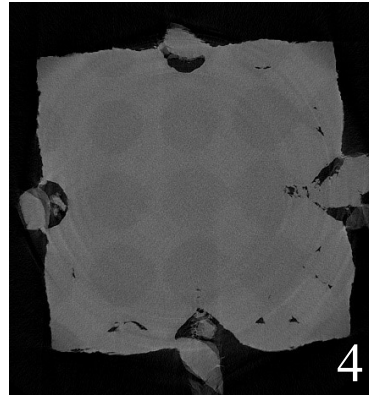
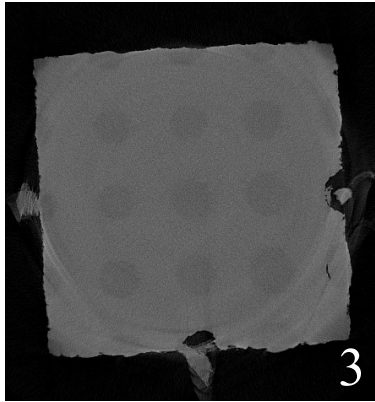


Fig 5.4: 3D scanning images of SC sample for 500 cycles.

Here each image represents one layer inside the sample. In these images, Light grey color represents the elastomer phase which is Tangoplus and the Dark grey represents the Plastic phase which is Vero white. Here Image 1 is the close top layer of the sample where there is no sign of damage. From images, 2 to it is observed that the damage inside the sample is slowly initiated near to the edges of the sample but in random locations. These are voids between the phases of the sample. From the rest of the images, we can observe the damage inside the layers of the sample. It is clear that the damage is slightly initiated inside of the sample under 50 cycles but most importantly it is in the plastic phase of the sample.





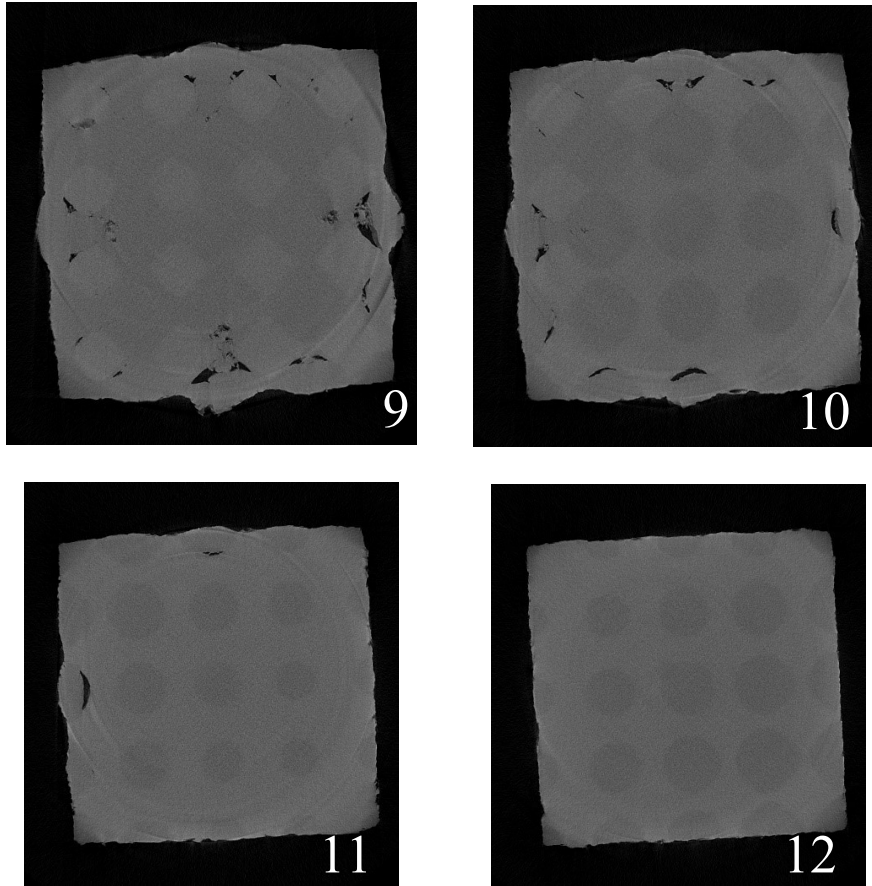
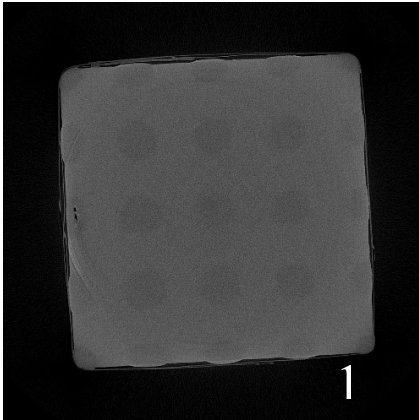
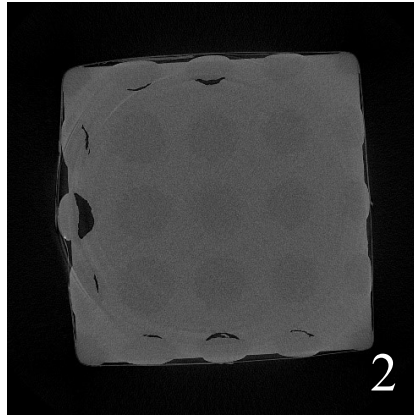


Fig 5.5: 3D scanning images of SC sample for 1500 cycles.

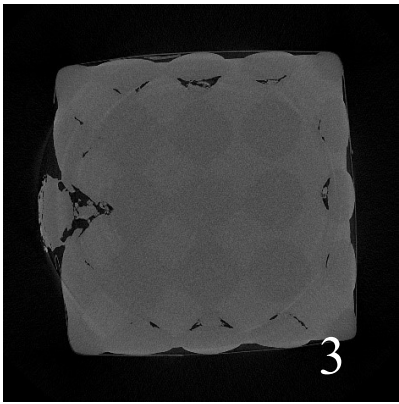
As the same sample has been put up to continuous loading, the damage inside of it is continued to increase. From the images 1 to 4, observe the damage is still maximum at the edges of the sample, from images 5 to 10 the damage is increased by breaking up the plastic phase and separating them. Images 11 and 12 shows the layers closer towards the base where there is no damage. Damage is continuously progressing and breaking the sample apart. As same as before, this damage is inside of the plastic phase.



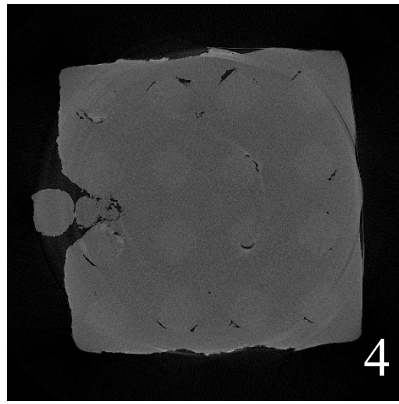
1



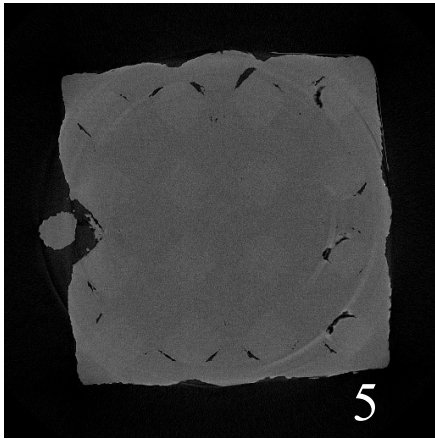
2



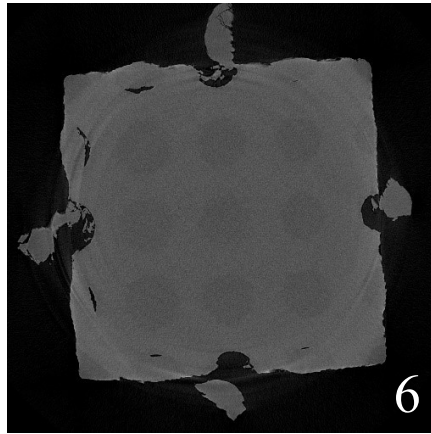
3



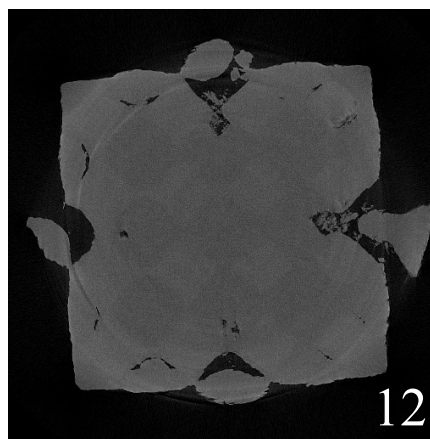
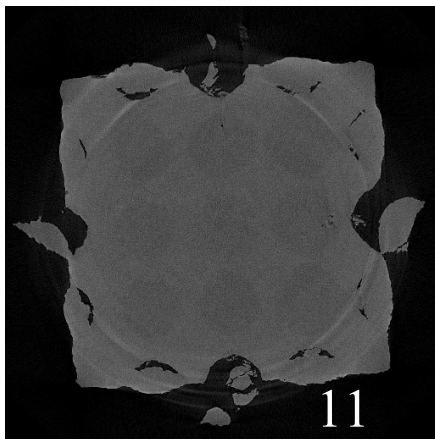
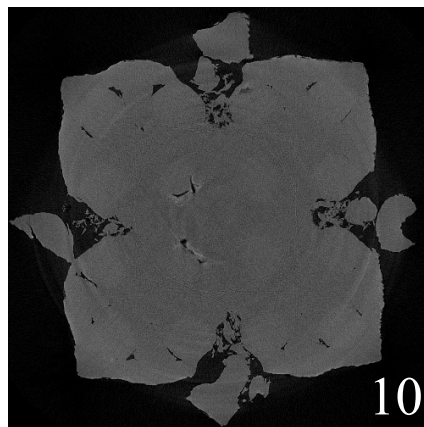
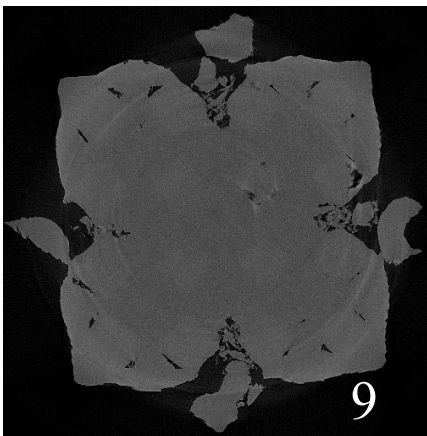
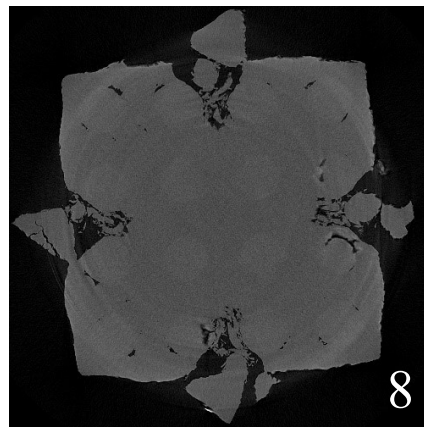
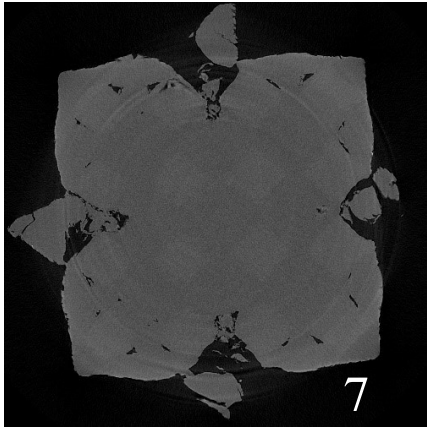
4



5



6



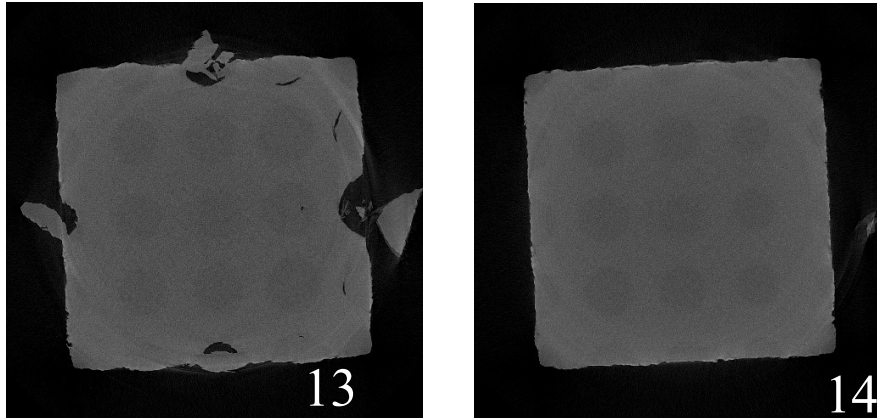


Fig 5.6: 3D scanning images of SC sample for 3500 cycles.

The same sample is subjected to 500 cycles multiple times, from the images 2 to 4 it is observed the one small part of the sample is almost separated due to breaking. From images 5 & 6 the damage initiation in other locations but closer to the edges is seen. From images 7 through 12, it is observed that the damages inflicted near to the edges is making the sample to break apart. Damage inside the sample is slowly progressing towards the center.

At this point, by observing the images above we can say that the internal structure of the sample is under soon to experience a catastrophic failure.

5.3 Data analysis and Results for 500 cycles for BCC sample

Same as the SC sample, the static analysis did not provide enough information on the BCC sample. So, the testing process is altered, and 500 cycles method is performed on the same sample multiple times with time lapse between testing's. sample relaxation allowed for BCC is completely different when compared to SC and FCC samples. As mentioned in the table below, first 500 cycle test was performed and allowed the sample to rest for 4 days at room temperature, then 6 days after next test and at last 10 days then

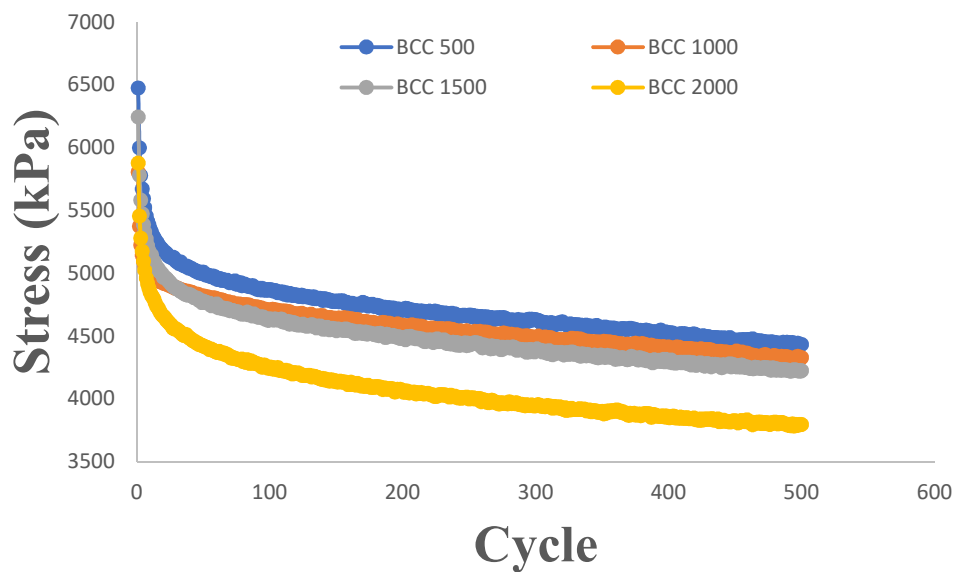
performed final testing. Because of the time constraint continuous testing's were not performed and the change in peak stress values is also minimal compared to SC sample.

Test (Cycles)	Relaxation time (days)
500	
1000	4
1500	6
2000	10

Table 5.2: Time lapse between the tests of BCC sample.

From the repeated testing on the same sample, data is gathered and analyzed.

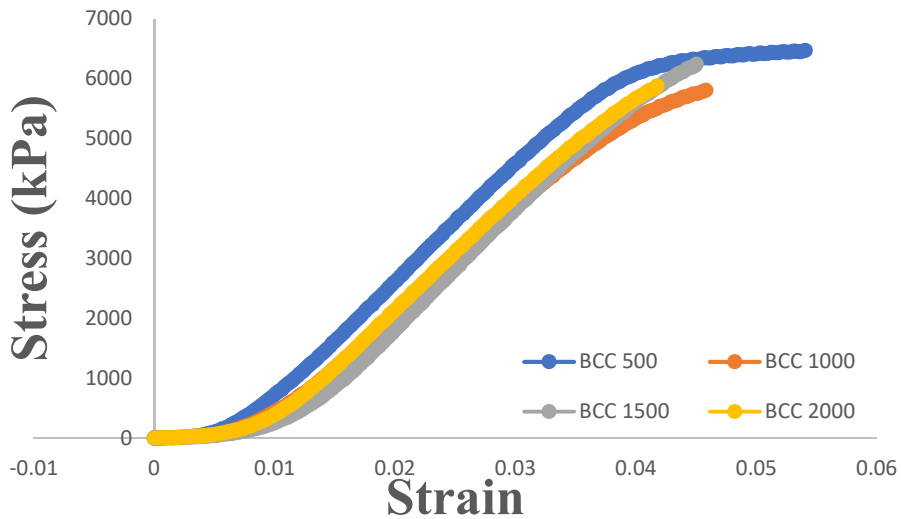
Results were plotted.



Plot 5.9: SN plot of BCC sample for 500 to 2000 cycles

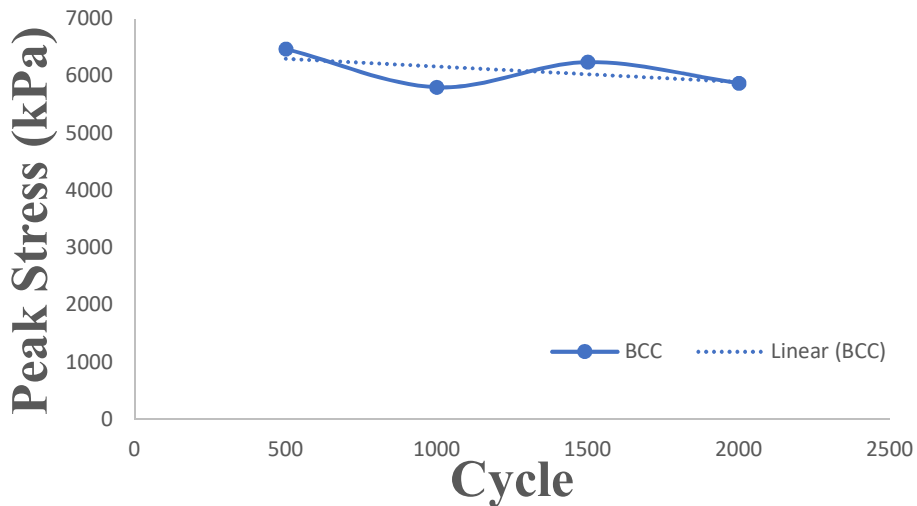
From the plot it is observed that even though there is a large time gap between the testing s on the sample, the peak stress values seem to be close and as same it is showing the initial drop of stress values due to plastic phase behavior in the sample and then the

stress stabilizing because of the elastomer phase. The relaxation did not show that many variations in the stress values. Now let's see the stress strain behavior of the sample.



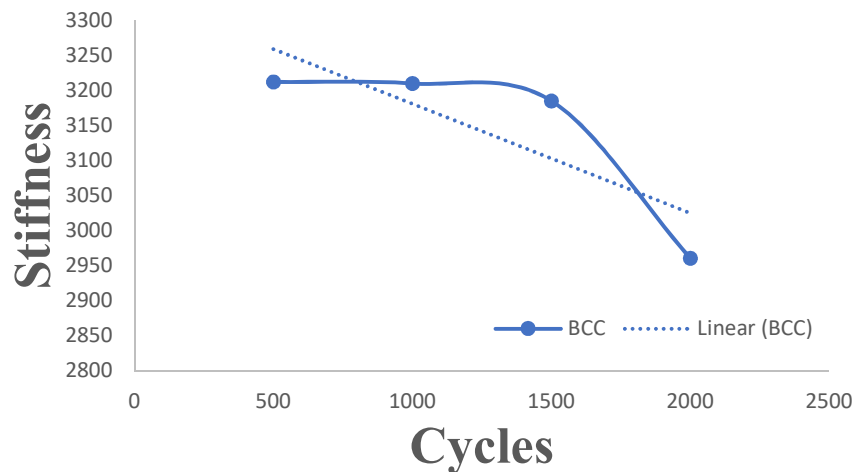
Plot 5.10: Stress-Strain plot of BCC sample for 500 to 2000 cycles

From the above plot, it is observed that BCC sample does not have that much energy absorption capacity as SC sample. but the peak stress values for each test seems to be dropping but very minimal. Peak stress regression is also calculated for BCC sample.



Plot 5.11 : Peak Stress regression of BCC sample for 500 to 2000 cycles

Stiffness of the sample describes the resistance offered by it under loading to resist deformation. Here based on the experimental data stiffness is calculated for this sample. linear regression performed to show the overall behavior, it is showing a decreasing trend.



Plot 5.12: Stiffness regression of BCC sample for 500 to 2000 cycles

From the plot, it is observed that till the 1500 cycles the sample shows the almost constant stiffness but for 2000 cycles the stiffness drops, this is because of the damage initiated inside the sample because of the continuous loading. A linear regression performed also shows a decreasing trend.

Now, images of the sample that was gathered from 3D scanning, we can visualize how the damage is initiated and progresses in the sample.

5.3.1 Imaging of BCC sample

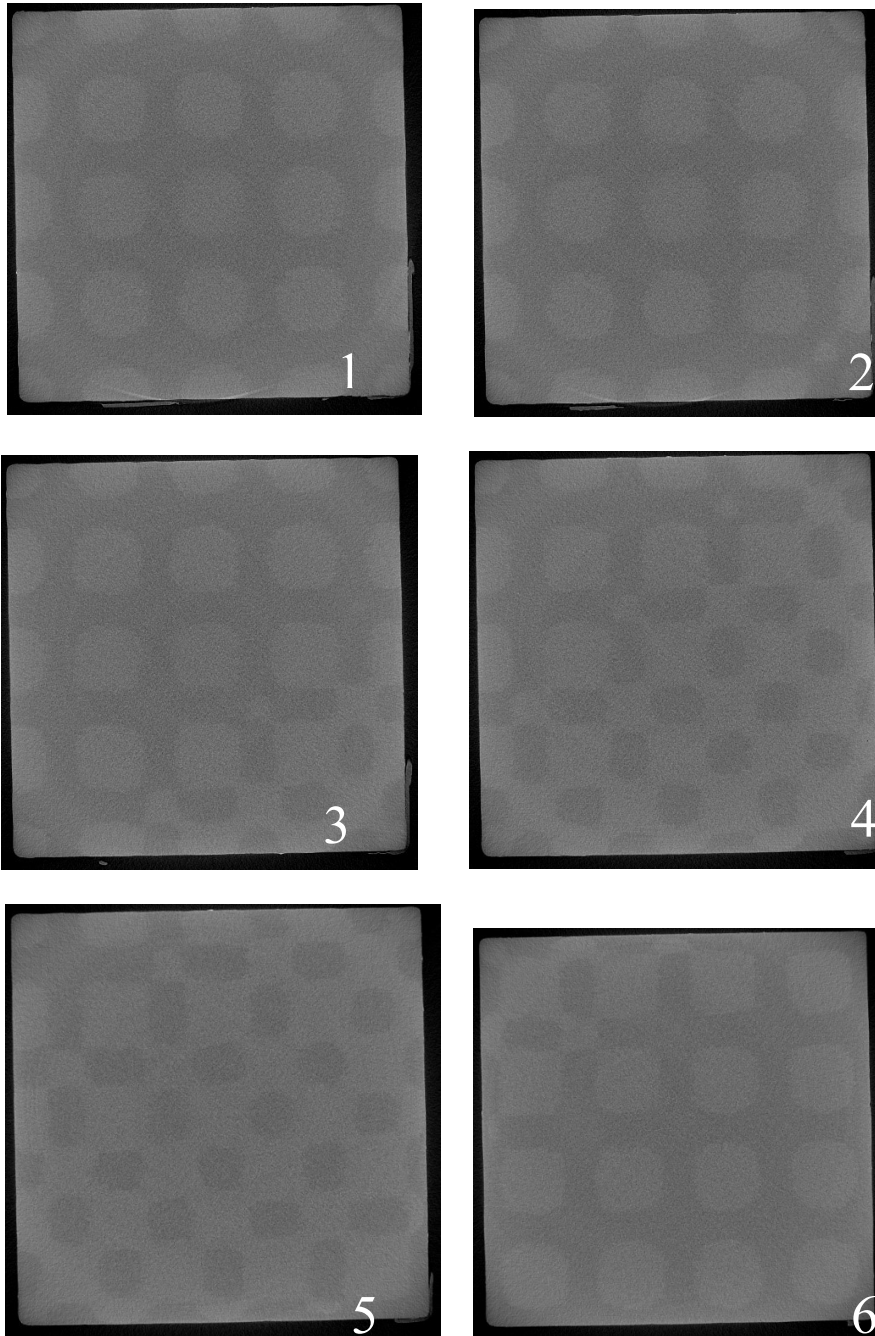


Fig 5.7 : 3D scanning images of BCC sample for 500 cycles.

It is observed from the images that, even though the sample is put to cyclic loading for 500 cycles, there is no trace of damage initiation in the structure.

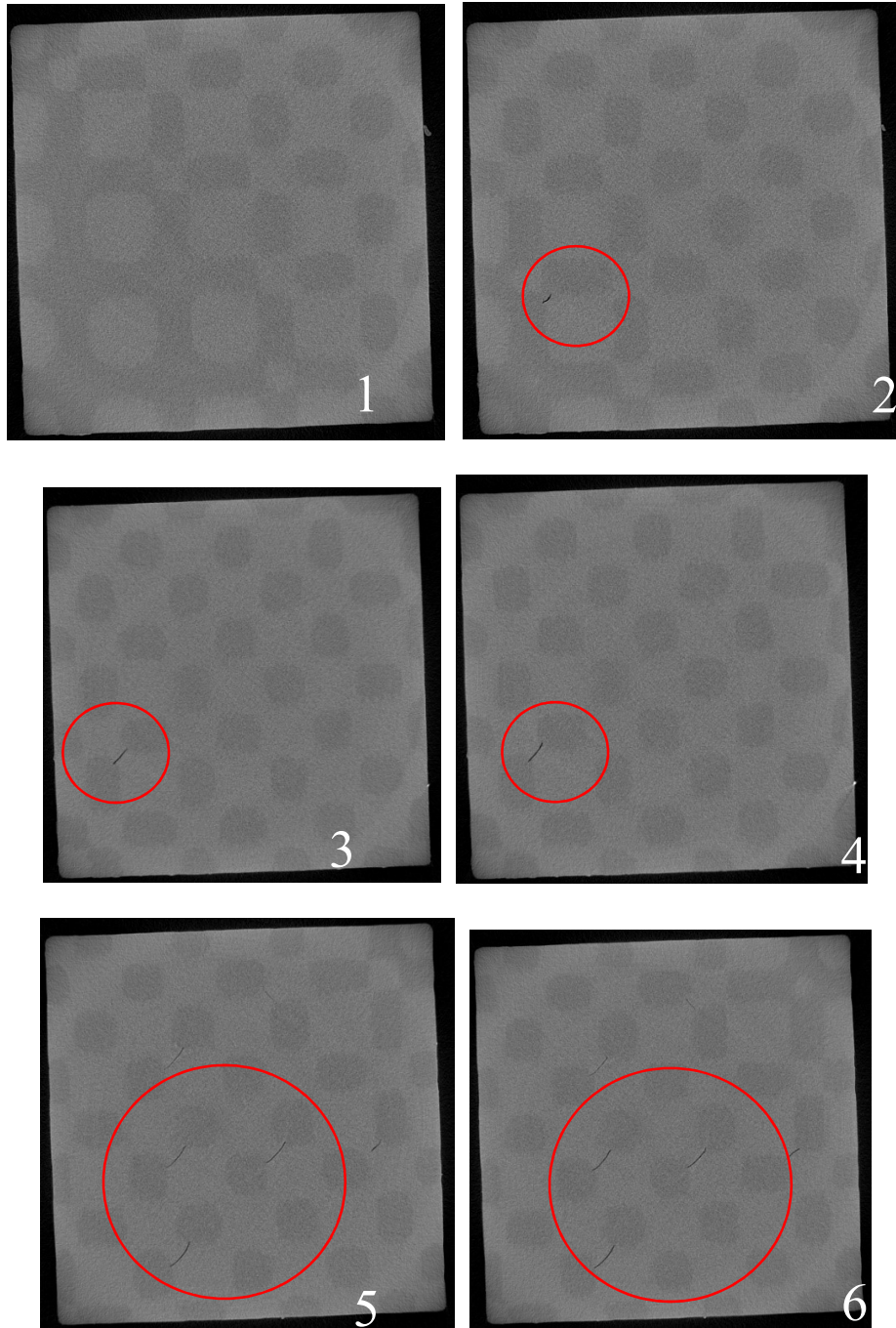


Fig 5.8: 3D scanning images of BCC sample for 1000 cycles.

From image 1, it is observed that there is no damage closer to the top surface of the sample. from images 2 to 4 there is a small sign of damage as a small void highlighted with a circle in the images. Due to the continuous application of loading, slowly sample starting

to take damage. From images 5 and 6 these small cracks can be seen in multiple locations.

Even though there is a sign of damage, it is minor.

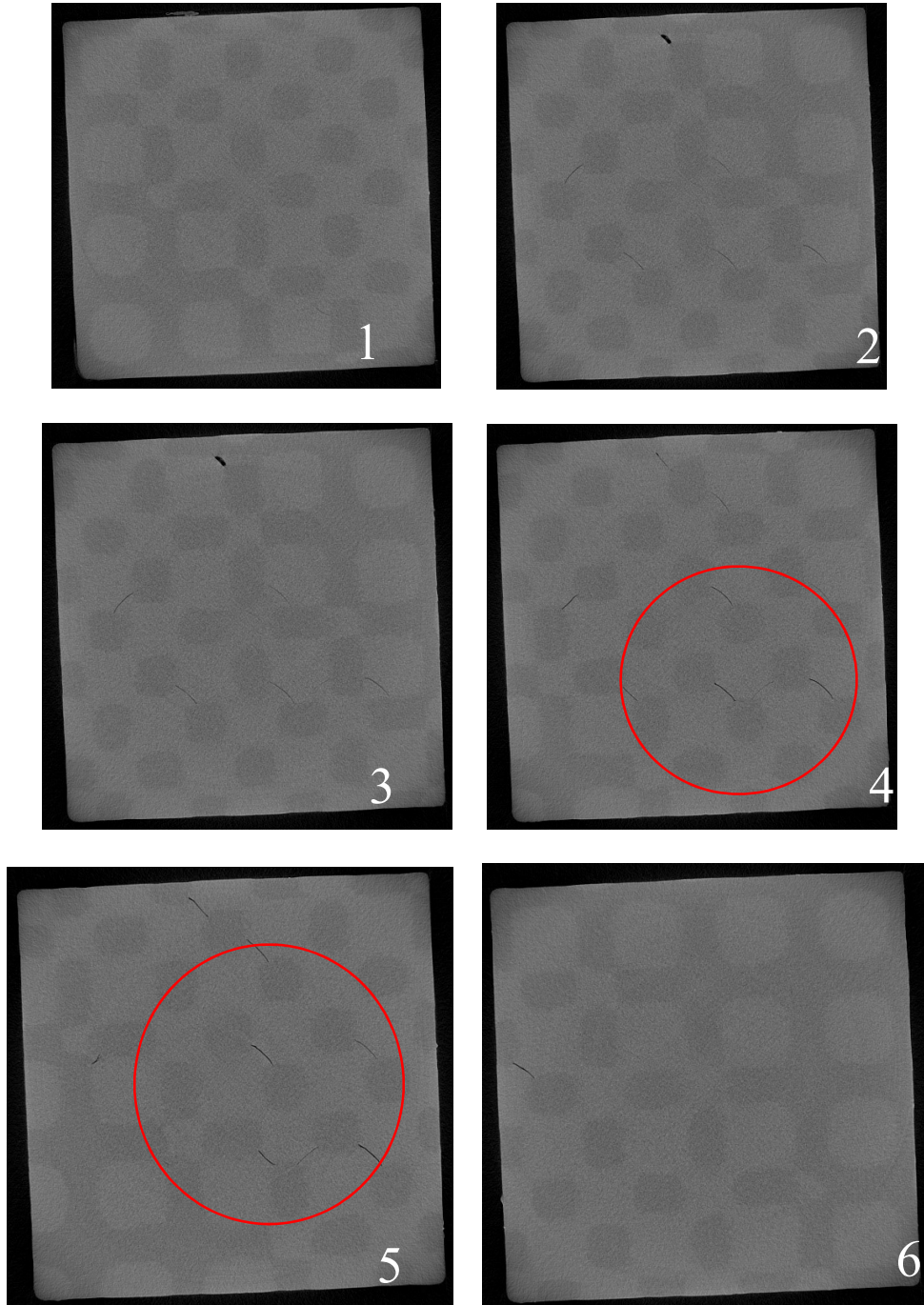


Fig 5.9: 3D scanning images of BCC sample for 1500 cycles.

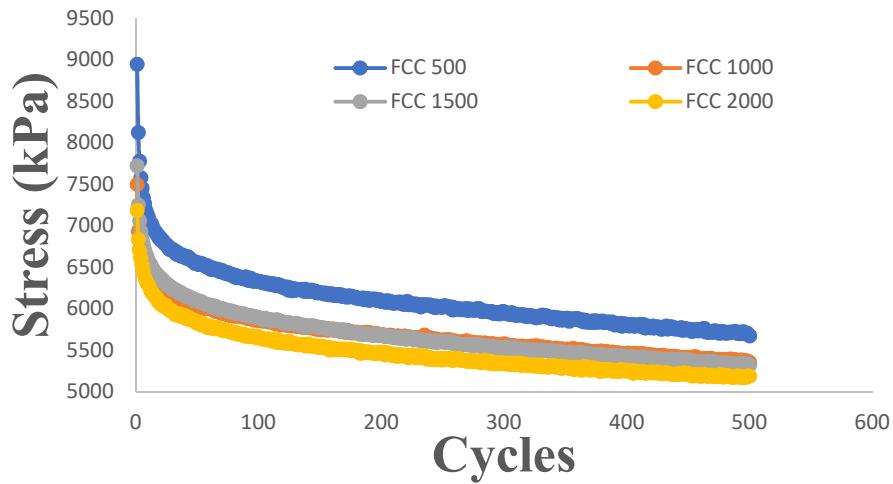
From the images 1 to 3, a small crack is observed, but as we move towards the center of the sample cracks formed at random locations in the sample which resulted in the minor separation of two phases in the sample. We can see the signs of damage that are visible inside the BCC structure highlighted in the circle. This damage is responsible for the stiffness regression as well as the peak stress regression in the sample.

5.4 Data analysis and Results for 500 cycles for FCC sample

As stated in the earlier results, high cyclic loading is opted to gather more data on the sample behavior. Tests were performed, data is gathered and analyzed, results were plotted. Here for the testing purpose, different relaxation time for the sample is considered which is completely different from SC and BCC sample.

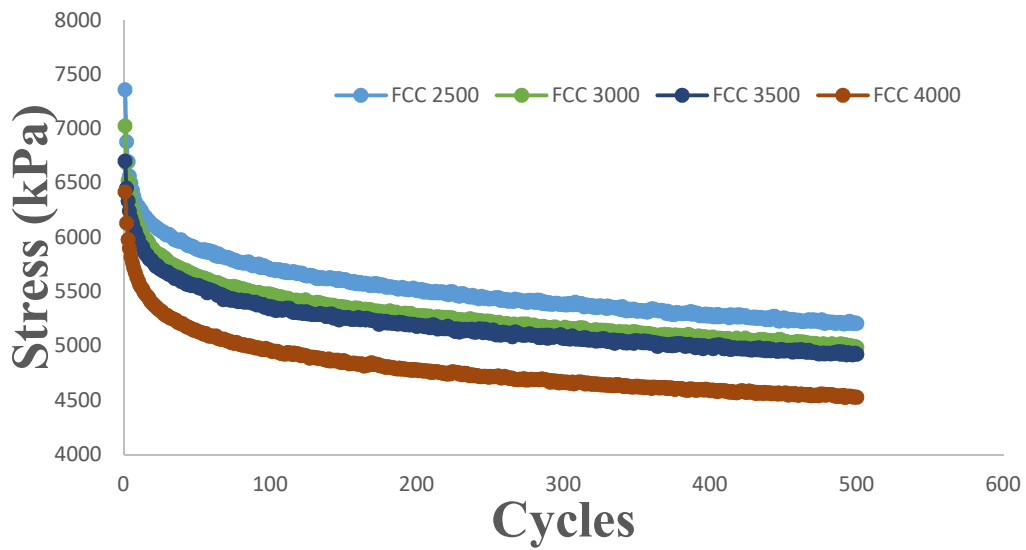
Test (Cycles)	Relaxation time (days)
500	
1000	1
1500	1
2000	1
2500	2
3000	1
3500	1
4000	10

Table 5.3: Time lapse between the tests of FCC sample.



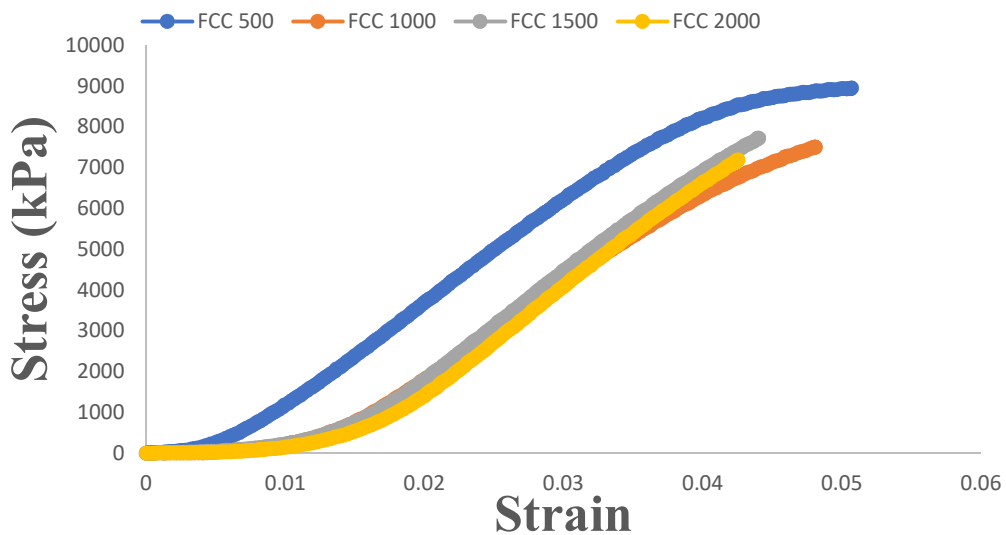
Plot 5.13: SN plot of FCC sample for 500 to 2000 cycles

Here from the plot, it is observed that peak stress values are close even though the time gap between the tests are kept to one day. For the third test, the sample was allowed to rest for two days, then the result is it almost shown the same behavior in the third test as shown during the second test. The stress values of the third and the second test are almost overlapping. Then the same one-day trend is continued. For the final test sample was allowed to rest for 10 days to visualize the behavior under continuous loading. For the last test which is 3500 to 4000 cycle test the stress values are drastically low compares to the earlier test values.



Plot 5.14: SN plot of FCC sample for 2500 to 4000 cycles

Let's observe the stress-strain behavior of the sample, which allows us to understand the energy absorption capability of the sample under continuous loading.

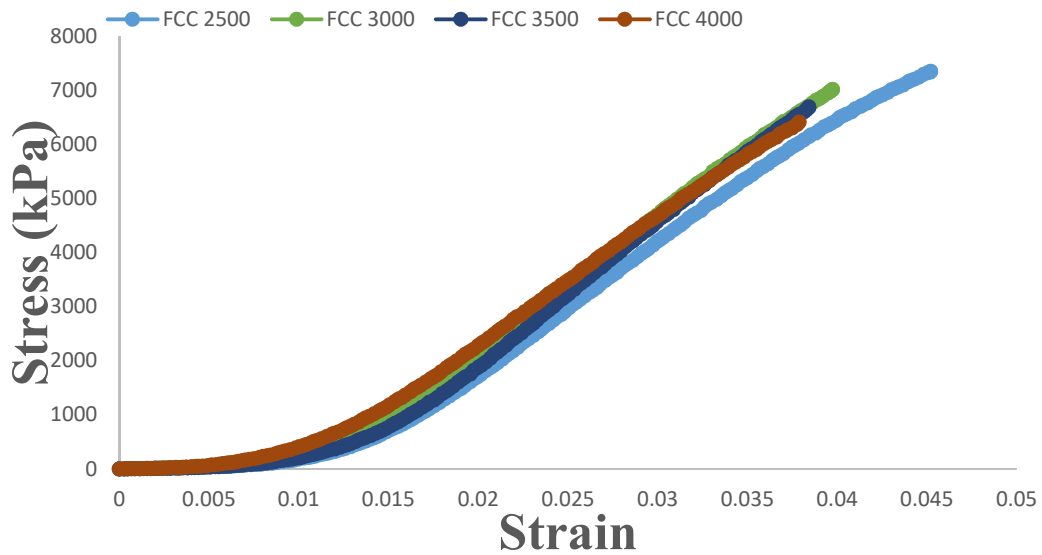


Plot 5.15: Stress-Strain plot of FCC sample for 500 to 2000 cycles

From the above plot, we can understand that the stress values keep on decreasing as the sample is under continuous loading, also the energy absorption during loading which

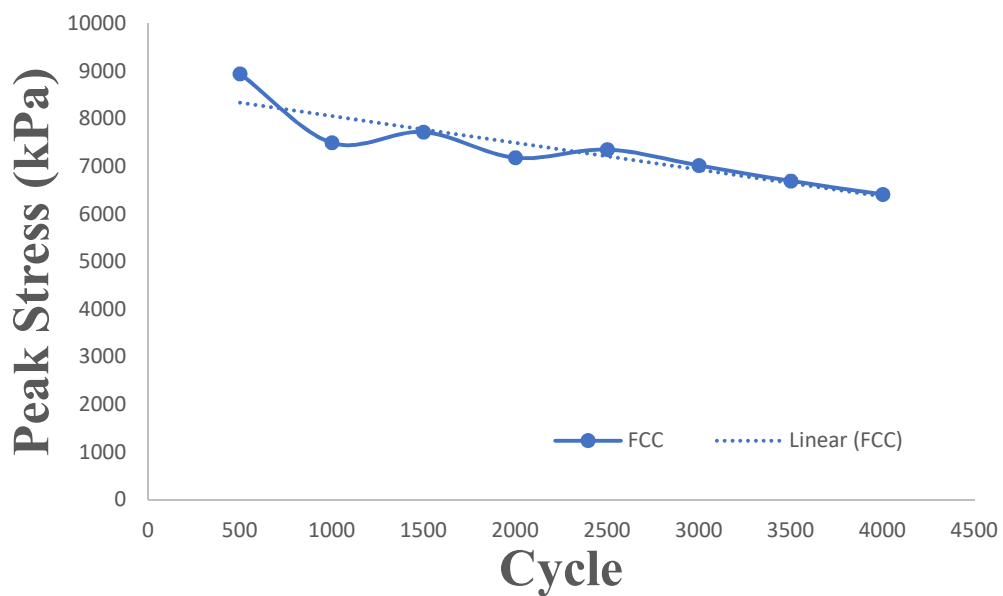
is represented by the area under the curve is also decreasing with every consecutive test.

this trend is continued for the rest of the results also.



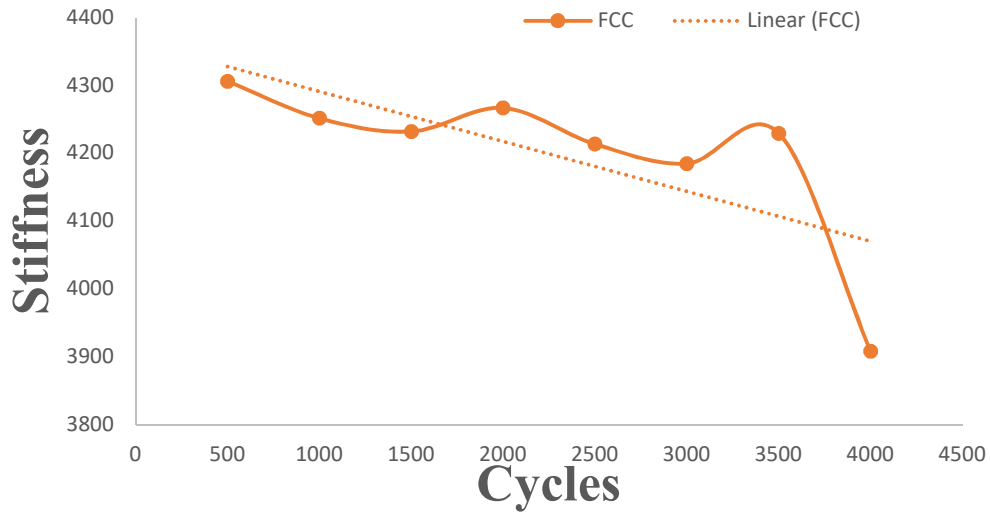
Plot 5.16: Stress-Strain plot of FCC sample for 2500 to 4000 cycles

Peak stress regression is also plotted for the FCC sample to visualize the decrease in the stress values with every consecutive test.



Plot 5.17: Peak stress regression of FCC sample for 500 to 4000 cycles.

Stiffness regression also calculated from the experimental values and plotted as follows.



Plot 5.18: Stiffness regression of FCC sample for 500 to 4000 cycles.

Here the stiffness degradation in the sample is very minimal until the seventh test which is up to 3500 cycles, but for the last test 3500 cycle to 4000 cycles the stiffness of the sample decreased drastically this is due to the damage inside of the sample due to continuous loading.

Now, from 3D scanning image so the FCC sample, we can visualize how the damage is initiated and progresses in the sample.

5.4.1 Imaging of FCC sample

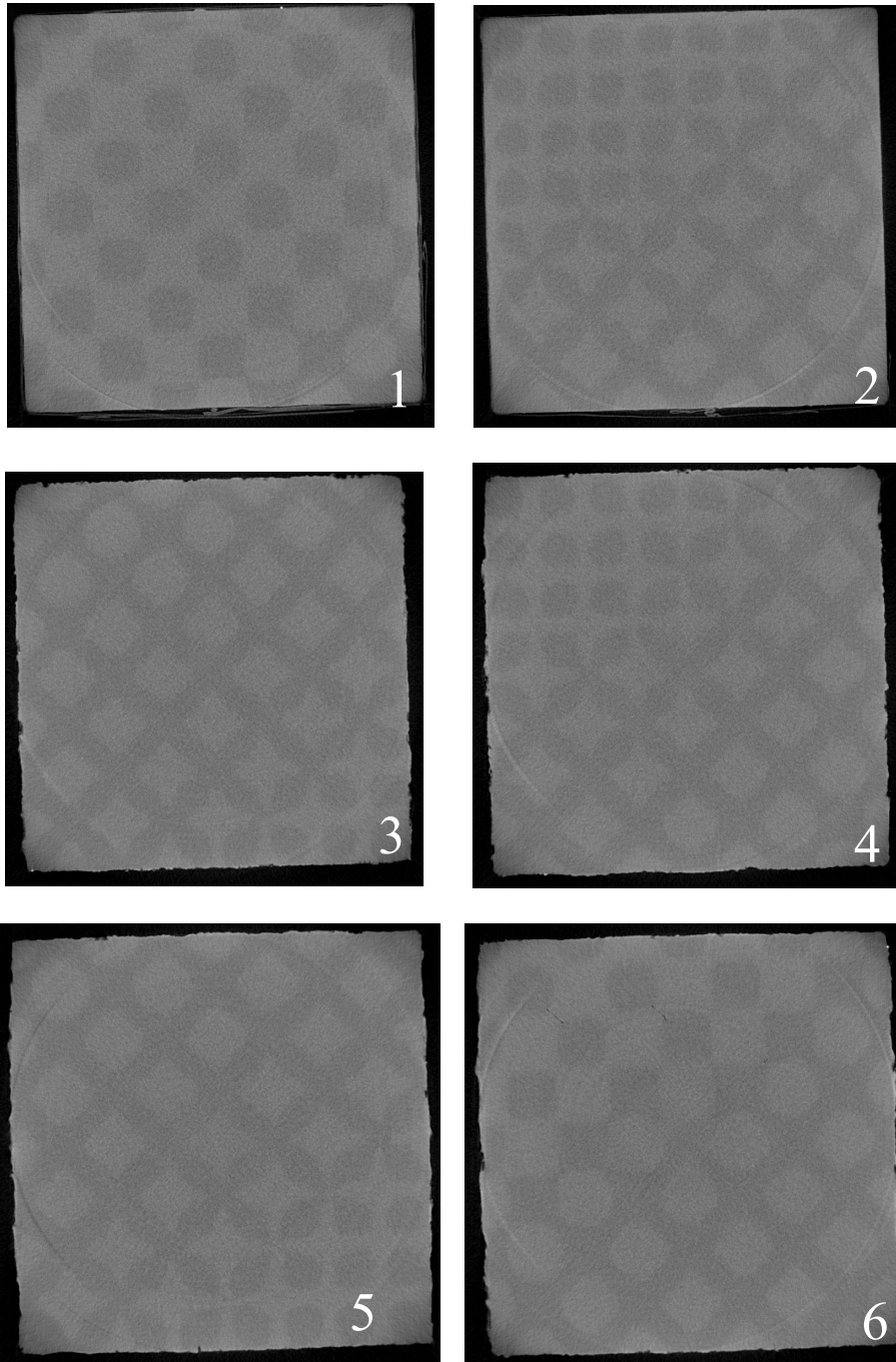
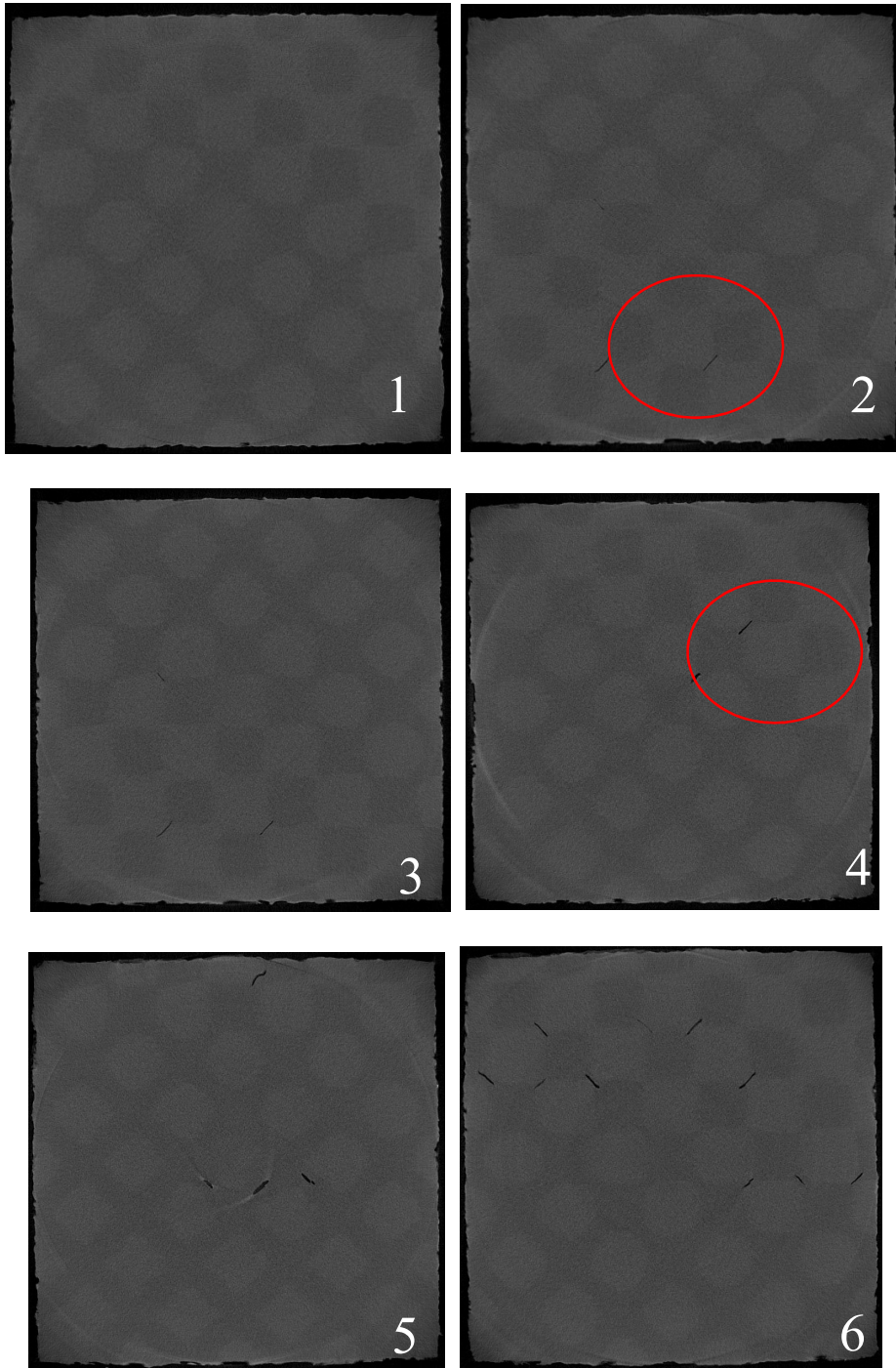


Fig 5.10: 3D scanning images of FCC sample for 500 cycles.

From the images, it can be observed that during the initial testing, there are no signs of damage in the structure of the sample.



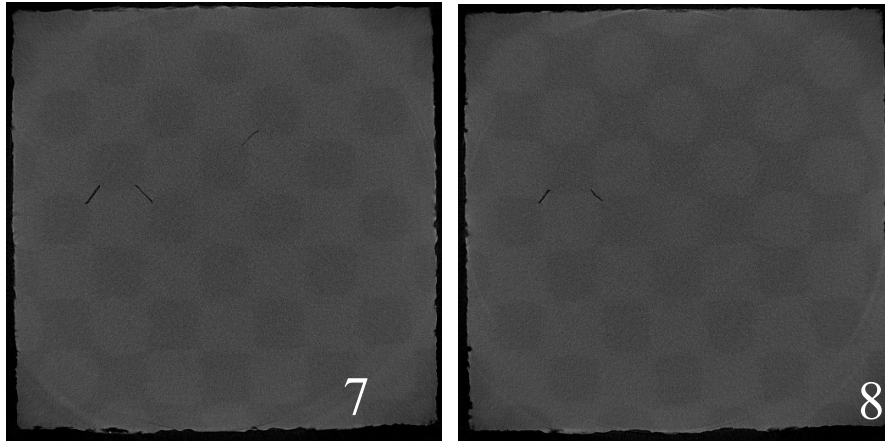
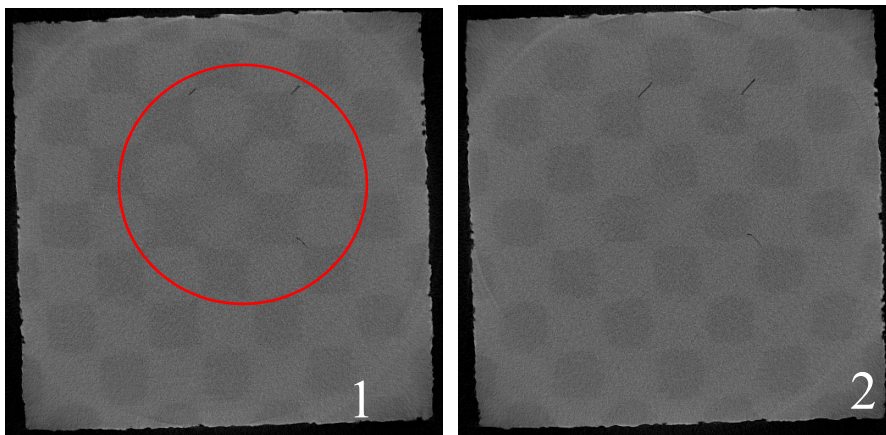
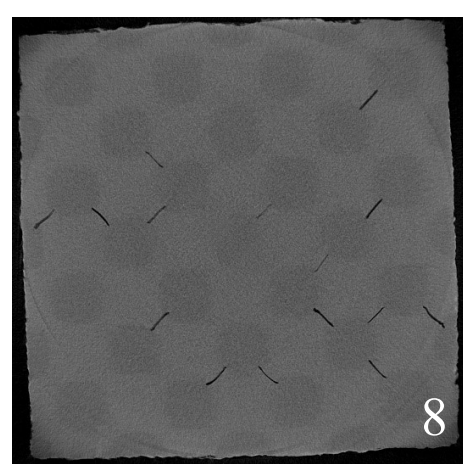
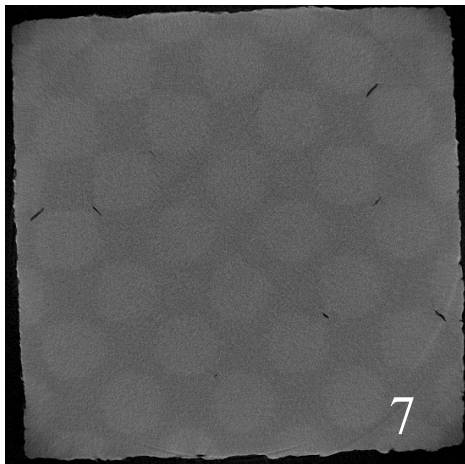
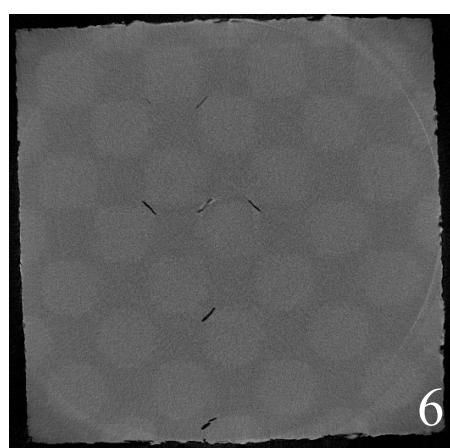
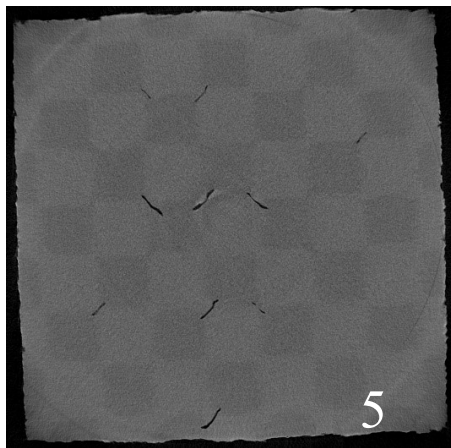
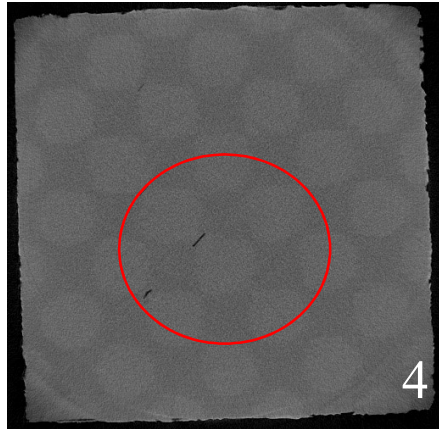
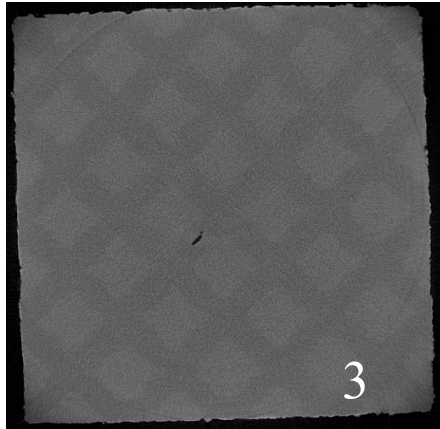


Fig 5.11: 3D scanning images of FCC sample for 2000 cycles.

From the image 1, there is no trace of crack. But from images 2 to 4 we can see small cracks appeared randomly highlighted in a circle. These cracks are progressing as the loading cycles are continuing. From the images 5 & 6 cracks are clearly visible because the separation between the phases is increasing with every cycle. From images 7 & 8, these layers are closer to the bottom of the sample have a minimum sign of visible cracks. So, We can say that a fair amount of damage inside the sample like cracks and small voids are observed.





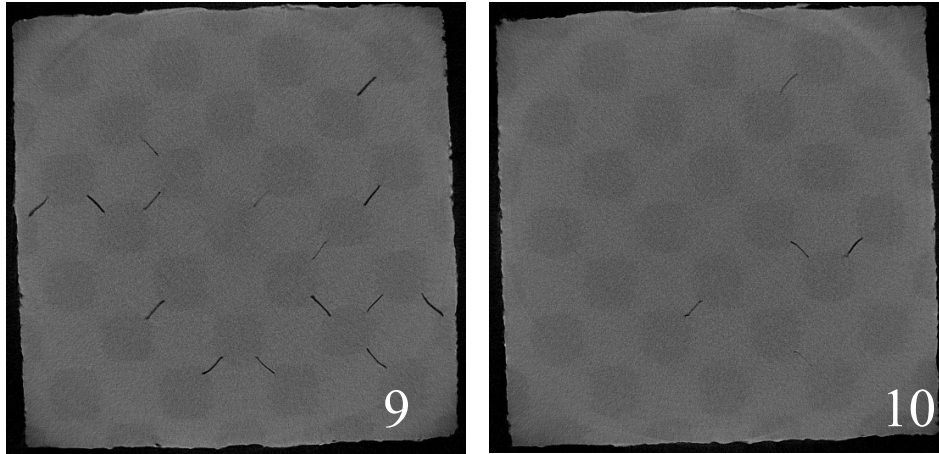


Fig 5.12: 3D scanning images of FCC sample for 3000 cycles.

From the images 1 through 10 we can observe the cracks are becoming more and more visible, this is due to the continuous application of load resulted in the deformations inside of the sample that led to the separation of phases. Since the load distribution inside the FCC is more efficient than BCC and SC the damage is seen all over the layer of the sample, unlike BCC and SC. From the images, more damage inside the sample is observed as the volume of cracks increased compared to last imaging.

5.5 Image Processing

Experimental investigations into the damage progression of the composite samples indicated a growth of voids in the sample with cycle time. An automated algorithm was developed to approximate the loss in area through voids to compare the damage progression in the BCC, FCC and SC samples. The images for this task were obtained through a micro-CT scanner, which captured images top-down through the thickness of the sample.

5.5.1 Methodology:

The process flow chart for the method is described below.

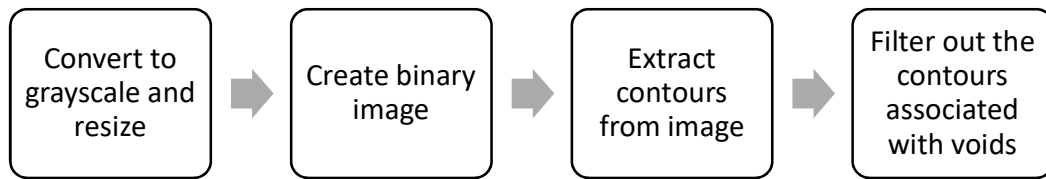
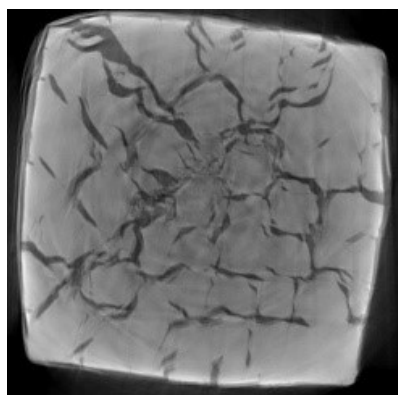
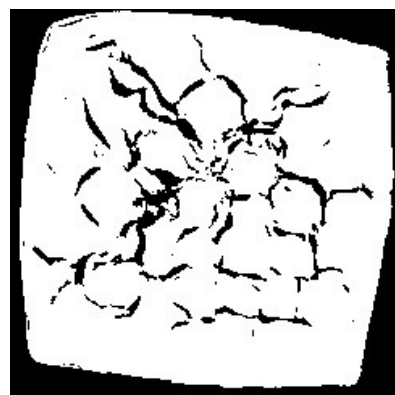


Fig 5.13: Overview of the algorithm to approximate void area

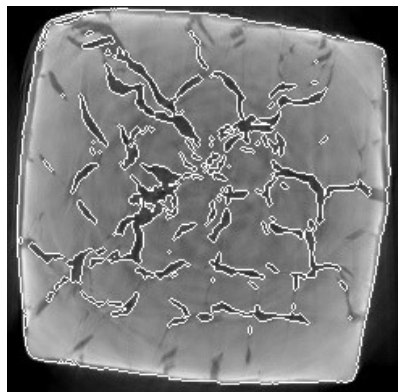
Images altered using algorithm are shown below following on above mentioned steps



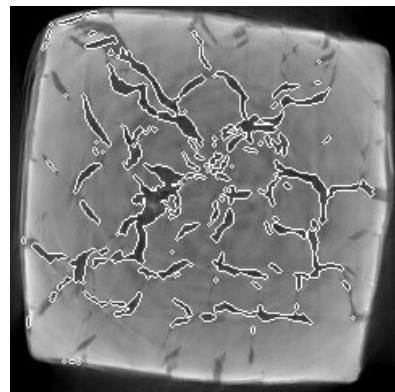
Grey scale image



Binary image



Contours extraction



voids filtering from the image

Fig 5.14: Overview of the images analysis to filter void area

1. Image preprocessing: RGB to Grayscale conversion and down-sampling

Each image from the dataset is imported serially and first converted into grayscale. The images are also resized to half their original size, as highly detailed (5K resolution) images extracted unwanted edges while processing with the Canny detector. Images of different resolutions would require different hysteresis thresholds. By down-sampling all the images down to a resolution of approximately 360x360, a standard technique of setting the Canny hysteresis threshold was possible.

2. Image binarization

Optimal threshold selection from the gray level histogram was accomplished using Otsu's binarization technique[22], a nonparametric algorithm. The reason why this method was hypothesized to work well was the clear distinction between void and material (background) pixels. This would lead to a well-defined boundary between the histogram intensities of the voids and the material. The threshold value returned by this algorithm was then used on the Canny edge detector algorithm [23] as:

$$T1 = 0.5 * I \dots\dots\dots(3)$$

$$T2 = I \dots\dots\dots(4)$$

where T1 and T2 are the hysteresis thresholds and I is the threshold intensity returned by the Otsu algorithm.

3. Extract edges from grayscale image

Edges from the grayscale image were extracted using the Canny edge detector. The Canny edge detector works as follows:[24]

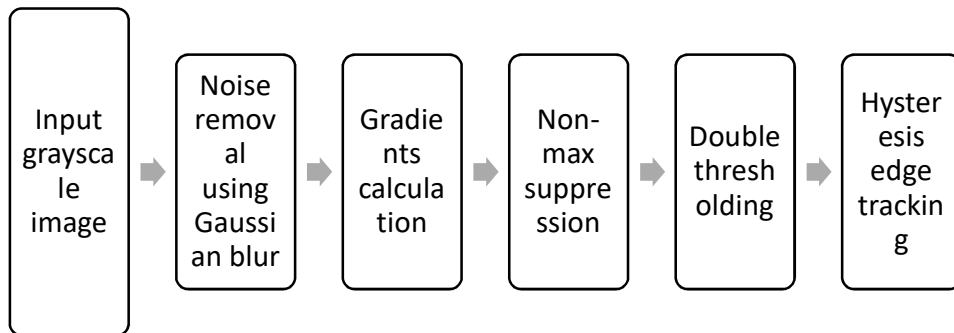


Fig 5.15: Canny edge detector algorithm

Edge detection involves finding differences in intensity gradients between neighboring pixels. The grayscale image is therefore smoothed by Gaussian blurring, using a 5x5 kernel. The matrix equation for a 5x5 kernel is given by:

$$H_{ij} = \frac{1}{2\pi(\sigma^*)^2} e^{\left(-\frac{(i-6)^2+(j-6)^2}{2\sigma^2}\right)} ; 1 \leq i, j \leq 5 \dots\dots\dots(5)$$

where σ^* is the std. deviation of the normal distribution centered at (0,0).

After blurring the image, the next step is to calculate the gradients of the image. The gradients are calculated using the Sobel operator, with kernel size 3. The image is convolved with two Sobel filters G_X and G_Y to detect edges in the X and Y directions respectively.

$$G_X = \begin{pmatrix} -1 & 0 & 1 \\ -2 & 0 & 2 \\ -1 & 0 & 1 \end{pmatrix} \text{ and } G_Y = \begin{pmatrix} 1 & 2 & 1 \\ 0 & 0 & 0 \\ -1 & -2 & -1 \end{pmatrix}$$

The magnitude of the gradient and the direction are then calculated:

$$|G| = \sqrt{G_X^2 + G_Y^2} \dots\dots\dots(6)$$

$$\theta = \tan^{-1} \frac{G_Y}{G_X} \dots\dots\dots(7)$$

The next step after finding the edges is the non-max suppression of pixels, a method to suppress the values with the lowest pixel intensities. The non-max suppression algorithm returns the pixel with the highest intensity from the edge matrix by evaluating the pixels that fall along the gradient direction obtained from the above equations.

The final step in the Canny edge detection process is the hysteresis thresholding step, where the pixels are categorized as strong, weak or irrelevant depending on whether they are above or below the threshold. The pixels in between the threshold are filtered (weak edges) as follows: If a weak edge pixel is surrounded by at least 1 strong pixel, then it is converted into a strong pixel.

4. Extract boundary contour from extracted edges

The external boundary contour needs to be extracted to find the approximate area of the sample. To do this, the contours were sorted by decreasing area, and the largest contour was used as the boundary contour.

5. Extract contours from binary image

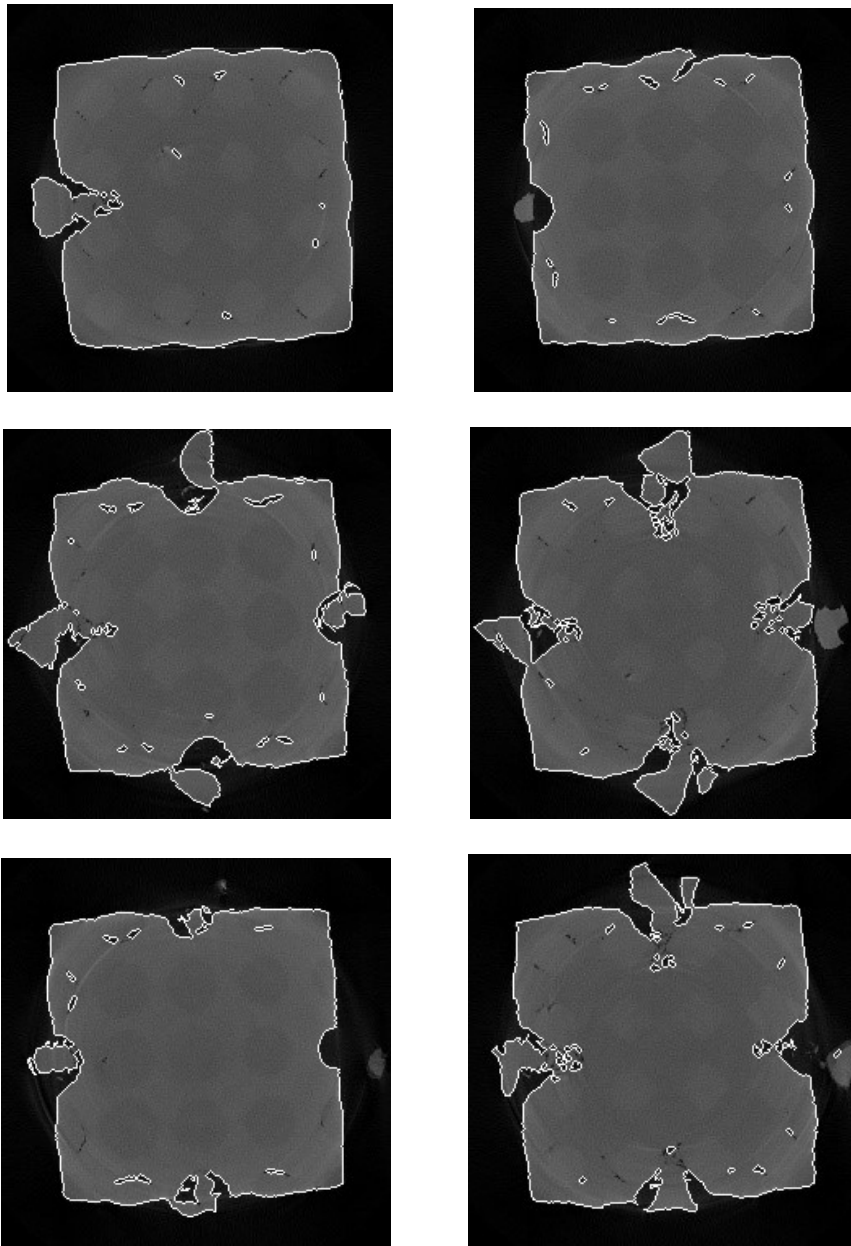
The contours were also extracted from the binary image by deploying the canny edge detector followed by contour extraction. The method used for contour extraction did not get rid of the hierarchies in the contours, thereby preserving both parent and child contours.

6. Iterate on contours extracted from binary image to check for voids

The contours extracted from the binary image were then analyzed individually to check for voids inside the sample. This was done by filtering through each contour and first checking whether it was internal to the boundary. A contour is defined to be internal to another if all the points of the first contour lay inside the parent contour. Since the image was binary, most of the voids were converted into pixels of intensity 0. The algorithm then

checked whether the current contour had greater than 15% of its interior pixels as 0. If it did, then this contour was considered a void, and the area of the contour was added to the void area.

Samples of gathered images with recorded void areas for all samples are shown as follows.



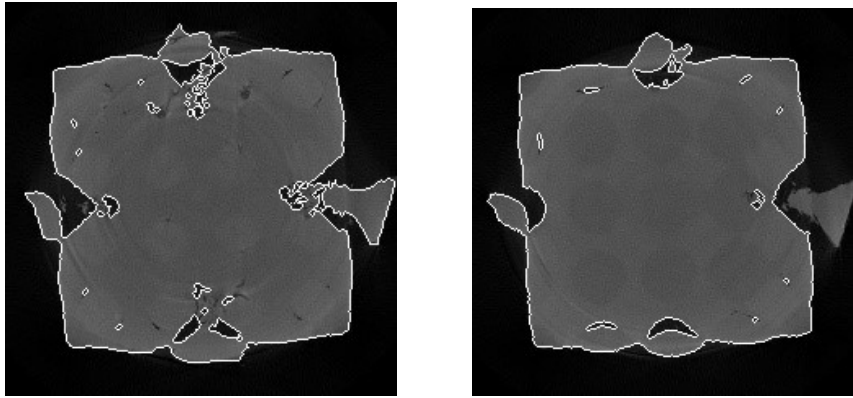
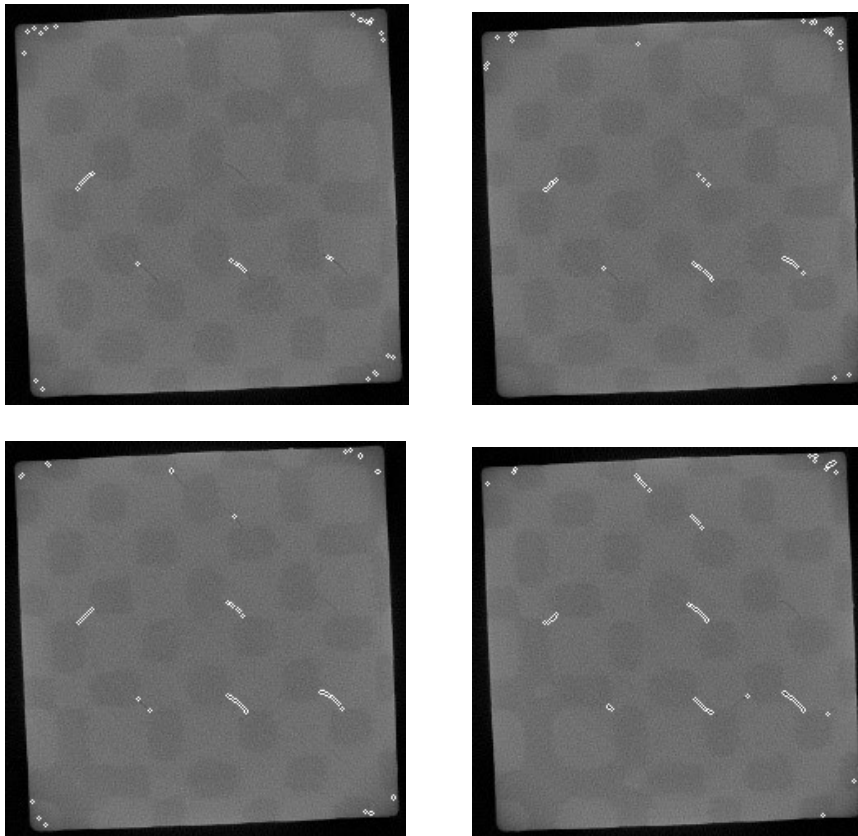


Fig 5.16: Contours extraction from SC sample images



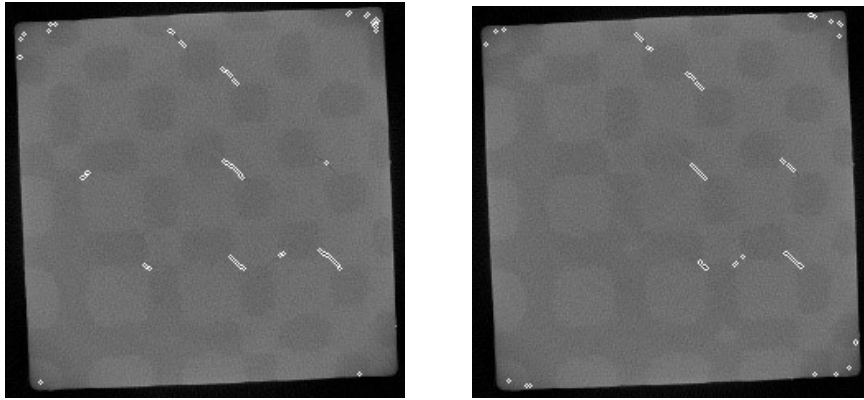
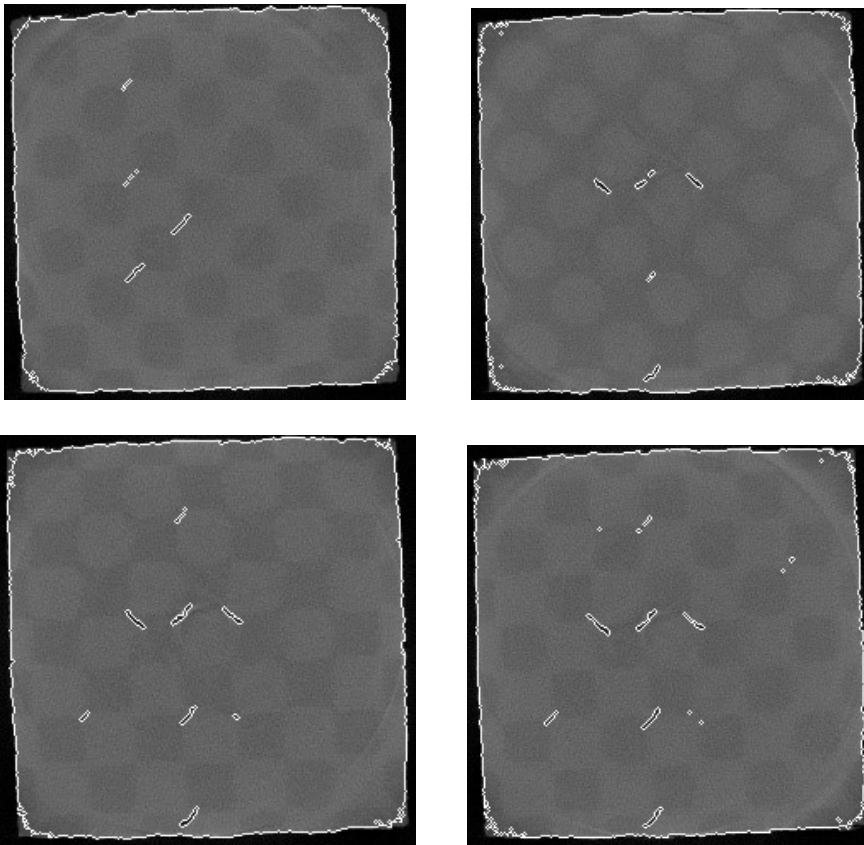


Fig 5.17: Contours extraction from BCC sample images



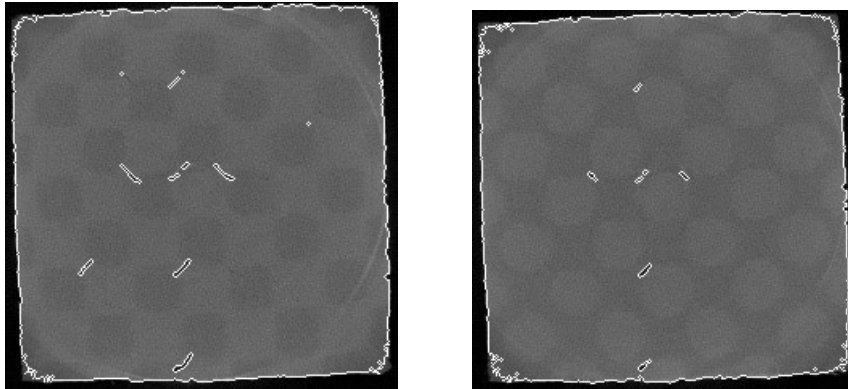
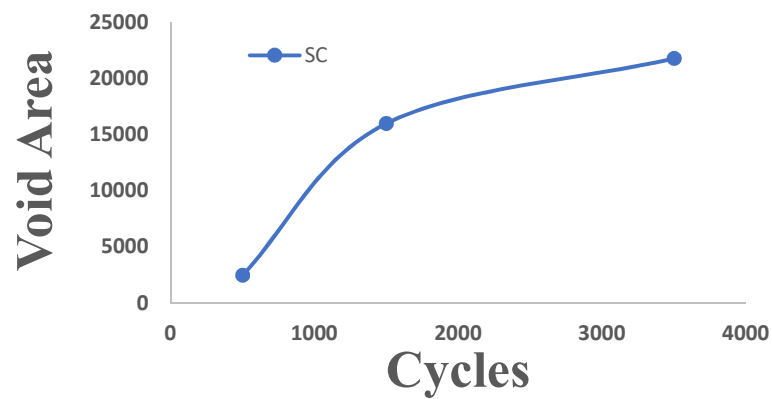


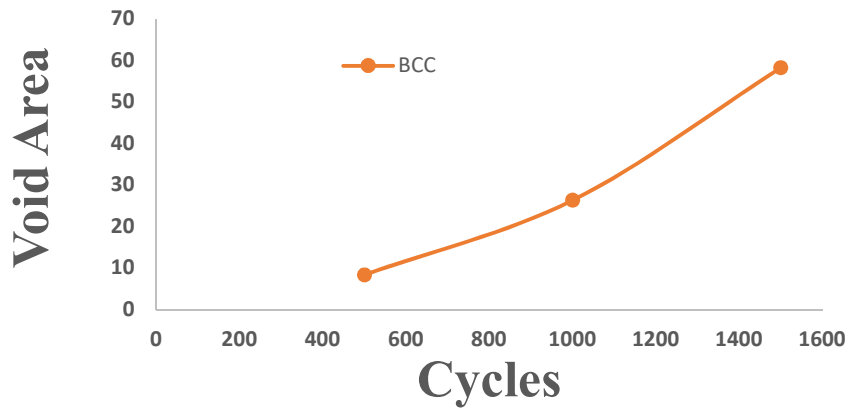
Fig 5.18: Contours extraction from FCC sample images

5.5.2 Results:

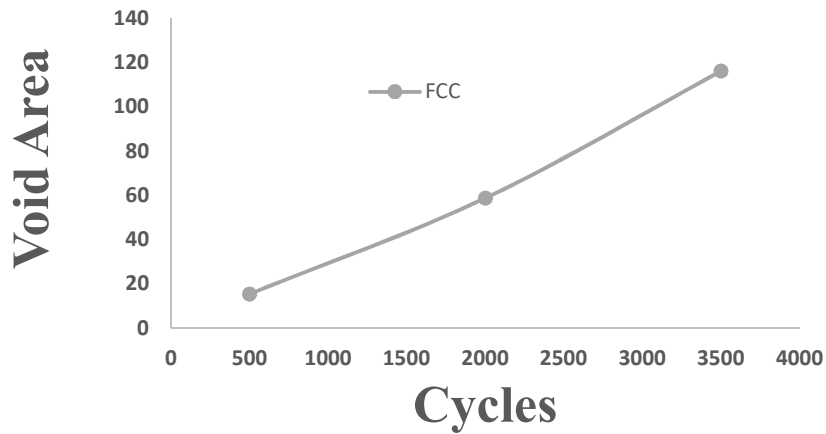
Results are generated by using the developed algorithm, in terms of pixels for all the available scanned images in the database. Void area progression in terms of pixels for every cycle is plotted to visualize the damage extension in the sample due to continuous change in loading on the sample.



Plot 5.19: Void area increase in SC sample



Plot 5.20: Void area increase in BCC sample

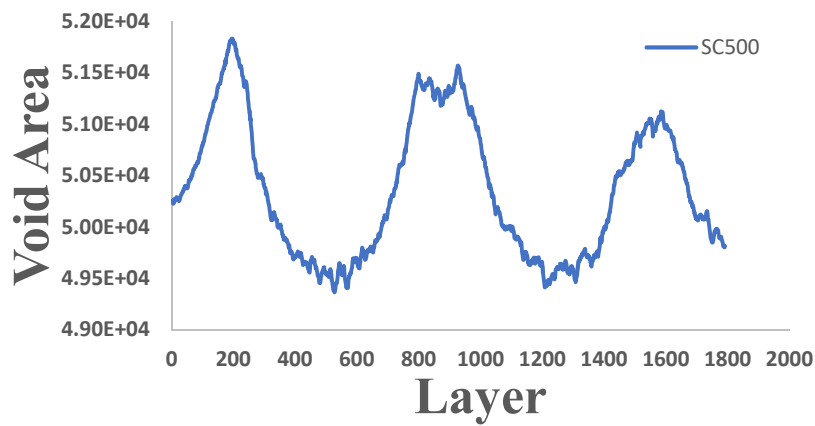


Plot 5.21: Void area increase in FCC sample

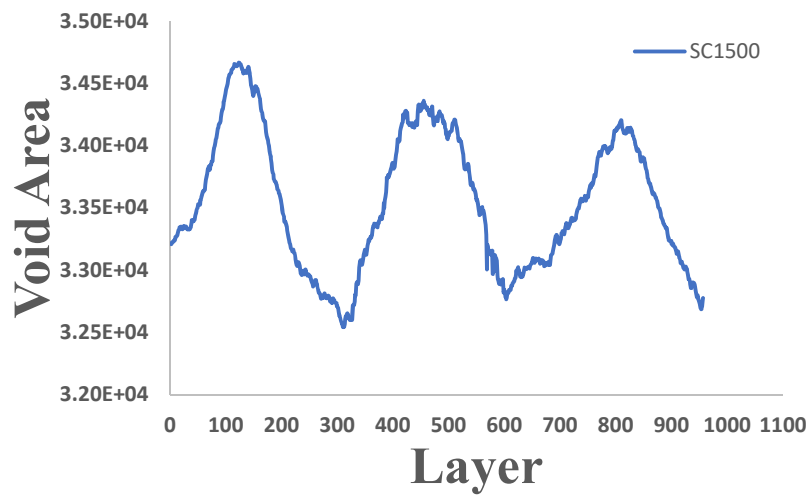
Total average area calculated for the image of the sample without damaged is about 51,889 pixels. Average void area is calculated for each test, since the damage inside the sample is not consistent throughout. From the above plots, we can observe the void area in the SC sample is more compared to other samples. The damage inside the SC is drastic and it is almost closer to half of the complete sample average area. The damage inside the SC sample is quite different where at the extreme loading case closer from 1500 cycles to 3500 cycles the amount of damage inside the sample is not much compared to preceding rise, this indicates the sample has sufficient damage inside and almost separation between the

phases is seen. But in other samples there is steady increase of the voids as the tests progressed.

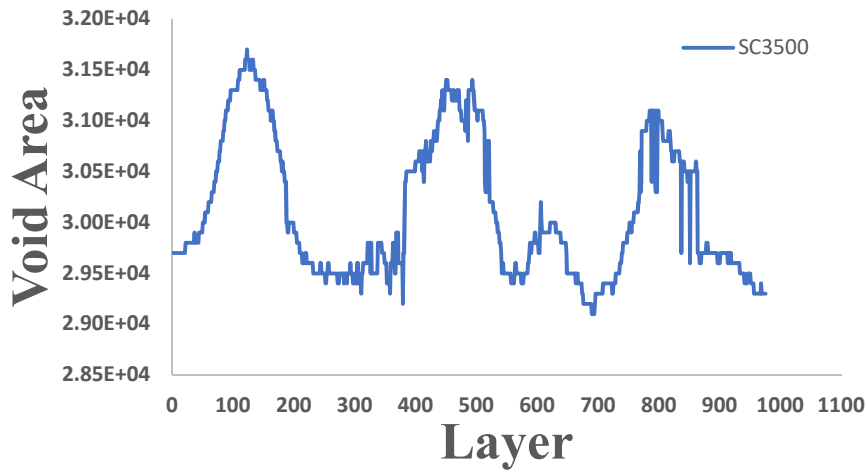
If we take a closer look into the damage inside the sample in multiple layers, inconsistency in the damage progression is observed. Each image extracted from the imaging process is considered a single layer for this analysis.



Plot 5.22: Damage variation inside of SC sample for 500 cycles

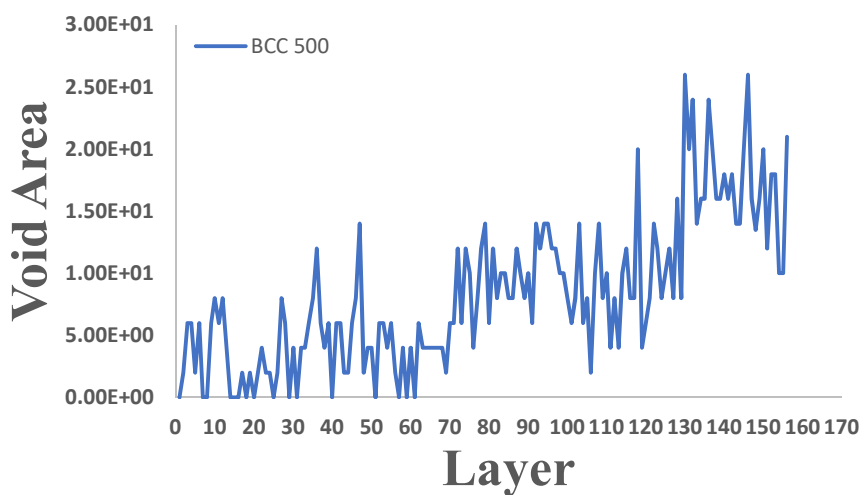


Plot 5.23: Damage variation inside of SC sample for 1500 cycles

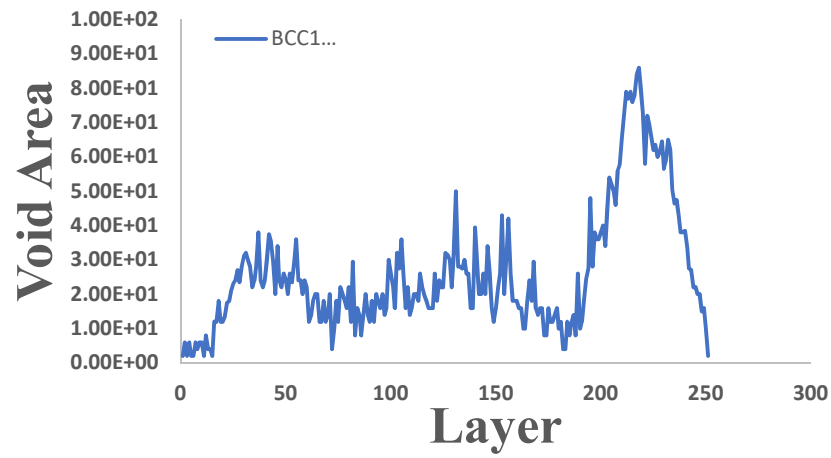


Plot 5.24: Damage variation inside of SC sample for 3500 cycles

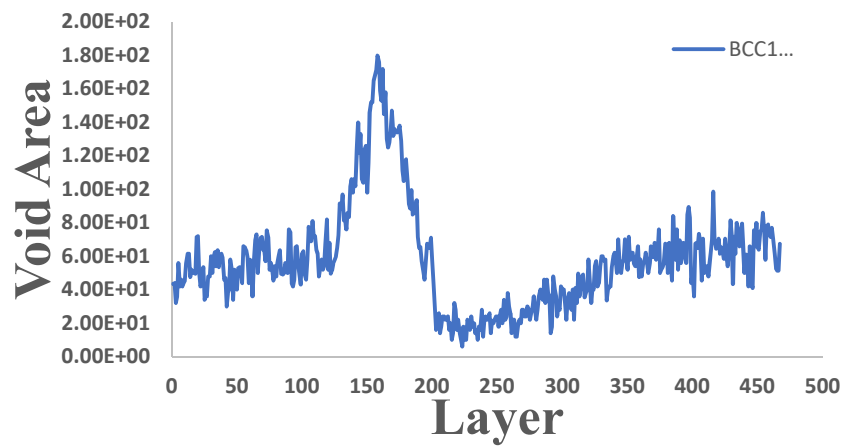
Damage initiated and the progression inside the sample is inconsistent, it might be because of these reasons. First, even though the material inside the sample is continuous, the arrangement of it in terms of loading direction might be resulting this variational behavior. Second reason could be the manufacturing of this sample. the material bonding in different locations in the sample might not be same. Same type of behavior seen in other samples but not extreme as this one.



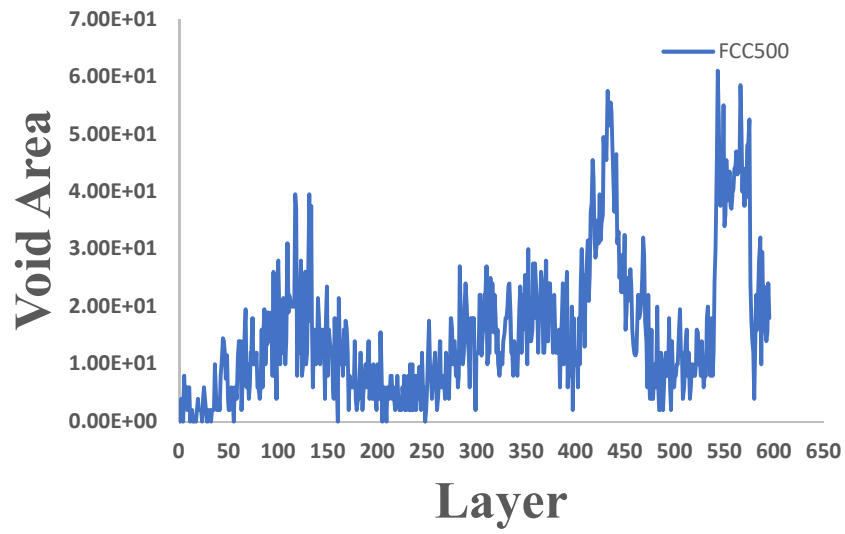
Plot 5.25: Damage variation inside of BCC sample for 500 cycles



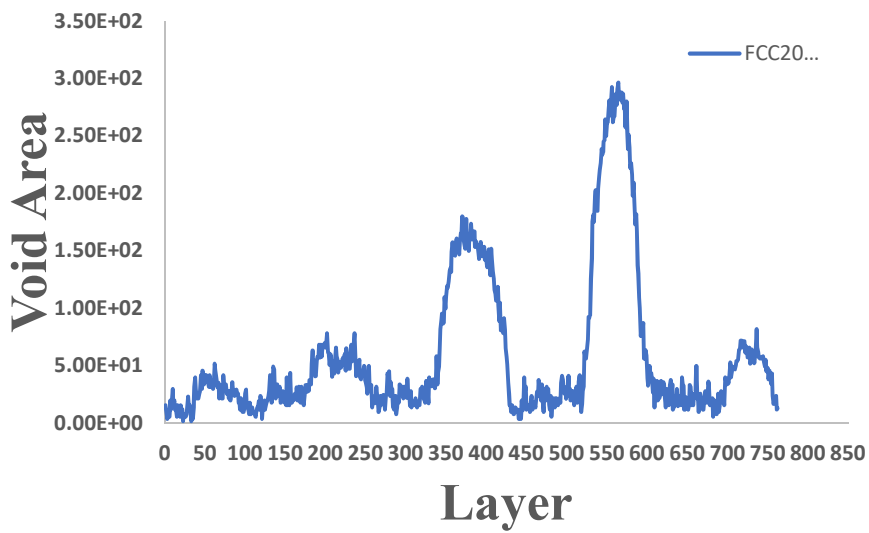
Plot 5.26: Damage variation inside of BCC sample for 1000 cycles



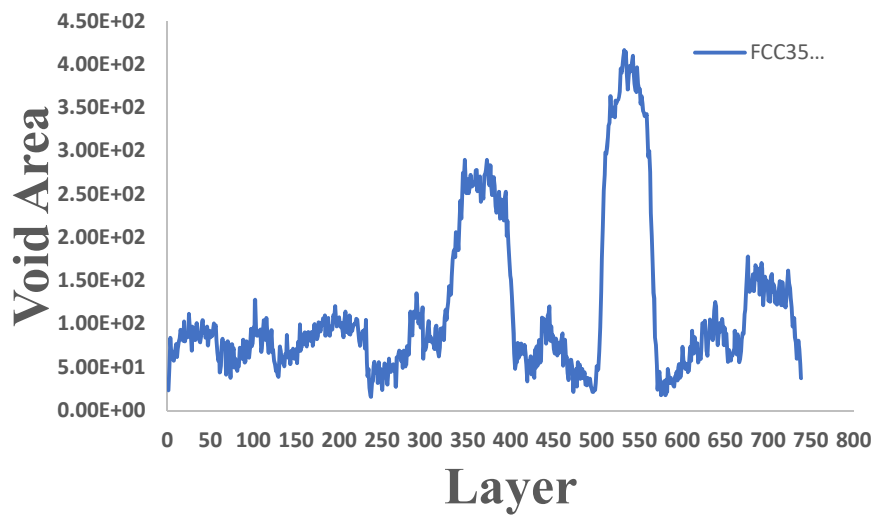
Plot 5.27: Damage variation inside of BCC sample for 1500 cycles



Plot 5.28: Damage variation inside of FCC sample for 500 cycles



Plot 5.29: Damage variation inside of FCC sample for 2000 cycles



Plot 5.30: Damage variation inside of FCC sample for 3500 cycles

here from this damage analysis the amount and the progression of the damage inside of the sample is quantitatively recorded.

CHAPTER – 6

CONCLUSION AND FUTURE WORK

6.1 Conclusion

The behavior of three co-continuous composite polymer structures studied under static loading gathered the results and visualized the damage pattern and the properties change in the sample mainly stress. From the images, FCC and BCC structures have purely shear deformation because the damage incurred in these samples are exactly 45 degrees in the direction of load applied. But for the simple cubic sample, the damage is in the direction of the loading axis, this is because of the alignment of the plastic phase in the same axis as loading that resulted in the pure compression behavior of sample, that generated buckling in the plastic phase resulting in the separation of elastomer and plastic phase with inflicting lot more damage compared to BCC and FCC.

The multi-cycle analysis is opted to study by forcing the samples into extreme conditions since the static analysis is not enough to record the behavior of the sample. From this, it is observed that the SC sample behaves differently than BCC and FCC. Stiffness regression is also one way to quantify the amount of damage in the sample, which was provided for all the samples based on experimental data.

This current study is also focused on validating the experimental results using imaging, all the samples are 3D scanned in Micro CT machine, to visualize the change in the internal structure of the sample after continuous testing. From the images, it is observed the damage criteria and pattern inside the samples. An effort was made by the images processing to calculate the pixel volume by excluding the damaged area inside of it. Results were showing the same periodic behavior as calculated from the experimental results.

Addition to the work done, images gathered from the scanning process are quantitatively analyzed using an algorithm developed to detect the voids in the sample to show the damage initiation, progression in one sample and all samples in comparison. As far the SC sample shows the progressively huge damage compared to other samples. Also, the damage inside the sample from top layer to bottom layer is also not consistent. Based on the results gathered, the hypothesis made earlier might be one of the reasons and the other reason might be the manufacturing of the samples did not result in the proper structural integrity which resulted in the uncommon and non-monotonic damage patterns in the samples. Further study is needed to study all these effects in detail.

6.2 Future work

As this study is completely focused on the mechanical characterization of the continuous polymer composites, there are some possible extensions adding onto this as future work.

Lattice structures have the tendency to behave differently when they are loaded on different slip planes that is different faces depending on the built of internal structure. So, potential addition to the future study is to analyze the behavior of these samples by loading them on different slip planes and validate to see the behavior is same or different.

The algorithm used for the quantitative analysis of the gathered images is not powerful enough to capture the smallest amount of details like hairline cracks and millimeter sized cracks from the images. So, another potential addition for the future work is to intensify the work to make the algorithm more sophisticated to detect even these cracks and many others without avoiding any. For now, the main focusing aspects that have to be added to validate the experimental results are stated below.

6.2.1 FEA Analysis

The analysis carried out in the experimental processes can be extended to simulations. Computer generated a 3D model of these co-continuous morphologies are being developed to analyze and characterize them based on multiple scenarios.

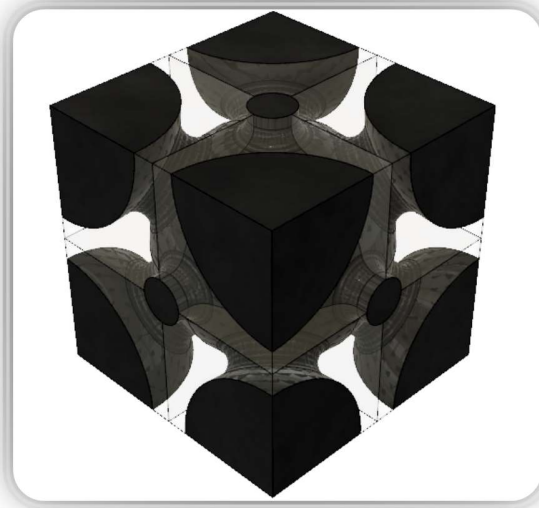


Fig 6.1: BCC 3D CAD model for FEA simulations

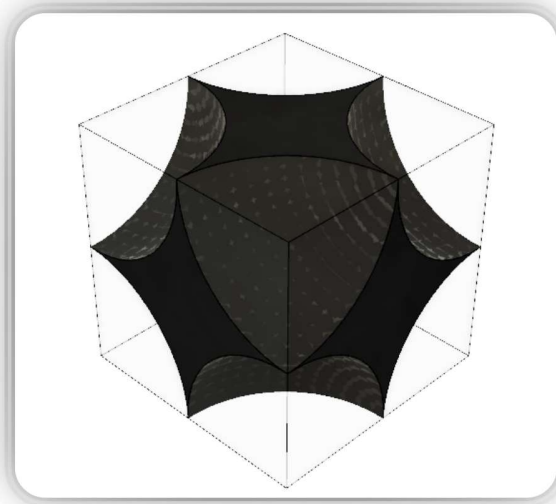
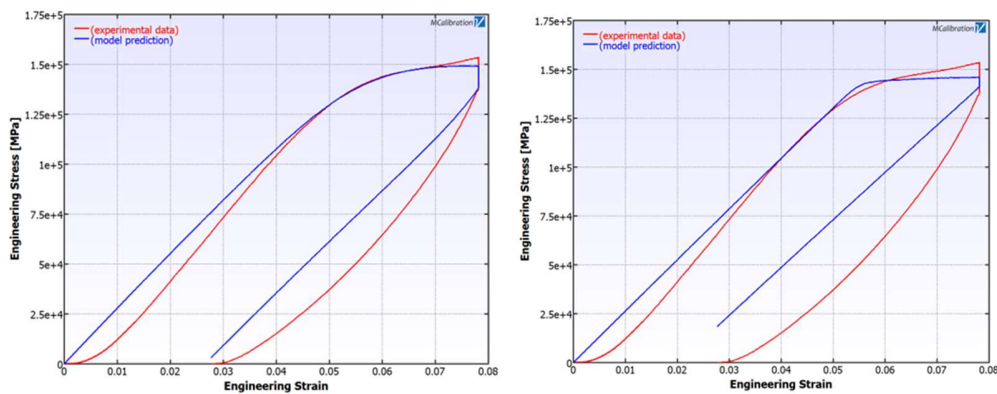


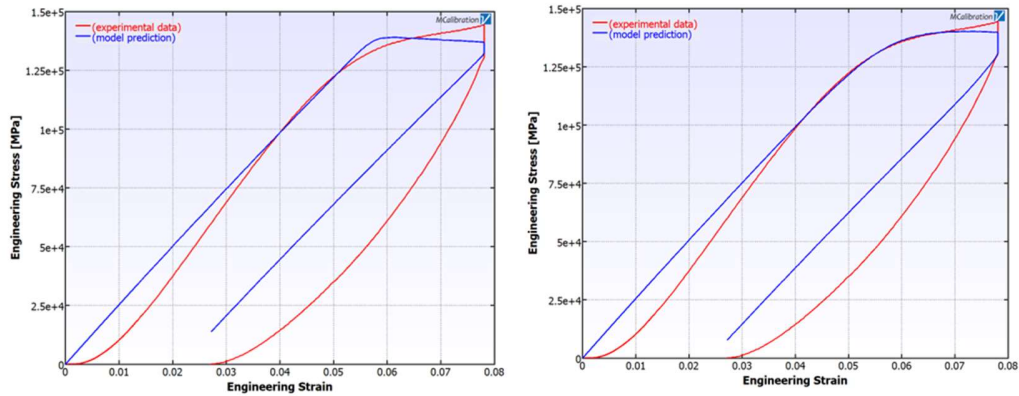
Fig 6.2: SC 3D CAD model for FEA simulations

6.2.2 Material calibration

The present study involved in the usage of polymer materials that highly shows non-linear behavior under mechanical loading. There are no theories to explain this phenomenon. There are some predefined models which are highly suited to explain and predict the nonlinear behavior of the polymers. A special software named “MCall” stands for material calibration distributed by Veryst materials can be used to analyze these materials using the already predefined material models in the Veryst material database. A sample calibration has been done to understand the prediction of the nonlinear behavior of the samples that are used for this study.

An input file is prepared by using the experimental data and loaded into the software. The appropriate material model is selected from the database and the calibration is performed. Sample plots are shown below.





Plot 6.1: Material calibration of samples

Here in this plot red line shows the imported experimental data and the blue line shows the calibrated data using the existing material model in the material database.

6.2.3 Characterization of 3D printed Metal sample

A new study is soon initiated in the group, in the material which is 3D printed using a special stainless-steel alloy which is Stainless Steel 316L. This Sample is fabricated into dog bone shape, to the dimensions that can fit inside the Micro CT machine, since this machine is also capable of Performing MTS operations. The main purpose of this study would be analyzing the sample behavior under loading and visualizing the effects of voids that are formed during fabrication. Sample scanning images of this sample are presented.



Fig 6.3: 3D printed Stainless Steel 316L alloy sample

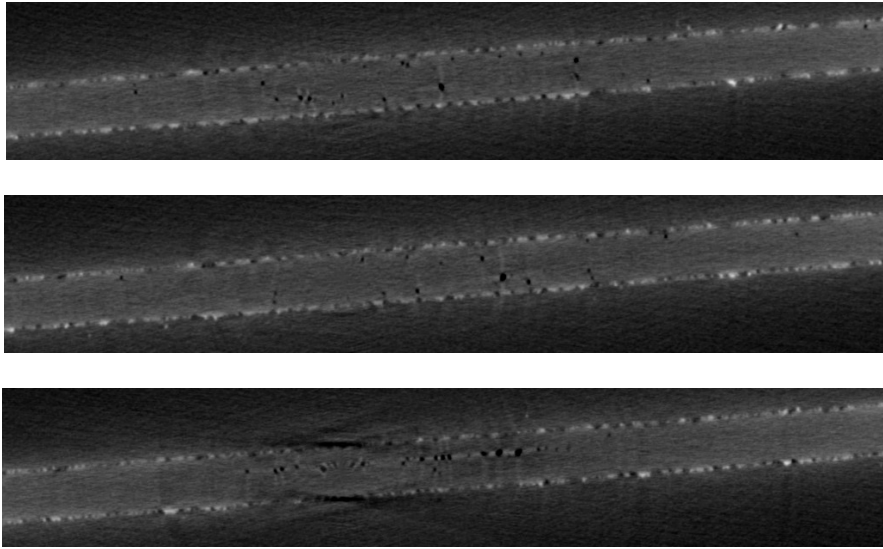


Fig 6.4: Micro CT imaging showing the voids in different layers of dogbone sample

REFERENCES

- 1 Wang, L., Lau, J., Thomas, E. L., & Boyce, M. C. (2011). Co-Continuous Composite Materials for Stiffness, Strength, and Energy Dissipation, 1524–1529. <https://doi.org/10.1002/adma.201003956>.
- 2 Zihlerl P. and Kamien R. D., “Soap Froths and Crystal Structures,” *Physical Review Letters*, Vol. 85, No. 16, 2000, pp. 3528-3531
- 3 Li, Le, "Kinetically Trapping Co-Continuous Morphologies in Polymer Blends and Composites" (2012). Open Access Dissertations. 529. https://scholarworks.umass.edu/open_access_dissertations/529
- 4 Cantrell, J., Rohde, S., Damiani, D., Gurnani, R., Disandro, L., Anton, J., ... Ifju, P. (n.d.). Experimental Characterization of the Mechanical Properties of 3D-Printed ABS and Polycarbonate Parts.
- 5 Bergström, J. (2015). Viscoplasticity Models. *Mechanics of Solid Polymers*,371-436. doi:10.1016/b978-0-323-31150-2.00008-x
- 6 Bergström, J. (2015). Plasticity Models. *Mechanics of Solid Polymers*,353-369. doi:10.1016/b978-0-323-31150-2.00007-8
- 7 Zaïri, F., Naït-Abdelaziz, M., Gloaguen, J., & Lefebvre, J. (2008). Modeling of the elasto-viscoplastic damage behavior of glassy polymers. *International Journal of Plasticity*,24(6), 945-965. doi:10.1016/j.ijplas.2007.08.001
- 8 Zaïri, F., Naït-Abdelaziz, M., Woznica, K., & Gloaguen, J. (2007). elasto-viscoplastic constitutive equations for the description of glassy polymers behavior at constant strain rate. *Journal of Engineering Materials and Technology*,129(1), 29. doi:10.1115/1.2400256
- 9 Spathis, G., & Kontou, E. (2015). Modeling of viscoplastic cyclic loading behavior of polymers. *Mechanics of Time-Dependent Materials*,19(3), 439-453. doi:10.1007/s11043-015-9272-x
- 10 Brown, R. P. (1999). *Handbook of polymer testing: Physical methods*. New York, NY: Dekker.
- 11 3D Printing and Its Applications. (2016). *International Journal of Science and Research (IJSR)*,5(3), 1532-1535. doi:10.21275/v5i3.nov162160
- 12 Bertram, A., & Glüge, R. (2015). One-Dimensional Material Theory. *Solid Mechanics*,1-42. doi:10.1007/978-3-319-19566-7_1
- 13 Silva, V. D. (2011). *Mechanics and strength of materials*. Berlin: Springer.

- 14 Forster, A. M. (2015). Materials Testing Standards for Additive Manufacturing of Polymer Materials: State of the Art and Standards Applicability. doi:10.6028/nist.ir.8059
- 15 Pegues, J. W., Roach, M. D., & Shamsaei, N. (2017). Influence of microstructure on fatigue crack nucleation and microstructurally short crack growth of austenitic stainless steel. *Materials Science and Engineering: A*, 707, 657-667. doi:10.1016/j.msea.2017.09.081
- 16 Ulu, K. N., Huneau, B., Verron, E., Béranger, A., & Heuillet, P. (2017). True stress controlled fatigue life experiments for elastomers. *International Journal of Fatigue*, 104, 171-182. doi:10.1016/j.ijfatigue.2017.07.007
- 17 Senatov, F., Niaza, K., Stepashkin, A., & Kaloshkin, S. (2016). Low-cycle fatigue behavior of 3d-printed PLA-based porous scaffolds. *Composites Part B: Engineering*, 97, 193-200. doi:10.1016/j.compositesb.2016.04.067
- 18 Hooreweder, B. V., & Kruth, J. (2017). Advanced fatigue analysis of metal lattice structures produced by Selective Laser Melting. *CIRP Annals*, 66(1), 221-224. doi:10.1016/j.cirp.2017.04.130
- 19 Willemse, R., Boer, A. P., Dam, J. V., & Gotsis, A. (1999). Co-continuous morphologies in polymer blends: The influence of the interfacial tension. *Polymer*, 40(4), 827-834. doi:10.1016/s0032-3861(98)00307-3
- 20 Zheng, Y., Ji, X., Yin, M., Shen, J., & Guo, S. (2017). Strategy for Fabricating Multiple-Shape-Memory Polymeric Materials via the Multilayer Assembly of Co-Continuous Blends. *ACS Applied Materials & Interfaces*, 9(37), 32270-32279. doi:10.1021/acsami.7b10345
- 21 Bonatti, Colin, and Dirk Mohr. "Mechanical Performance of Additively-Manufactured Anisotropic and Isotropic Smooth Shell-Lattice Materials: Simulations & Experiments." *Journal of the Mechanics and Physics of Solids*, vol. 122, 2019, pp. 1–26., doi:10.1016/j.jmps.2018.08.022.
- 22 N. Otus, "A Threshold Selection Method from Gray-Level Histograms," *IEEE Trans. Syst. Man. Cybern.*, 1979.
- 23 M. Fang, G. Yue, and Q. Yu, "The Study on An Application of Otsu Method in Canny Operator," *Proc. 2009 Int. Symp. Inf. Process. Huangshan, P. R. China, August 21-23*, vol. 2, no. 4, pp. 109–112, 2009.
- 24 J. Canny, "A Computational Approach to Edge Detection," *IEEE Trans. Pattern Anal. Mach. Intell.*, 1986.

APPENDIX A
MICROSOFT VISUAL STUDIO CODE DEVELOPED AND USED FOR
THE IMAGE ANALYSIS

```

# Import libraries - Install using pip
import numpy as np
import cv2
import argparse
import statistics
import matplotlib.pyplot as plt
import os
from imutils import paths
# construct the argument parse and parse the arguments
ap = argparse.ArgumentParser()
ap.add_argument("-i", "--images", required=True,
                help="path to input directory of images")
args = vars(ap.parse_args())
area = []
# Iterate through each image in the directory
for imagePath in paths.list_images(args["images"]):
    # Extract filename from full image path
    base = os.path.basename(imagePath)
    fileName = os.path.splitext(base)[0]
    # Load image and resize it
    im=cv2.imread(imagePath)
    width_orig, height_orig = im.shape[:2]
    print("Width, Height of original:", width_orig, height_orig)
    im=cv2.resize(im, None, fx=0.5, fy=0.5)
    width_mod, height_mod = im.shape[:2]
    print("Width, Height of resize:", width_mod, height_mod)
    # Convert BGR to Grayscale
    gray = cv2.cvtColor(im, cv2.COLOR_BGR2GRAY)
    overlay = gray.copy()
    overlay_interior = gray.copy()
    blur = cv2.GaussianBlur(gray, (1,1), 0, None, 0)
    cv2.imshow("Blurred", blur)
    # Calculate and plot histogram of gray image
    hist = cv2.calcHist(gray, [0], None, [256], [0,256])
    plt.hist(im.ravel(),256,[0,256]); plt.show()
    # Blur image
    kernel = np.ones((9,9), np.float32)/25
    blur = cv2.filter2D(gray, -1, kernel)
    # Feature Extraction
    ret, binary = cv2.threshold(gray, 30, 255,
cv2.THRESH_BINARY|cv2.THRESH_OTSU)
    # ret, binary = cv2.threshold(gray, 30, 255, cv2.THRESH_BINARY)
    # Edge Extraction using Canny Edge Algorithm
    canny = cv2.Canny(gray,0.5*ret, ret)
    # Black canvas images for outputs

```

```

img_black = np.zeros_like(canny)
img_allContoursBlack = img_black.copy()
img_externalContour_damage = img_black.copy()
img_largestContour_damage = img_black.copy()
img_selectedContours = np.zeros_like(canny)
'''

cv2.imshow("Gray", gray)
cv2.imshow("Binary", binary)
cv2.imshow("Canny", canny)
'''

# Morphological operation - Dilate the edges
kernel = np.ones((2,2),np.uint8)
dilate_canny = cv2.dilate(canny,kernel,iterations = 3)
# Extract outer boundary contour from dilated image
_, boundaryContours, _ = cv2.findContours(dilate_canny, cv2.RETR_EXTERNAL, \
cv2.CHAIN_APPROX_NONE)
# Extract contours from binary image
_, contours, _ = cv2.findContours(binary, cv2.RETR_TREE, \
cv2.CHAIN_APPROX_NONE)
cv2.drawContours(overlay, contours, -1 , 255 , 1)
cv2.drawContours(img_allContoursBlack, contours, -1, 255, 1)
# cv2.imshow("All Contours", img_allContoursBlack)
# Extract the largest contour from the boundarycontours list
boundaryContoursSorted = sorted(boundaryContours, key=lambda x:
cv2.contourArea(x, True))
largestBC = boundaryContoursSorted[0]
largestBC = np.intp(largestBC)
cv2.drawContours(img_black, largestBC, -1 , 255 , 1)
'''

cv2.drawContours(overlay, secondLargestContour, -1, 155, 1)
cv2.imshow("boundary contour", img_black)
cv2.imshow("contours", overlay)
'''

areaContour = []
# Damaged contours
_, boundaryContours_damage, _ = cv2.findContours(img_allContoursBlack,
cv2.RETR_EXTERNAL, \
cv2.CHAIN_APPROX_NONE)
cv2.drawContours(img_externalContour_damage, boundaryContours_damage, -1, 255,
1)
boundaryContoursSorted_damage = sorted(boundaryContours_damage, key=lambda
x: cv2.contourArea(x, True))
largestBC_damage = boundaryContoursSorted_damage[0]
largestBC_damage = np.intp(largestBC_damage)
cv2.drawContours(img_largestContour_damage, largestBC_damage, -1, 255, 1)

```

```

cv2.drawContours(overlay_interior, largestBC_damage, -1, 255, 1)
'''
cv2.imshow("largest contour damage", img_largestContour_damage)
cv2.waitKey(0)
areaContour.append(-cv2.contourArea(largestBC_damage, True))
print(-cv2.contourArea(largestBC_damage, True))
'''
# Iterate on contours from binary image to check for voids
for i,c in enumerate(contours):
    numZeros = 0
    num255 = 0
    numPoints = 0
    relFreqZeros = 0
    interior_intensities = []
    img_singleContour = np.zeros_like(gray)
    inside = 0
    void = 0
    for j in c: # Check whether the contour is inside the boundary
        if cv2.pointPolygonTest(largestBC, (j[0][0], j[0][1]), False) == -1:
            # print("Outside")
            inside = 0
            continue
        else:
            # print("Inside")
            inside = 1
    if inside == 1:
        cv2.drawContours(img_singleContour, contours, i, color=255, thickness=-1)
        # cv2.imshow("single contour", img_singleContour)
        # cv2.waitKey(0)
        pts = np.where(img_singleContour == 255)
        interior_intensities.append(binary[pts[0], pts[1]])
        interior_intensities = np.array(interior_intensities, dtype=np.uint8)
        # print(interior_intensities)
        numZeros = (interior_intensities==0).sum()
        # print("Number of 0 pixels:", numZeros)
        num255 = (interior_intensities == 255).sum()
        # print("Number of 255 pixels:", num255)
        numPoints = len(interior_intensities[0])
        # print("Total number of pixels:", numPoints)
        relFreqZeros = numZeros/numPoints
        relFreq255 = num255/numPoints
        if relFreqZeros > 0.15:
            cv2.drawContours(overlay_interior, c, -1, 255, 1)
            areaContour.append(cv2.contourArea(c,True))
            # print(-cv2.contourArea(c,True))

```

```
area.append(sum(areaContour))
# cv2.imshow("Interior contours", overlay_interior)
# cv2.waitKey(0)
# Save output images to file (contour overlay and binary)
cv2.imwrite("D:/data/rahul/madhava/madhavaImages/BCC1500_1/" + fileName +
"_contours.jpg", overlay_interior)
# cv2.imwrite("D:/data/rahul/madhava/madhavaImages/BCCL/" + fileName +
"_allContours.jpg", overlay)
cv2.imwrite("D:/data/rahul/madhava/madhavaImages/BCC1500_1/" + fileName +
"_binary.jpg", binary)
# cv2.imwrite("D:/data/rahul/madhava/madhavaImages/originals/" + fileName +
"_gray.jpg", gray)
np.savetxt("BCC1500_1.csv", area, delimiter="\n")
```

-Credits to Rahul Rathnakumar for algorithm